

5-2012

Effect of Building Morphology on Energy and Structural Performance of High-Rise Office Buildings

Mohamed Krem

University of Massachusetts Amherst, mkrem@engin.umass.edu

Follow this and additional works at: https://scholarworks.umass.edu/open_access_dissertations

Part of the [Civil and Environmental Engineering Commons](#)

Recommended Citation

Krem, Mohamed, "Effect of Building Morphology on Energy and Structural Performance of High-Rise Office Buildings" (2012). *Open Access Dissertations*. 579.

<https://doi.org/10.7275/xb97-6f66> https://scholarworks.umass.edu/open_access_dissertations/579

This Open Access Dissertation is brought to you for free and open access by ScholarWorks@UMass Amherst. It has been accepted for inclusion in Open Access Dissertations by an authorized administrator of ScholarWorks@UMass Amherst. For more information, please contact scholarworks@library.umass.edu.

EFFECT OF BUILDING MORPHOLOGY ON ENERGY AND STRUCTURAL PERFORMANCE OF
HIGH-RISE OFFICE BUILDINGS

A Dissertation Presented

by

MOHAMED ALI MILAD KREM

Submitted to the Graduate School of the
University of Massachusetts Amherst in partial fulfillment
of the requirements for the degree of

DOCTOR OF PHILOSOPHY

May 2012

Civil and Environmental Engineering

EFFECT OF BUILDING MORPHOLOGY ON ENERGY AND STRUCTURAL PERFORMANCE OF
HIGH-RISE OFFICE BUILDINGS

A Dissertation Presented

by

MOHAMED ALI MILAD KREM

Approved as to style and content by:

Sanjay R. Arwade , (Co-chair)

Simi T. Hoque , (Co-chair)

Sergio Brena, Member

Benjamin S.Weil, Member

Richard N. Palmer, Department Head
Civil and Environmental Engineering Department

DEDICATION

This dissertation is dedicated to my patients and my wife and my children.

ACKNOWLEDGMENTS

Special thanks go to my advisors Professor Sanjay R. Arwade and Professor Simi T. Hoque, who always gave me useful suggestions and orientation, and always encouraged me to challenge the deeper exploration throughout my academic years at the University of Massachusetts-Amherst. Special thanks go to Professor Sergio F. Breña who always welcomed my questions and answered them with pleasure; and to Professor Benjamin S. Weil for editing some of my work. Special thanks go to my friend Carl Fiocchi who helped me to understand some features of using Ecotect 2011. Special thanks go to all my instructors and all staff (Jodi Ozdarski, Caroline Nofio, and others) in Civil and Environmental Engineering Department. Also, many thanks go to my sponsor the Ministry of Education and Scientific Research in Tripoli, Libya.

Finally, special thanks to my family: my wife and my children I appreciate their patience on this four-year journey to obtain my PhD degree in this country faraway from our home country, Libya. I appreciate their hardships and homesickness. Special thanks also go to my family in our home country: my mother and my father and my siblings and my relatives and friends, all of whom wish us great success and have waited for our safe and fruitful return.

Many thanks all of you for your support and your belief in me.

I wish to be the pride of all of those.

ABSTRACT

EFFECT OF BUILDING MORPHOLOGY ON ENERGY AND STRUCTURAL PERFORMANCE OF HIGH-RISE OFFICE BUILDINGS

MAY 2012

MOHAMED ALI MILAD KREM, B.Sc., NASSER UNIVERSITY

M.Sc., AL-MERGEH UNIVERSITY

Ph.D., UNIVERSITY OF MASSACHUSETTS AMHERST

Directed by: Professor Sanjay R.Arwade and Professor Simi T. Hoque

The civil engineering and architectural communities are highly focused, these days, on designing buildings that maximize utilization of energy available from natural resources. This dissertation presents a quantitative study of the effect of high-rise office building morphology on energy and structural performances for the major climates. The parameters of the building morphologies are varied – the building footprint shape, the placement of the structural core/walls, and the building orientation. The energy analysis is performed using Autodesk Ecotect Analysis 2011; while using SAP2000 for the structure analysis and design. The key observations are: 1) the building morphology has a significant effect on the annual energy consumption, 2) placement of the structural core/walls in the east and west sides significantly improve the energy performance, 3) the tradeoff in the cost of placing the structural core/walls to maximize operating energy efficiency is too great, 4) for built to code buildings the energy demand may be considered marginally sensitive to changes in aspect ratio, and 5) high quality thermal properties of code-built envelope systems offer more flexibility to designers with regard to the building site planning without creating negative impacts on total energy demand.

TABLE OF CONTENTS

	Page
ACKNOWLEDGMENTS.....	v
ABSTRACT.....	vi
LIST OF TABLES.....	x
LIST OF FIGURES.....	xii
CHAPTER	
1. INTRODUCTION.....	1
2. LITERATURE REVIEW.....	7
3. BACKGROUND.....	14
3.1 Thermal mass.....	14
3.2 Thermal mass properties.....	14
3.3 Thermal mass in Buildings.....	15
3.4 Thermal transmission through building.....	18
3.4.1 Heat transfer.....	18
3.4.2 Office building heat gain.....	19
3.5 Design and analysis of tall building.....	22
3.5.1 Structural lateral load systems.....	23
3.5.2 Outrigger-Braced Structures.....	24
4. INVESTIGATING THE EFFECT OF BUILDING MORPHOLOGY AND CORE PLACEMENT ON ENERGY PERFORMANCE OF SKYSCRAPER OFFICE BUILDINGS ..	32
4.1 An approach.....	32
4.1.1 Description of building models variables.....	33
4.1.2 The thermal analysis.....	38
4.1.3 The modeling.....	38

4.1.4	Modeling assumptions.....	40
4.1.5	The analysis.....	41
4.1.6	Thermal analysis results.....	42
4.2	Preliminary calculation of building stiffness.....	51
4.2.1	Building stiffness.....	53
4.2.4	Results.....	55
4.3	Summary of energy analysis and Preliminary calculation of building stiffness.....	56
4.4	Energy demand with equivalent percentages of opaque surfaces (EPO).....	59
4.4.1	Modeling.....	59
4.4.2	Summary of EPO analysis.....	62
4.5	Thermal mass modeling.....	64
4.5.1	Equivalent distributed of the opaque surfaces (EDO).....	64
4.5.2	Doubling the wall's thickness.....	65
4.5.3	Summary of EDO analysis.....	68
5.	STRUCTURAL ANALYSIS.....	70
5.1	Introduction.....	70
5.2	Description of building models variables:.....	71
5.2.1	Building model loading.....	72
5.2.2	Base structural system.....	73
5.2.3	Supplementary lateral load resistance.....	76
5.2.4	Displacements results, SLLR:.....	78
5.2.5	Summary of the structural analysis.....	81
6.	MATERIAL USED EMBODIED ENERGY AND TOTAL COSTS (OPERATIONAL, EMBODIED ENERGIES AND MATERIAL USED).....	84
6.1	Material used embodied energy.....	84
6.1.1	Summary of the material used embodied energy.....	86

6.2 Cost analysis.....	87
6.2.1 Cost calculation Assumptions	88
6.2.2 Cost of operational energy	88
6.2.3 Cost of material used for BSS and SLLR	89
6.3 Total cost: Operational, Embodied energies and Material costs	94
6.3.1 Summary of the cost estimating.....	95
7. SENSITIVITY OF ENERGY DEMAND TO BUILDING FOOTPRINT ASPECT RATIO AND BUILDING ORIENTATION.....	99
7.1 Introduction	99
7.2 Building Materials and Method	100
7.3 Analytical Approach:	102
7.3.1 Thermal analysis	102
7.3.2 Demand sensitivity–glazing walls built to code	106
7.3.3 Demand sensitivity with non-code-compliant glazing on walls.	110
7.3.4 Summary of results	114
8. CONCLUSIONS AND RECOMMENDATIONS AND FUTURE WORK	115
8.1 Conclusions	115
8.2 Recommendations	116
8.3 Future work.....	117
APPENDIXES	
A. PRELIMINARY ANALYSIS.....	119
B. COST INDEX.....	131
BIBLIOGRAPHY	134

LIST OF TABLES

Table	Page
2.1 Yeang’s passive design strategies with respect to building morphology [1]	9
2.2 Energy efficient building shape [8]	12
4.1 Structural layers and thermal resistance of the materials	36
4.2 Description of the climate zones characteristics for the representative cities	39
4.3 Thermal analysis conditions.....	40
4.4 Annual heating and cooling loads.....	52
4.5 Lateral stiffness and torsional susceptibility of different building models	57
4.6 Thermal analysis results of EPO	62
4.7 Thermal analysis results of EDO	67
4.8. Thermal mass results of Sides configuration (initial configuration)	68
4.9 Thermal mass effect Sides configuration of 46% opaque	69
5.1 lateral displacements result of BSS models.....	76
5.2 The lateral displacements result with SLLR	82
6.1 Embodied energy of the material used (for BSS & SLLR).....	85
6.2 The operational energy extreme differences in annual energy the cost	90
6.3 Total material used cost index.....	93
6.4 Summation all costs operational, embodied energies and material for fifty years life span	96
7.1 Energy demand verses SAR (N-S orientation).....	107
7.2 Energy demand ratio, EDR, (model of 1:4 aspect ratio).....	111
7.3 Sources of heat gain (Wh) in July- built to code envelope (model of 1:4 aspect ratio).....	113

7.4 Breakdown heat gain (Wh) in July in Arid climate – regular glass envelope (model of 1:4 aspect ratio)	114
--	-----

LIST OF FIGURES

Figure	Page
3.1 Thermal mass material use in construction in Upper Egypt [24]	16
3.2 Heat gains through the thermal mass material: (a) Heat gain in winter; (b) Heat dispose in summer “after [25]”	17
3.3 Heat transfer through a wall “after [27]”	20
3.4 Heat gain/loss through an office building components “after [27]”	21
3.5 Height comparison of steel building systems [29].....	23
3.6 Height comparison of concrete building systems [29]	24
3.7 Outrigger-Braced Structures [30]	25
3.8 a) outrigger system with a central core: (b) outrigger system with offset core[29].....	27
3.9 (b) cantilever bending of core; (c) tie-down action of cap truss [29].....	28
3.10 One outrigger at top, $z = L$ [29].....	30
3.11 Optimum locations of outriggers: (a) single outrigger; (b) two outriggers; (c) three outriggers; (d) four outriggers[29]	31
4.1 Proposal by K. Yeang for optimal floor-plan and placement of structural cores to minimize building energy consumption in four climates [1].....	33
4.2 Plan views and an elevation of the buildings	35
4.3 Plan view of dodecagon shape- equivalent to the Central configuration	42
4.4 Ecotect 3D models	43
4.5 Sun-path diagram – building’s walls shadow.....	43
4.6 The thermal analysis result of the four models in the arid climate	46
4.7 The thermal analysis result of the four models in the cool climate	47
4.8 The thermal analysis result of the four models in the temperate climate.....	48

4.9 The thermal analysis result of the four models in the tropical climate	49
4.10 3D of how the different building types might deform under wind loads	58
4.11 Plan views and an elevation of the buildings (EPO)	61
4.12 The variance in EUI between the initial and EPO for the four configurations in each climate zone	63
4.13 Plan views and an elevation of the buildings (EDO)	66
4.14 Plan views Central and Sides (thermal mass analysis)	68
5.1 Torsional displacements: (a) Half sides; (b) Edge model	76
5.2 Building plan views and schematic structural system for the buildings with three outriggers with/without belt trusses (connecting columns perpendicular to the plane of outriggers)	80
5.3 Lateral displacements at the roof (service wind loads P_w and $0.75 P_w$)	83
6.1 Financial comparison of the operational energy cost for a 50 year life span with respect to the Central configuration	91
6.2 Material cost index BSS and SLLR	92
6.3 Financial comparison of the total cost for a 50 years life span with respect to the Central configuration.....	97
7.1 Building orientation considered in this study	101
7.2 Building plan view and envelope thermal properties	103
7.3 Sensitivity of EUI to the change in surface area ratio.....	109
7.4 Monthly passive solar heat gain ratio (model of 1:4 aspect ratio).....	112

CHAPTER 1

INTRODUCTION

For thousands of years, tall buildings and towers have fascinated human beings; they have been built primarily for defensive or religious purposes as evidenced by the Pharaonic temples (pyramids) of Giza, Egypt, the Mayan temples of Tikal, Guatemala, the Kutub Minar of Delhi, India, and the gothic cathedrals of Europe.

In the modern era, high-rise buildings are a reality of contemporary life in cities and there are several reasons for this. Urban real estate is a premium due to the lack of available land, which drives up the cost of land and forces restrictions on indiscriminate expansion (or sprawl) to preserve green space, natural habitats, or agricultural land. High-rise buildings (vertical construction) present an effective way to reduce traffic congestion in cities, as they can provide many services to citizens in a single building [1]. Rapid population growth of urban communities increases the need for housing, and with limited buildable land, leads to pressure to develop high-rise residential apartments. The limitations and the conditions of the terrain and topography in some urban areas may make the construction of high-rise buildings the only viable solution. This is particularly true for many cities in Asia and South America such as Rio de Janeiro and Hong Kong [2]. As a result of the high concentration of businesses in city centers, high-rise commercial buildings are a solution to keep these institutions as near to each other as possible.

Meeting operational performance requirements and maintaining occupant comfort in high-rise buildings is a challenging design problem. The energy demands for

large scale HVAC system (Heating, Ventilating, and Air Conditioning) loads are significant. Not only are the site energy costs high, the attendant environmental consequences of using non-renewable energy sources are great.

Improving the energy efficiency of high-rise buildings is a key component in increasing the sustainability of the environment. More than one-third of the world's energy consumption is attributed to the construction and building industry [3]. Given the dramatically increased energy demand, there is a critical need to design and construct buildings that are more sustainable. Energy efficient buildings minimize building resource consumption, operations and life cycle costs, and can improve occupant health and comfort [4].

High-rise buildings should be designed in a manner to reduce the need for fossil fuels (oil, gas and coal) and promote greater reliance on passive/renewable energy strategies. This concept is reflected in what is known these days as sustainable architecture or green building. A green building is one that focuses on reducing the impact of buildings on the environment. In general, a green building is one that meets the needs of the present generation without compromising the ability of future generations to meet their needs as well [1]. For designers and architects such as Reed [5], green buildings are designed, implemented, and managed in a manner that places the environment first. One of the key goals of the green building movement is to reduce the material, constructional, and operational costs of buildings, and also reduce the excessive depletion of natural resources. One way this is accomplished is by drawing on the synergies between the building components (its materials and geometry) and the

local climate. Once building construction ends, a building becomes a part of its environment, and is exposed to the effects of the sun, wind, and rain. If a building is designed with these different environmental conditions in mind, it may take advantage of available solar or wind energy or avoid its negative impact. This has the potential to reduce energy loads, leading to reduced carbon dioxide emissions and ensuring a healthy and sustainable building.

Substantial progress has been made towards improved energy efficiency through design and technological innovations such as passive ventilation systems, daylighting and sun shading, high performance heating, cooling, and ventilation (HVAC) systems, and the introduction of novel materials to the building envelope. However, the impact and influence of the structural system on building energy efficiency has been largely neglected and therefore serves as the focus of this thesis. We consider whether structural and energy performance considerations can be integrated and optimized concurrently. And we analyze tradeoffs in the design of structural systems for both structural and energy performance.

In his book *The Green Skyscraper* [1], architect Ken Yeang suggests that in different climate zones, the structural core (structural wall) should be arranged in different locations to reduce the yearly energy consumption of the building. Furthermore, he argues the shape of the building footprint should be modified based on the climate zone in which the building is to be constructed. In Yeang's analysis, three parameters are varied - the shape of the building footprint, the placement of the structural core or walls, and the orientation of the building. The first two (which we

define as **building morphology**) of these parameters have clear implications for structural performance since buildings with asymmetric distribution of stiffness are known to be susceptible to damaging torsional modes of vibration when subjected to wind or earthquake loading. However, Yeang does not address the implications of different footprints and core placements on structural performance. As for the third parameter, building orientation has much less effect on the structural performance unless the building is located where wind direction is strongly biased.

This study begins with an investigation of the relationship between structural form and environmental performance, which use Yeang's proposals as an approach to limit the variables in this investigation. Four buildings are modeled in Ecotect Analysis 2011 corresponding to four major climate zones. Each building's thermal properties are assigned according to International Energy Conservation Code 2009 (IECC) [6]. These four building configurations are examined under equivalent opaque surfaces in their envelopes. The output for energy performance is presented in terms of annual heating and cooling loads (Mwh/year). The results suggest that building morphology has a significant effect on the annual energy consumption in a high-rise office building.

Second, the structural performance of the four study models is analyzed: 1) hand calculations so preliminary estimating of the stiffnesses for the base structural system (BSS) are made, and also based on the directional method [7]. We were able to make preliminary findings for what height BSS can meet the serviceability requirement (according to the ASCE 7-10 for loading and lateral displacement limit); 2) structural analysis and design by using SAP2000 (ASCE 7-10 is used to estimate wind loads). For a

set of given building conditions (loading and height, etc.), the results demonstrate that supplementary lateral load resistance system (SLLR) is needed. An outrigger system is used as the RLLS for the four buildings in this study. The output (under serviceability control) is represented in terms of additional structural material needed for RLLS to supplement the BSS in order to meet the specification.

Third, a cost analysis of these systems is conducted. The unit cost of a kilowatt-hour based on the Energy Information Administration database (EIA), while the material cost (material used in BSS and RLLS) have been estimated by using Reed Construction data (RC means). The outputs (total operational and material cost for a building life span of 50 years) show that buildings with asymmetric distribution of stiffness are the most costly, in terms of both energy expenditures and additional material costs.

Fourth, the sensitivity of energy demand to two parameters of passive design related to building layout and site are examined. The key parameters are building footprint aspect ratio and building orientation, both of which are considered important factors in passive design. Four high-rise office buildings (glazed curtain wall) with four different aspect ratios (1:1, 1:2, 1:3, and 1:4) are thermally analyzed in four climate zones: cool, temperate, arid, and tropical. Each building's thermal properties are assigned according to 2009 IECC code. Energy demand is calculated for each model with respect to two opposing orientations. The outcome shows that for buildings in Cool, Arid, and Temperate climate zones, the energy demand may be considered marginally sensitive to changes in aspect ratio, while in the Tropical climate zone, changes in aspect ratio do not significantly affect energy demand. Moreover, the energy demand of high-

rise office buildings is not sensitive to the passive solar gain as long as the exterior envelopes are built to IECC 2009 requirements for thermal performance.

In the following chapters, the details of these four studies are presented. Chapter 2 provides a literature review of existing scholarship in this area as well as a thorough explanation of Yeang's proposal. Chapter 3 presents background about thermal properties, referring to the green building, and mentioning about the lateral resistance systems for tall buildings. Chapter 4 focuses on the energy analysis and the preliminary structural calculations. Chapter 5 frames the structural modeling, analysis and design using SAP2000. Chapter 6 focuses on the cost calculation (operational, embodied energy and material costs). Chapter 7 addresses the sensitivity of energy demand to two parameters of passive design related to building layout and site. Finally, chapter 8 illustrates our conclusions, recommendations, and future work.

CHAPTER 2

LITERATURE REVIEW

The design of high performance buildings is becoming increasingly urgent, and efforts are being made by engineers and architects to reduce the environmental impact of buildings to conserve resources and secure our energy future. In the present study, we consider the building morphology and its influence on energy and structural performance. However, there is a lack of research to support a correlation between energy performance and structural performance.

In his book *The Green Skyscraper* [1], architect Ken Yeang suggests that building morphology, i.e. aspect ratio, the shape of the building footprint, orientation, and placement of structural vertical core/walls can be designed to maximize passive-mode systems. For Yeang, there is an ideal aspect ratio for each different climate zone, which is presented in Table 2.1. He states that for the four major climate zones, the long axis of the footprint should be oriented east-west except in a cool climate. The rationale is to control the amount of exposed area to the sunlight for each individual side of the building.

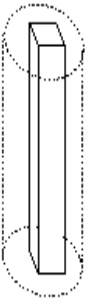


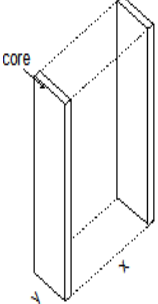
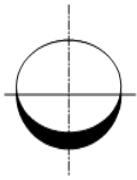
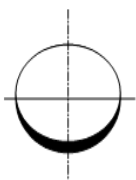
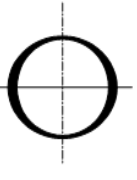
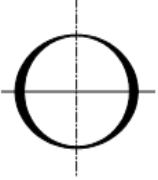
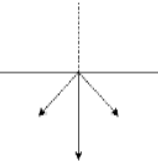

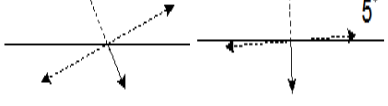
Building orientation is another critical aspect of passive design. The goal is to orient the building in accordance to sun path and wind direction. Orientation helps to increase or decrease the heat gained from the sun by either maximizing or minimizing the amount of time that the building is exposed to direct sunlight. Yeang provides an example for a building located in the tropical climate zone: to reduce insolation (i.e. direct solar heat gain), the short axis of the building footprint should be on the north-

south axis and the building oriented with 5° north of east. Also, he suggests that for each one of the major climate zones there is a critical angle of orientation for passive design, see Table 2.1.

The third aspect of passive design in Yeang's book is the placement of structural vertical cores. Choosing the ideal position of the structural vertical cores with regard to the climate zones may help to modulate building interior temperatures. In principle, heavy and opaque structural cores provide shade and thermal mass to the building, potentially helping to keep it cool or to restrict heat penetration in the building. Thus, one would place the vertical cores to avoid or accommodate direct solar gain according to a climate zone. Yeang suggests that in a cool climate where solar gain can help to offset heating energy costs, it is optimal that the structural core is placed in the center of the building where it cannot block any of the sun's direct rays. In a temperate zone the structural core is placed on the north face, in a tropical zone cores are placed on both east and west sides and in an arid zone cores cover 50% of east and west sides, see Table 2.1.

To reduce energy consumption using passive methods in high-rise structures, Yeang provides a set of directives: for each one of the major climate zones, the structural walls should be arranged in different locations and the shape and the orientation of the building should be modulated to reflect the unique demands of the climate [1]. Walker [8] shows that simple shaped houses are typically more efficient to cool and heat than houses with irregular shapes (Table 2.2).

Table 2.1 Yeang's passive design strategies with respect to building morphology [1]

Climate passive methods	Cool	Temperate	Arid	Tropical
Vertical core corresponding to the sun path				
				
Aspect ratio Y:X	1:1	1:1.6	1:2	1:3
Orientation				

A simple shape house has a smaller surface area and consequently less exposure surface to the impact of the ambient weather change, resulting in less heat loss in the winter and less heat gain in the summer. It also demands less construction materials and erection. Moreover, he recommended that in hot and humid climates the building

shape should be designed to minimize solar heat gain to reduce cooling demand. Furthermore, multi-story homes are generally more efficient because they have less exposure area to the sunlight compared to same size single-story houses. Moreover, building elongated in an east-west direction could greatly affect the overall energy efficiency (Table 2.2).

Cheung et al. [9] published a study in 2004 that describes an investigation of the effects of six passive design strategies (insulation, thermal mass, glazing type, window size, color of external wall and external shading devices) on the annual cooling energy for a high-rise apartment building in Hong Kong. This study shows that a reduction in energy consumption for cooling load of 31.4% can be obtained, as a result of modifying building envelope to match the local climate. However, this achievement is specific to this building type and this particular climate.

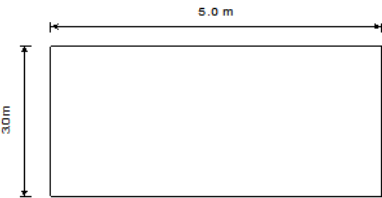
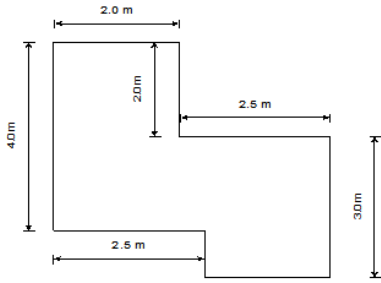
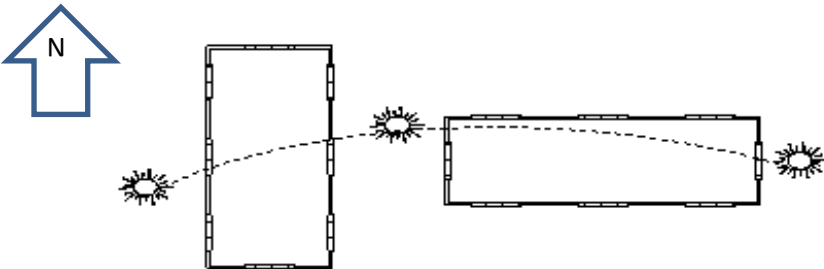
Jones et al. [10] widely studied passive solar design and the balancing between the energy conservation and the solar energy strategies to save in the cost of annual energy demand with respect to the climates. Furthermore, he developed a method for the optimum mix of energy conservation and solar energy. He emphasized that the designer decision should always involve the “trade-off between the cost of the improvement versus the increased performance.”[10] He recommended that energy conservation is more appropriate and less solar where cooling is significantly demanded. Also, he recommended that the features of passive solar heating can increase cooling loads in summer time, therefore shading tactics to reduce this effect should be considered. Mazria [11] provided a complete guide to passive solar home, greenhouse

and building design, which illustrates many different applications of direct heat gain concepts for both commercial and residential buildings. In terms of building shape he recommended that for all climates the sufficient building elongated is in an east-west direction, which results in more exposed surface area facing south, minimizing heating needed in winter and cooling in summer. Also he emphasized that in the case of climates where heating is needed in winter, place the building on the site that receives the most sun during the hours of maximum solar radiation 9:0 am to 3:0 pm “to insure that-the, outdoor areas and gardens placed to the south will have adequate winter sun, and help minimize the possibility of shading the building in the future by off-site developments” [11].

A number of studies have focused on natural ventilation design strategies to reduce energy loads. Chow [12] shows that a structural wall projecting from the building façade could guide prevailing winds to drive passive ventilation of a tall building. Li and Mak [13] used simulation to evaluate the performance of wind catcher devices designed for passive ventilation. Mak, C.M., et al. [14] investigated the effect of wing walls on passive ventilation and found potential synergies between the structure and environmental performance.

Finally, the structural engineering profession has been attempting to define the proper role for the structural engineer in the pursuit of sustainability of the built environment. Anderson & Silman [15] and Webster [16] identify how the structural engineer may work with an integrated design team of architects, engineers, builders and owners to make the structure sustainable.

Table 2.2 Energy efficient building shape [8]

Item	Model 1	Model 2
shape	 <p>Simple shape</p>	 <p>Irregular shape</p>
size	150 m ²	150 m ²
Exterior walls area (4m height)	64 m ²	76 m ²
Orientation	 <p>Lesser energy efficient higher energy efficient</p>	

The Structural Engineering Institute of the American Society of Civil Engineers recently published *Sustainability Guidelines for the Structural Engineer* [17], which emphasizes material selection and life cycle cost analysis as the basis for structural sustainability.

Managing material resources is another crucial factor in reducing total life-cycle energy, as material usage has a significant impact on embodied energy. Lee, B. et al. [18] illustrate that the embodied energy for industrial buildings made of the concrete is significantly more than those made of the steel or even hybrid structures. Australia's

guide to environmentally sustainable homes [19] and TecEco sustainable technologies [20], show that the concrete in its basic form has relatively low embodied energy, but its high usage in construction results in higher total embodied energy than any other material. According to the American Institute of Architects Sustainable Design Resource Guide, 90% of 1.0 MJ/kg embodied energy of concrete of compressive strength 17.5 MPa is attributable to the production of Portland cement. Ashley, E. and Lemay, L. [21] show that the embodied energy of virgin imported structural steel is 35.0 MJ/kg, while recycled steel has an embodied energy of 10.1 MJ/kg. In his study Ken Yeang [1] illustrates that the amount of embodied energy of concrete-frame structure is almost the same as that from the steel structure, but the concrete structure is less recyclable at the end of its useful life than the steel structure.

However, these publications promise to significantly affect the way structural engineering is practiced, yet none the above studies directly address the interplay of structural form and energy efficiency, which is our primary interest.

CHAPTER 3

BACKGROUND

3.1 Thermal mass

Thermal mass may be defined as the building's materials ability to store heat, i.e. its thermal storage capacity, for extended periods. A material with good thermal mass will absorb heat from an available source like sunlight during the daytime or from the heating system in the building, store it, and release it when the sun sets and air temperature drops or the other source turns off. The main characteristic of a material's thermal mass is its density and specific heat; the capacity to retain heat varies for different materials. The material that has higher density and specific heat capacity has a higher thermal mass, which can be calculated as following [22].

$$\text{Thermal Mass} = M \times C_p \times \Delta T \dots \dots \dots (3.1)$$

Where M is the mass of substance, ΔT change in temperature, and C_p is the specific heat of substance.

3.2 Thermal mass properties

Materials with high density typically have a higher thermal mass; for example normal weight concrete has higher thermal mass than light weight concrete, mod brick has low thermal mass, and insulation materials have almost no thermal mass. A good thermal mass material with high density characteristics also has to be conductive. However, if conductivity is too high (e.g. steel) energy is absorbed and given off too quickly, compromising its ability to be a heat sink for thermal storage.

3.3 Thermal mass in Buildings

There are some known thermal mass materials built-up in building elements such as water, soil, rock, concrete, brick, cement, and ceramic tile. These represent the bulk of building construction materials. In buildings with mechanical heating, ventilation, and air conditioning (HVAC) systems, the presence of a thermal mass material may affect the heating and cooling loads because it can lead to raised or lowered temperatures inside the building. Thermal mass within the insulated building envelope may also help to reduce fluctuations and dampen extremes in temperature inside the building [23].

In ancient times people built their shelters against earth berms and hillsides to take advantage of the earth as a thermal mass to protect them from the heat during the day and cold at night. During the day, building surfaces (walls and roof) that are exposed to direct sunlight must have the capacity to absorb solar energy and by the night they radiate this energy out as heat. The thermal mass absorbs thermal energy passively during the day and releases this stored energy at night. In these kinds of buildings, maintaining thermal comfort for occupants inside buildings depends largely upon the thermal mass of the walls and roofs. In climates with low heating energy demands such as the temperate-arid zone of Upper Egypt [24], using materials with high thermal storage capacity in their construction helps to modulate interior temperatures (see Figure 3.1).

Today, thermal mass is usually used in conjunction with passive design techniques [25]. Indeed, thermal mass may help to mitigate operational energy loads

and is most appropriate where there is a big difference between day and night outdoor temperatures. However, in the winter time thermal mass sometimes might not be efficient, becomes buildings often use mechanical heating systems, and the thermal mass might absorb some heat produced from heating system [23].

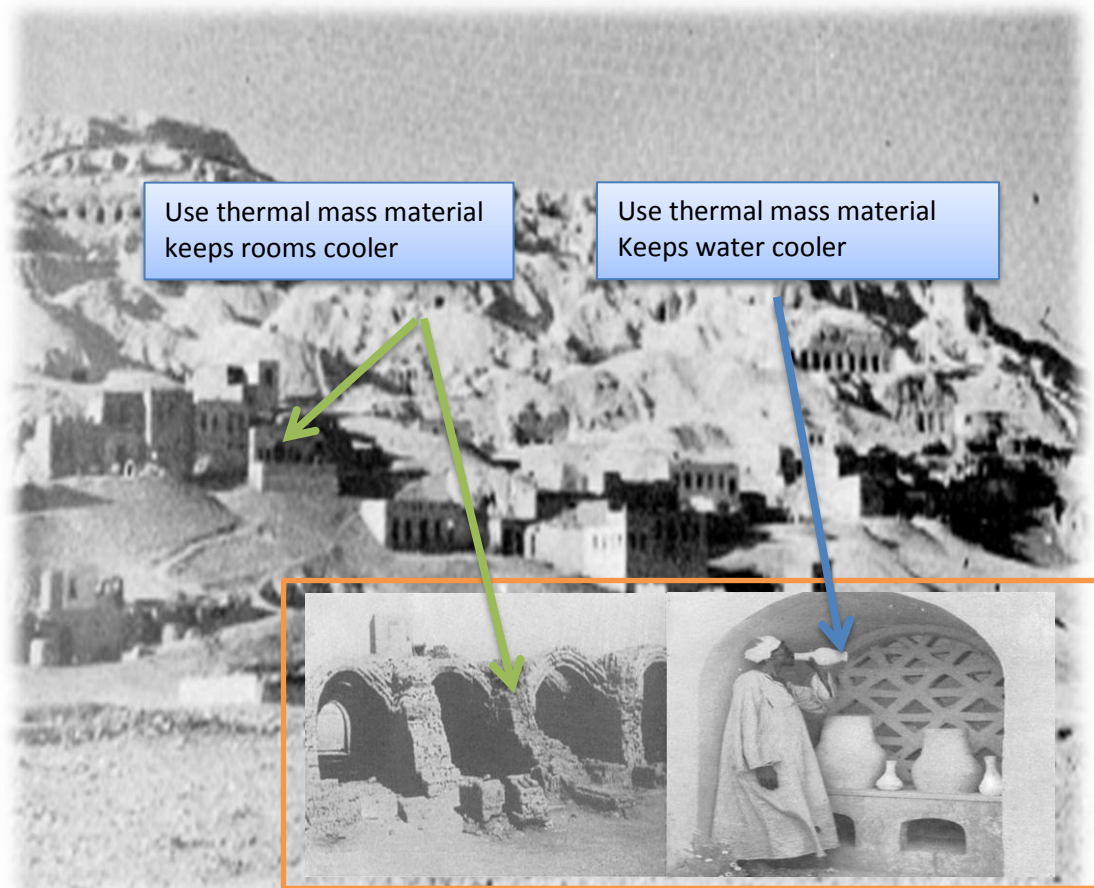


Figure 3.1 Thermal mass material use in construction in Upper Egypt [24]

Figure 3.2 shows how the heat is gained by allowing sunlight and is stored in the thermal mass during the day and released in the night time which leads to warming the room. This is a desired solution if nighttime heating is desired. On the other hand, in the summer, if nighttime heating is not desirable, then strategies to cool the thermal mass have to be implemented. One solution is to allow for air cooling, that is, convective

currents to pass over the thermal mass to draw out the stored energy resulting comfortable atmosphere inside the building[25].

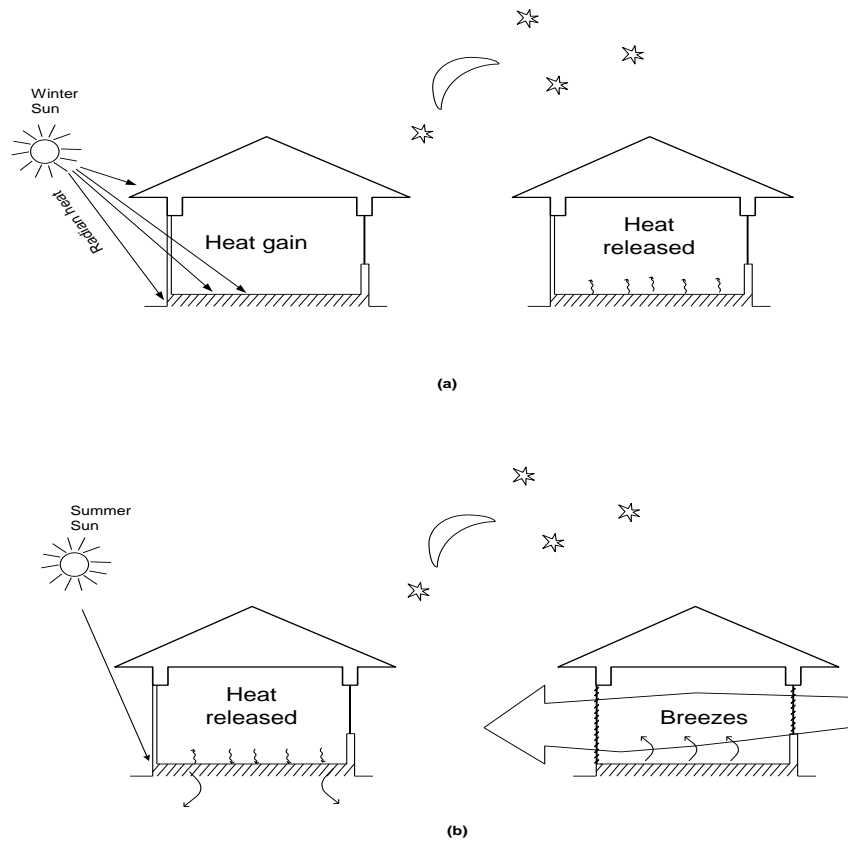


Figure 3.2 Heat gains through the thermal mass material: (a) Heat gain in winter; (b) Heat dispose in summer “after [25]”

Thermal mass in a building envelope slows down heat flow through the walls, roof, and floor, potentially allowing a reduction in insulation requirements. Buildings constructed with materials that have high thermal mass like concrete could have a unique energy saving advantage because of their inherent thermal mass. These materials absorb energy slowly and hold it for much longer periods of time, and then release it as heat energy.

3.4 Thermal transmission through building

Most of the common building materials that are used in contemporary construction absorb and transfer heat. The total amount of heat transferred through the building elements can be determined by calculating the resistance to heat transfer (R-value) of each material in the building assembly [26].

3.4.1 Heat transfer

Heat transfer is flow of heat energy from a high temperature body to a lower temperature body, which is fundamental to the second law of thermodynamics. There are three primary mechanisms of heat transfer: conduction, convection, and radiation (see Figure 3.3). Conduction is defined as the transfer of heat energy from the higher temperature to lower temperature particles that are in contact. This mode of heat transfer occurs in a stationary material (solid bodies and non-movable fluids), conductive heat transfer is given by:

$$Q_k = k A \frac{\partial T}{\partial x} \dots \dots \dots (3.2)$$

Where Q_k is the rate of heat flux by conduction (Watts), k is the thermal conductivity (W/m k), A is the surface area (m^2), $\partial T/\partial x$ change of temperature with respect to x which is wall thickness (k/m). Heat transfer by convection is a combination of conduction and fluid motion, where convection occurs wherever a surface is in contact with a fluid at a temperature that is different from its own. Convective heat transfer is given by:

$$Q_c = h A(\Delta T) \dots \dots \dots (3.3)$$

Where Q_c is the rate of heat flux by convection (Watts), h is the heat transfer coefficient ($W/m^2 k$), ΔT is the difference in the surface temperature ($T_{surface}$ and $T_{ambient}$) (k). Heat transfer by radiation occurs by electromagnetic waves that are emitted from a hot body towards cold body (such as heat transferred from the sun to the earth). Radiation heat transfer is given by:

$$Q_R = A \sigma (T_{surface}^4 - T_{ambient}^4) \dots \dots (3.4)$$

Where Q_R is the heat flux by radiation, σ is the Stefan- Boltzmann constant ($W/m^2 k^4$).

Transmission of heat through a wall can be summarized as: Heat transfer by convection Q_c and radiation Q_R from the hot air (air film) surrounding the external wall surface. Then heat transfer by conduction Q_k through the wall. Once the heat reaches the internal surface, it is transferring again by convection Q_{Ri} and radiation Q_{Ci} from the wall surface to the cold air and surrounding surfaces inside the room. Where the rate of heat transfer mainly depends on the wall thermal resistance property, which is R-value ($R= 1/U$) the resistance to heat flow, is equal to the inverse of thermal conductance (U-value) which may be defined as the amount of heat flow of through a material. Note, high R-Value materials could be used as insulation materials.

3.4.2 Office building heat gain

Heat gain is the thermal energy that a room may gain from external and internal sources. External sources of heat gain are heat transferred to indoors due to the difference between outside and inside temperature. This gain occurs through the building envelope walls, ceiling, windows, ventilation systems, and air leakage. Internal

sources of heat gain are the heat generated by occupants, the heat produced by lighting, and the heat resulting from the equipment (Figure 3.4) [26].

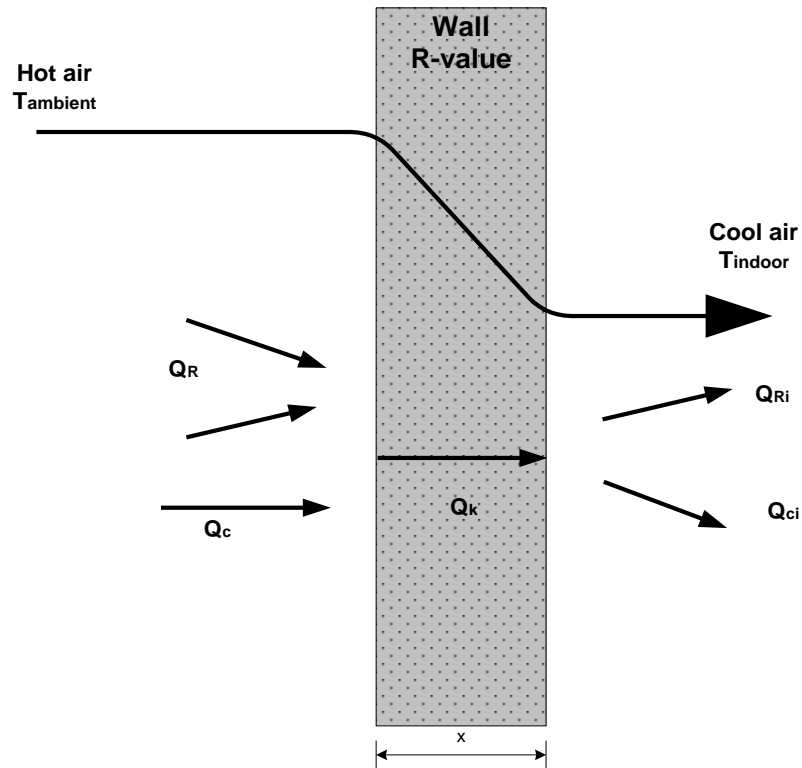


Figure 3.3 Heat transfer through a wall “after [27]”

Daytime heat flow through an exterior wall is due to solar radiation on exterior surface and the outside ambient temperature. Nighttime heat gain through a wall is typically a result of thermal lag effects, as a result of thermal mass heat storage. A wall of high thermal capacity may considerably dampen the inside temperature swings, when ambient temperature fluctuates, whereas, a wall of low thermal capacity has little damping effect; thus any variations in outside temperature will almost immediately affect the inside temperature.

Heat gain through glass windows may occur in two ways [26] a) Sensible transmission through glass (caused by the difference between inside and outside temperatures), b) Solar gain through the glass. This gain depends on building orientation as sun-path and location of windows on a building greatly influence the extent of direct solar heat gain through glazed surfaces. Solar heat gain can mainly be controlled by the solar heat gain coefficient of the glass (SHGC) [6].

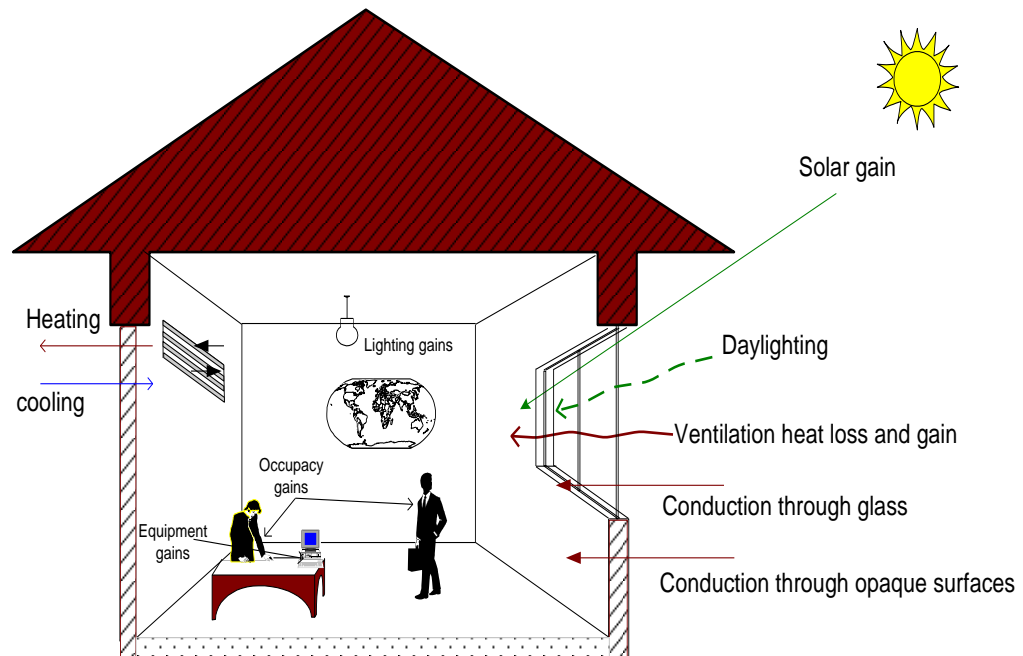


Figure 3.4 Heat gain/loss through an office building components “after [27]”

Heat transfer through unintended air exchange is a result of infiltration or exfiltration. Infiltration occurs through the small cracks and improper seals on windows and doors. The allowable infiltration rate is 0.5 air change per hour for most air-

conditioning cases [28] and may be less (0.25 air change per hour) in case of high performance buildings or if special measures have been taken to prevent infiltration.

The heat gain as a result of occupants in a building is a combination of sensible and latent heat. Sensible heat gains from occupants results from the difference between the human body temperature and the temperature of the air inside the room. Latent heat is characterized by an increase in the moisture content of the air, which can be attributed to occupant respiration. Heat gain by the occupants depends on the number of people in the room and the rate of heat released by each person, which depends on the degree of activity. Heat gain from lighting depends on light equipment efficiency and lighting level. Heat gain from equipment depends on number of machines and their efficiency [26, 28].

3.5 Design and analysis of tall building

During the design and construction process, structural engineers and architectural designers work together on the building design and on the elements of construction such as the location of partitions, stairs and elevators, positioning of columns and lateral resistance systems, as well as choice of materials. The structural engineer calculates the gravity loads and identifies the forces which will be generated on the building due to wind and earthquake loads.

The challenge for structural engineers is to design a lateral resistance system that fulfills the requirements of architectural design. This task starts with estimating the lateral loads and identifying the full extent of possible deformations that can be

produced by the horizontal loads. The engineer performs analytical studies to obtain a series of strengths and deformation to determine the structural system components.

3.5.1 Structural lateral load systems

Lateral resistance systems have evolved for both steel and concrete. Figure 3.5 and Figure 3.6, respectively, show various lateral resistance systems that are grouped into specific categories, each with an applicable height range [29]. In this study we will use the outrigger systems, so we will discuss briefly the behavior of this system under the wind load, in the following section.

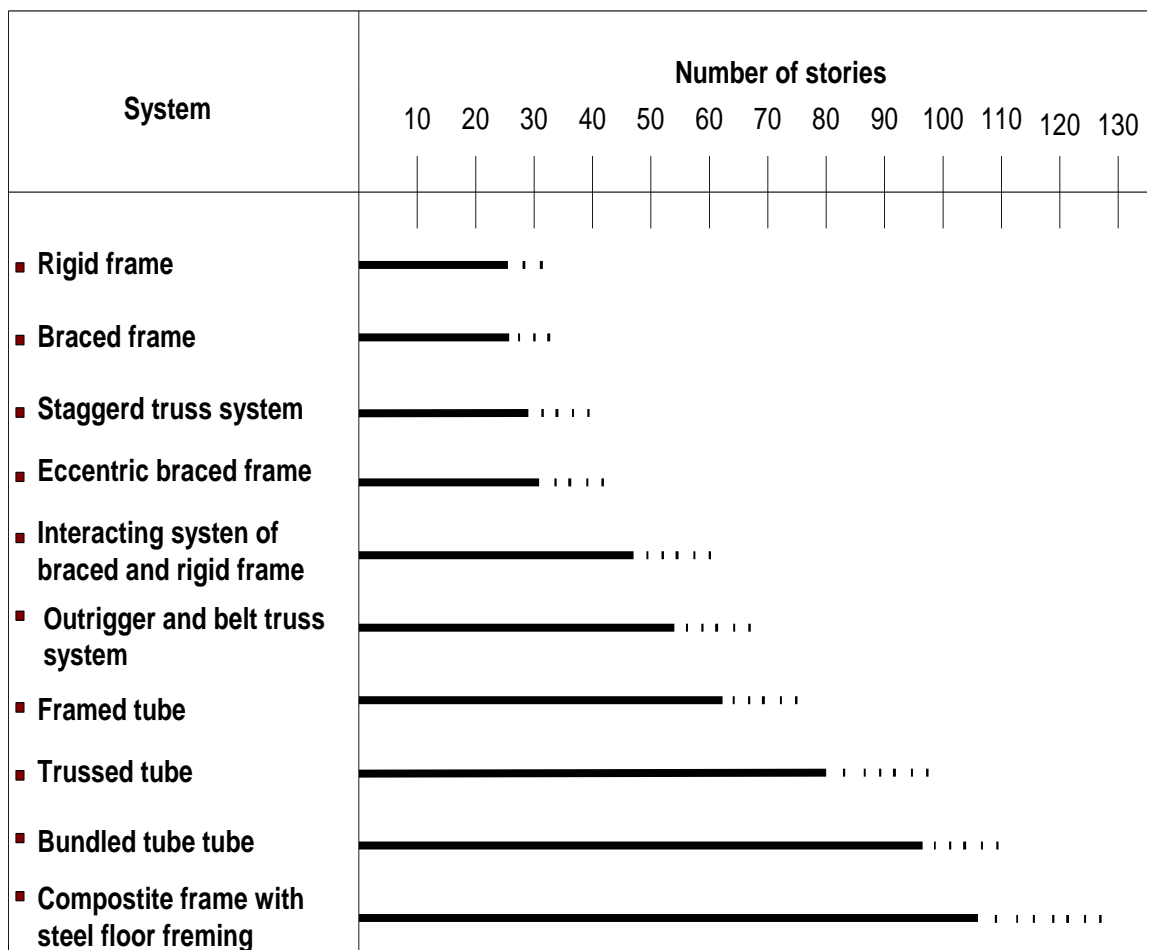


Figure 3.5 Height comparison of steel building systems [29]

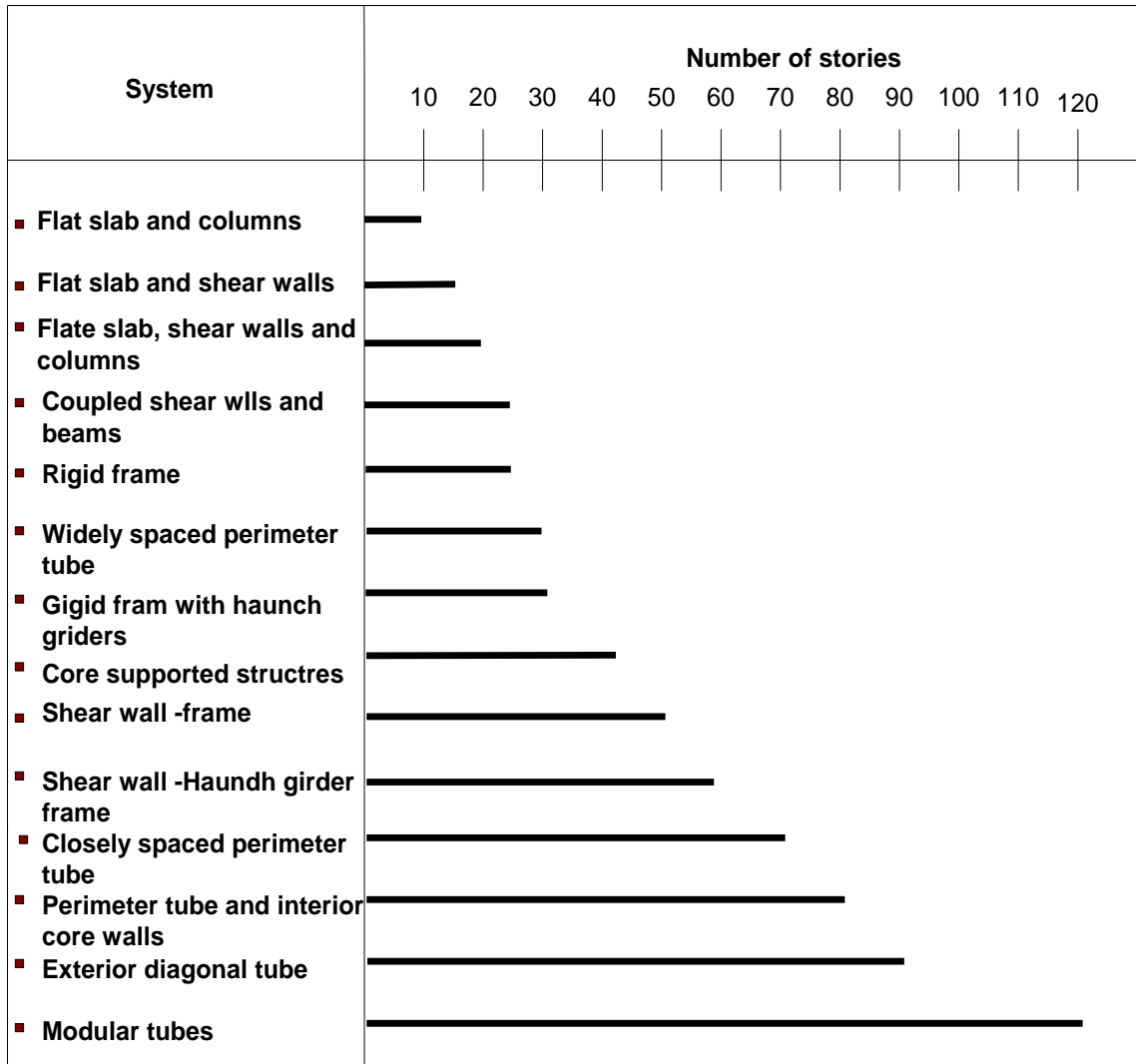


Figure 3.6 Height comparison of concrete building systems [29]

3.5.2 Outrigger-Braced Structures

The main information summarized from the book written by Bungale S. Trananath [29] (*Wind and Earthquake Resistant Buildings: Structural Analysis and design*). The outrigger system is a central core made of braced frames or shear walls, with trussing or gardening horizontal cantilever “outrigger” connecting the core to the outer columns. Joining the columns to the core by those outriggers makes the structure behave as partly composite cantilever. The outrigger systems may be formed in any combination

of steel, concrete, or composite construction [30, 29]. Under lateral loading, the outriggers restrain the core against overturning through tension in the windward columns and compression in the leeward columns (Figure 3.7). Outrigger-braced structures have been used in building up to 70 stories [29].

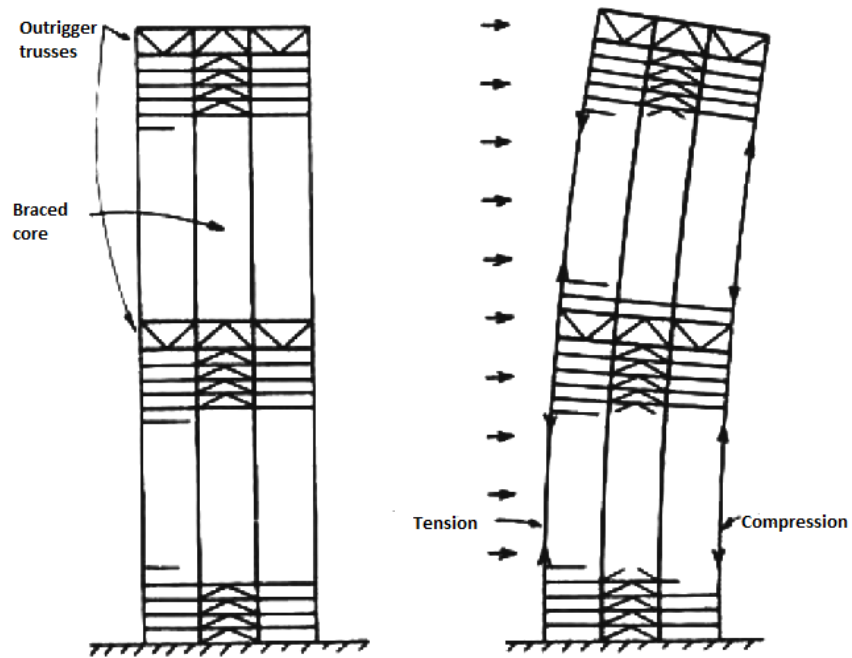


Figure 3.7 Outrigger-Braced Structures [30]

3.5.2.1 Outrigger systems behavior

As we mentioned the core is connected to the edge columns by relatively stiff horizontal members (the outrigger). These outriggers may be located with extending on both sides; it could also be located on one side of the building with outriggers extending to the building columns on one side (Figure. 3.8) [29, 30]. When subjected to lateral loads, the basic structural response is: the column-restrained outriggers resist the

rotation of the core, resulting in smaller lateral deflections and moments in the core. The external moment is now resisted by the axial tension and compression of the exterior columns connected to the outriggers, not only by the bending of the core. As a result, the effective depth of the structure is increased when it flexes as a vertical cantilever, “by the development of tension in the windward columns, and by compression in the leeward columns” [29].

To assist in restraining the outriggers one usually uses other peripheral columns, which can be done by attaching a deep spandrel girder, or a truss “belt truss,” [29], around the structure at the levels of the outriggers. One or two stories usually comprise the depth of the outriggers and belt truss [30].

To simplify the outrigger system behavior, consider a building stiffened by a story high outrigger at the top, as shown in Figure 3.9. The restraining action produced by the cap truss generates a restoring couple at the building top, resulting in a point of contra flexure in its deflection curve. Thus, the bending moment in the core is reduced by this reversal in curvature. The tension and compression forces work as a couple to produce rotation opposite to the rotation produced by the core. Therefore, the outrigger at the top may be considered a restraining spring located at the free end [16].

With the assumption that the cap truss is rigid, “the axial elongation and shortening of columns is equal to the rotation of the core multiplied by their respective distances from the center of the core” [29]. Considering the distance of the equivalent column is $d/2$ from the center of the core, the axial deformation of the columns would be then equal to $(\theta \times d/2)$, where θ is the core rotation.

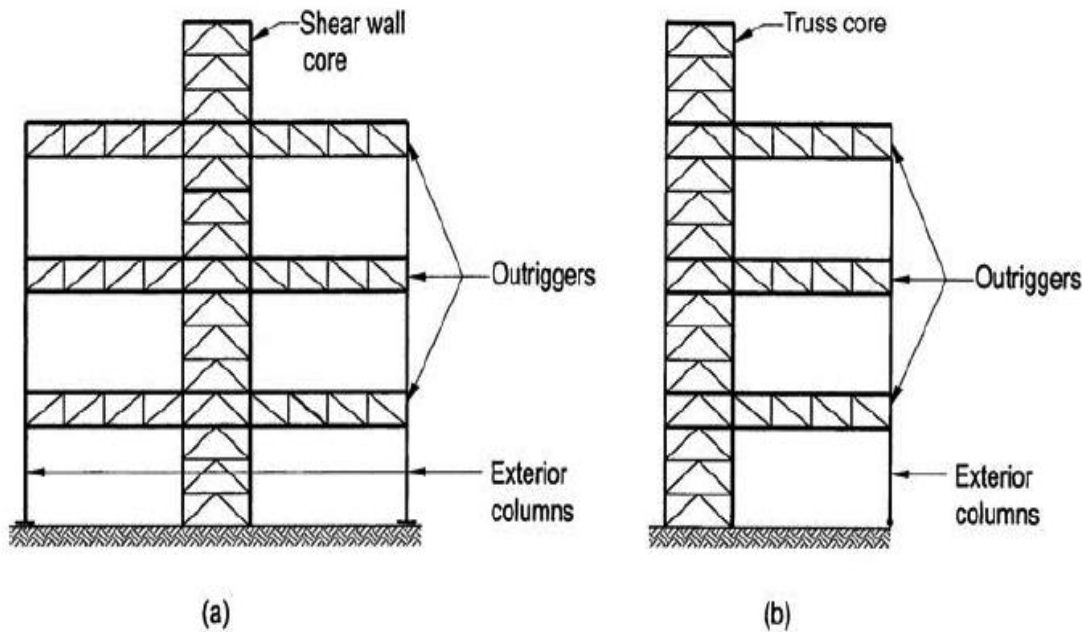


Figure 3.8 a) outrigger system with a central core: (b) outrigger system with offset core[29]

With the equivalent spring stiffness being calculated for unit rotation of the core, the axial deformation of the equivalent columns is equal to $d/2$ units. The corresponding axial load P in the columns is as following:

$$P = \frac{AE d}{2L} \dots \dots \dots (3.1)$$

where A is the area of columns; E is the modulus of elasticity; d is the distance between the exterior columns; L is the building height (Figure. 3.10). The rotational stiffness of the outrigger at the top is given by the axial load in the equivalent columns multiplied by their distance from the center of the core.

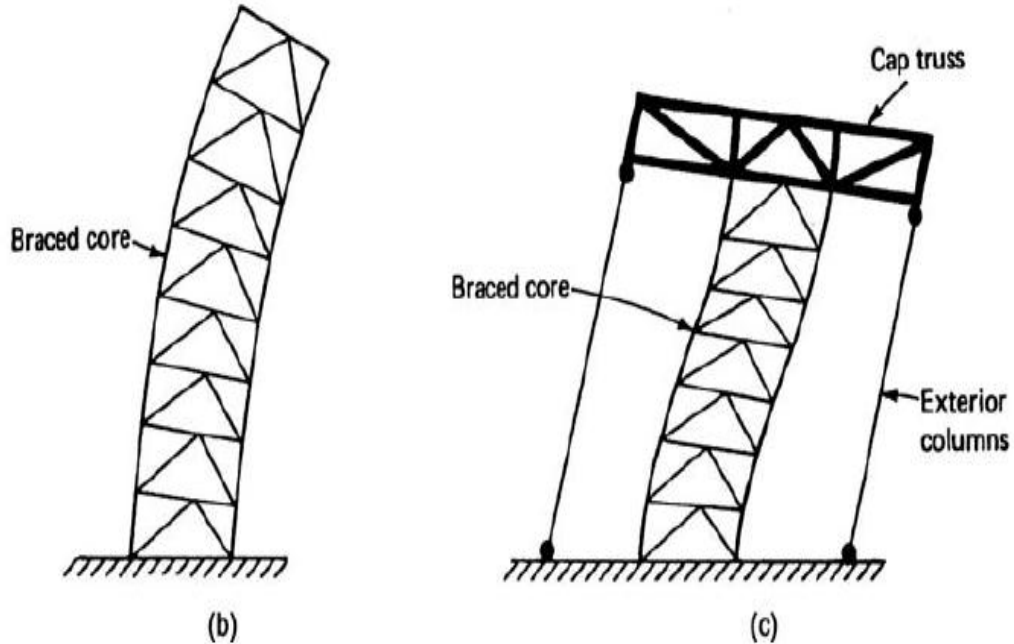


Figure 3.9 (b) cantilever bending of core; (c) tie-down action of cap truss [29]

The rotational stiffness (K) for the two equivalent columns is located at a distance $d/2$ from the core.

$$K = \frac{P \times d}{2} \times 2 = Pd \dots \dots \dots (3.2)$$

To calculate the lateral deflection, the rotation compatibility condition at $z = L$ can be written as:

$$\theta_w - \theta_s = \theta_L \dots \dots \dots (3.3)$$

where θ_w is the rotation of the cantilever at $z = L$ due to a uniform lateral load W , in radians; θ_s is the rotation due to spring stiffness is in a direction opposite to the rotation due to external load, located at $z = L$, in radians; θ_L is the final rotation of the cantilever at $z = L$, in radians. For a cantilever with uniform moment of inertia I and modulus of elasticity E subjected to uniform load W .

$$\theta_w = \frac{WL^2}{6EI} \dots \dots \dots (3.4)$$

If M_1 and K_1 represent the moment and stiffness of the spring located at $z=L$, then Eq.

(3.3) can be rewritten as

$$\frac{WL^2}{6EI} - \frac{M_1L}{EI} = \frac{M_1}{K_1} \dots \dots \dots (3.5)$$

$$M_1 = \frac{\left(\frac{WL^2}{6EI}\right)}{\left(\frac{1}{K_1} - \frac{L}{EI}\right)} \dots \dots \dots (3.6)$$

The resulting deflection Δ_1 at the building top can be obtained by superimposing the deflection of the cantilever due to external uniform load W , and the deflection due to the moment induced by the spring, thus:

$$\Delta_1 = \Delta_{load} - \Delta_{spring} \dots \dots \dots (3.7)$$

$$= \frac{WL^4}{8EI} - \frac{M_1L^2}{2EI} \dots \dots \dots (3.8)$$

$$= \frac{L^2}{2EI} \left(\frac{WL^2}{4} - M_1 \right) \dots \dots \dots (3.9)$$

With the same concept and based on the expression for lateral deflection y , at distance x measured from the top and is equal to $(L - z)$; where for a cantilever subjected to a uniform lateral load ((Figure. 3.10) is given by:

$$y = \frac{W}{24EI} (x^2 - 4L^3x + 3L^4) \dots \dots \dots (3.10)$$

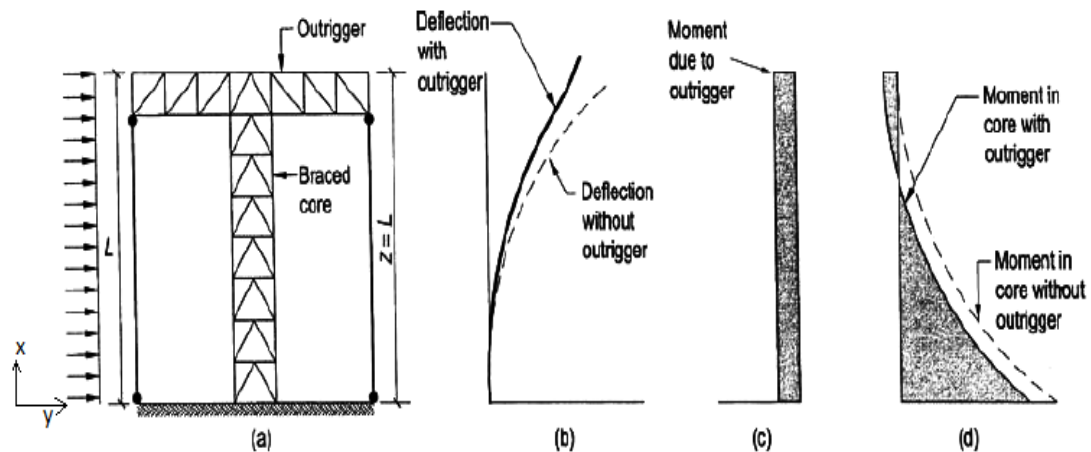


Figure 3.10 One outrigger at top, $z = L$ [29]

Thus, if M_2 , M_3 , and M_4 are the moments of the spring corresponding to different heights, we can calculate the lateral deflation at any height, so, lateral deflation at $z = 3L/4$, $z = L/2$, and $z = L/4$ are:

$$\Delta_{3L/4} = \frac{WL^4}{8EI} - \frac{M_2 3L}{4EI} \left(L - \frac{3L}{8} \right) \dots\dots (3.11)$$

$$\Delta_{L/2} = \frac{WL^4}{8EI} - \frac{M_3 3L}{2EI} \left(L - \frac{L}{4} \right) \dots\dots (3.12)$$

$$\Delta_{L/4} = \frac{WL^4}{8EI} - \frac{M_4 3L}{4EI} \left(L - \frac{L}{8} \right) \dots\dots (3.13)$$

3.5.2.2 Optimum Locations of Outrigger Trusses

It's been recommended that the optimum level of the outriggers for minimizing the drift for a single outrigger is at approximately mid-height (Figure. 3.11). A two-outrigger system would have one placed at 1/3 and the other placed at 2/3 of the building height [30]. For a three-outrigger system, they should be at the 1/4, 1/2, and 3/4 heights, and so on. Therefore, for the optimum performance of an n -outrigger

structure, the outriggers should be placed at $1/n + 1$, $2/n + 1$, $3/n + 1$, $4/n + 1 \dots n/n + 1$ height locations [29].

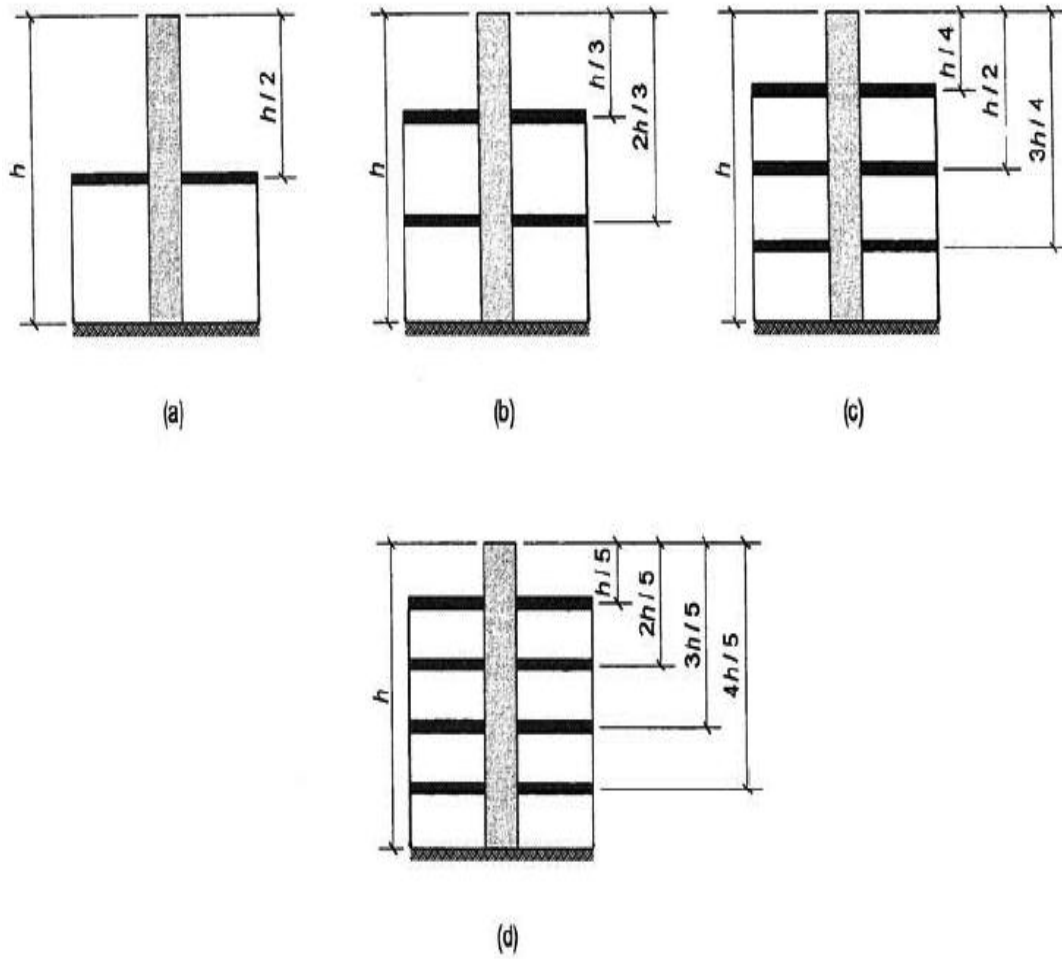


Figure 3.11 Optimum locations of outriggers: (a) single outrigger; (b) two outriggers; (c) three outriggers; (d) four outriggers[29]

CHAPTER 4

INVESTIGATING THE EFFECT OF BUILDING MORPHOLOGY AND CORE PLACEMENT ON ENERGY PERFORMANCE OF SKYSCRAPER OFFICE BUILDINGS

4.1 An approach

In his book *The Green Skyscraper* [1], architect Kenneth Yeang suggests that in different climate zones the structural core should be arranged in different locations to reduce the yearly energy consumption of the building. He also argues the shape of the building footprint should be modified based on the climate zone in which the building is to be constructed (Figure 4.1). In Yeang's analysis, three parameters are varied - the shape of the building floor plan, the placement of the structural cores/walls, and the orientation of the building. The first two of these parameters have clear implications for the structural performance, while building orientation has much less effect on the structural performance unless the building is located where wind direction is strongly biased.

In the present work, we consider two parameters, the shape of the building footprint and the placement of the structural cores (structural walls, to evaluate the structural and energy performance of four different building morphologies in four different climate zones. We then present the results of structural and energy consumption calculations for each of the sixteen morphology/climate scenarios.

In this study, as in Yeang's, two main characteristics are modulated to optimize energy performance: the position of the vertical structural core/walls and the aspect ratio and shape of the building footprint.

4.1.1 Description of building models variables

All other morphological descriptors such as the square footage, number of stories, building height, occupancy, schedules, and envelope materials, for the four skyscraper office buildings are constant. All buildings modeled in this study are 200 m in height, 50 stories that are 4.0 m floor to floor height, with a total conditioned floor area of 135000 m². Figure 4.2 shows the plan views for these models, and the locations of the primary mass (opaque surfaces) and the glazing walls (transparent surfaces) for each configuration. The primary material for the structural core/wall (opaque walls) is reinforced normal weight concrete, and the glazed (curtain) walls are two layers of standard glass with 10 % metal framing.

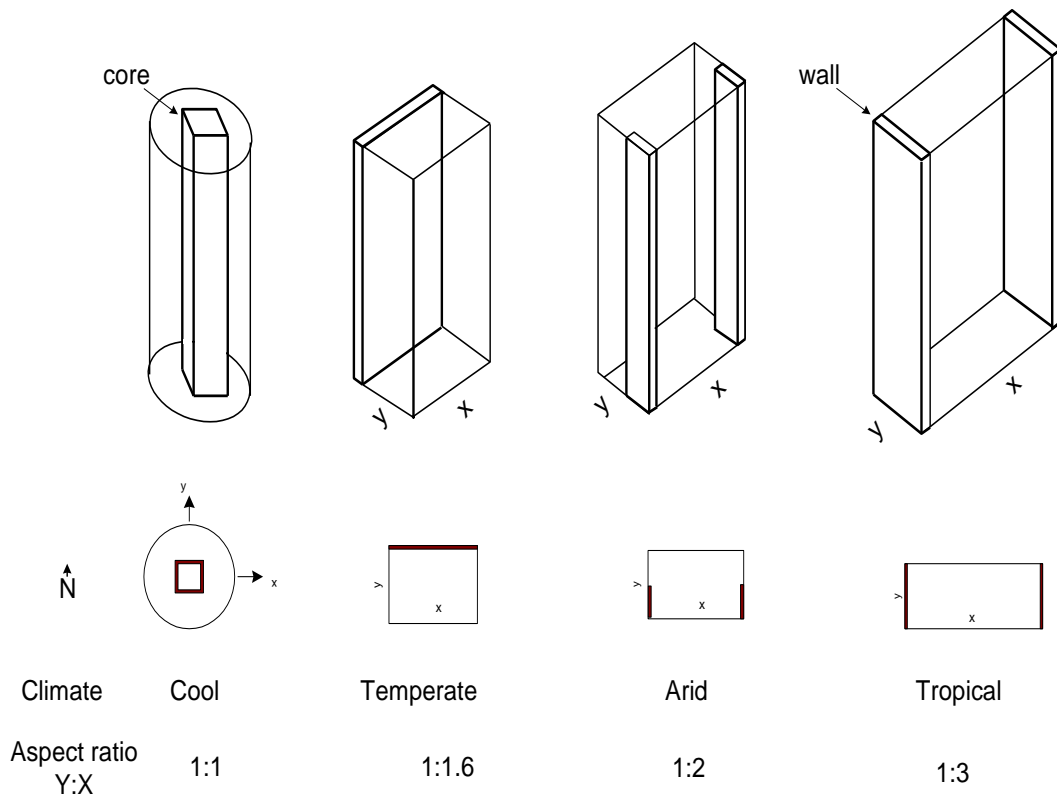


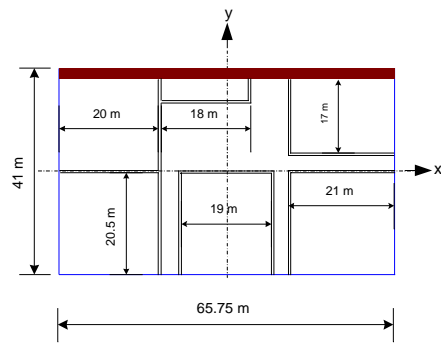
Figure 4.1 Proposal by K. Yeang for optimal floor-plan and placement of structural cores to minimize building energy consumption in four climates [1]

To simplify the analysis, we have neglected the effect of surrounding buildings and of building orientation, in essence assuming that the buildings are erected on flat open ground and are aligned with the cardinal directions.

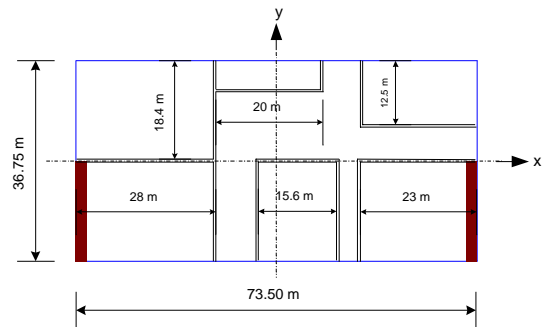
The materials selected for the exterior envelope of all four models meet the requirements of thermal resistance of the 2009 International Energy Conservation Code, IECC [6], for each specific climate zone. There are three different material palettes (with associated thermal resistances) for the four buildings. In other words, there is a prescribed material palette for the buildings in the tropical zone 1, for buildings in the temperate zone and arid zones (both zone 3), and for buildings in cool zone 5. Structural layers and thermal resistance of the material are presented in Table 4.1.

All four building morphologies are simulated in each of the four major climate zones (cool, temperate, arid, and tropical, according to the Koppen classification [31]). Additionally, we have selected specific cities as representative of the conditions in each climate zone, and use the climatic conditions at these four cities in the energy performance simulations: Boston, Massachusetts for the cool zone, Sacramento, California for the temperate zone, Las Vegas, Nevada for the arid zone, and Honolulu, Hawaii for the tropical zone. The climate characteristics for the representative cities are provided in Table 4.2 [32].

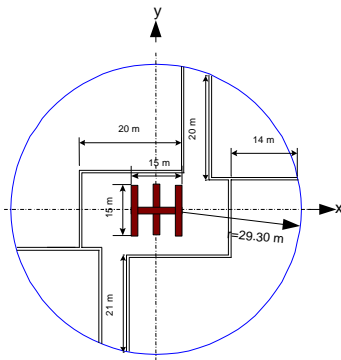
Building energy consumption is highly dependent on occupancy and scheduled usage of the interior space. Since our goal is to isolate the influence of building morphology on energy consumption, we assume that occupancy and scheduling characteristics are constant across all climate zones and building types.



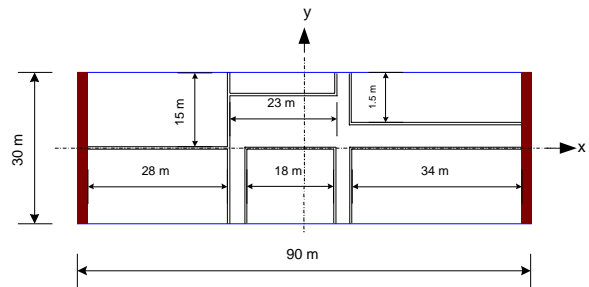
Plan view -Edge configuration
 [31% opaque ; 69% glazed curtain walls]



Plan view -Half Sides configuration
 [17% opaque ; 83% glazed curtain walls]



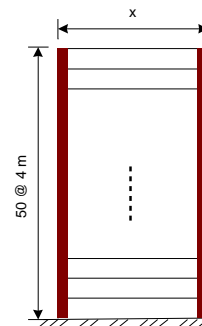
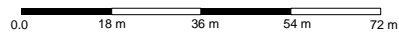
Plan view -Central configuration
 [100% glazed curtain walls]



Plan view -Sides configuration
 [25% opaque ; 75% glazed curtain walls]

- Core/walls: opaque surfaces
- Non-core: glazed curtain walls
- Partitions

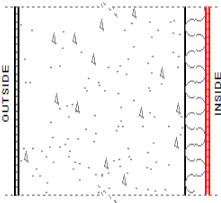
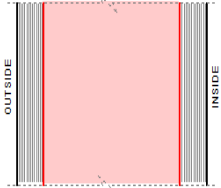
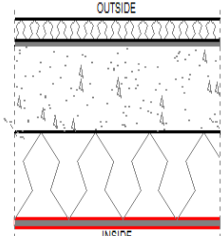
Note: - Percentages given are only for the building envelope.



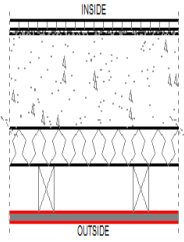
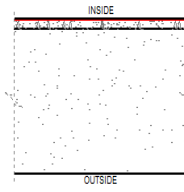
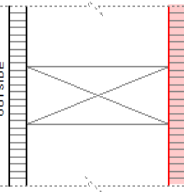
Elevation

Figure 4.2 Plan views and an elevation of the buildings

Table 4.1 Structural layers and thermal resistance of the materials

Element	Material			Layers	Zone 1 (Tropical)		Zone 3 (Arid & Temperate)		Zone 5 (Cool)	
	Zone 1 (Tropical)	Zone 3 (Arid & Temperate)	Zone 5 (Cool)		U-value W/m ² K	R-value m ² K/W	U-value W/m ² K	R-value m ² K/W	U-value W/m ² K	R-value m ² K/W
Cores walls	*450 mm concrete III	450mm concrete III 22 mm polystyrene foam 10 mm plaster in either side	450 mm concrete III 45 mm polystyrene foam 10 mm plaster in either side		1.65	0.61	0.74	1.36	0.49	2.05
Glazing walls	*6 mm single glazed metal framing	6 mm double glazed metal framing, 15 mm gap with low-conductance gas fill	6 mm double glazed metal framing, 13 mm gap with low-conductance gas fill		6.81	0.15	3.40	0.294	9.3	0.107
Roof	27 mm Aggregate 6 mm asphalt 100 mm concrete III 19 mm poly. foam 10 mm plaster	27 mm Aggregate 6 mm asphalt 100 mm concrete III 27 mm poly. foam 10 mm plaster	27 mm Aggregate 6 mm asphalt 100 mm concrete III 27 mm poly. foam 10 mm plaster		0.37	2.71	0.267	3.75	0.267	3.75

(Continue)

Element	Material			Layers	Zone 1 (Tropical)		Zone 3 (Arid & Temperate)		Zone 5 (Cool)	
	Zone 1 (Tropical)	Zone 3 (Arid & Temperate)	Zone 5 (Cool)		U-value W/m ² K	R-value m ² K/W	U-value W/m ² K	R-value m ² K/W	U-value W/m ² K	R-value m ² K/W
Floor suspended concrete	10 mm ceramic tiles 5 mm screed 100 mm suspended concrete floor 50 mm air gap 10 mm plaster ceiling underneath	10 mm ceramic tiles 5 mm screed 100 mm suspended concrete floor 20 mm polystyrene 50 mm air gap. 10 mm plaster ceiling underneath	10 mm ceramic tiles 5 mm screed 100 mm suspended concrete floor 40 mm polystyrene 50 mm air gap. 10 mm plaster ceiling underneath		1.81	0.55	0.86	1.17	0.27	3.75
Slab on ground	100mm concrete 5 mm screed 10 mm ceramic tiles	100mm concrete 5 mm screed 10 mm ceramic tiles	100mm concrete 5 mm screed 10 mm ceramic tiles		0.88	1.14	0.88	1.14	0.88	1.14
Partition	80mm framed wall as air gap 10mm plaster board either side	80mm framed wall as air gap 10mm plaster board either side	80mm framed wall as air gap 10mm plaster board either side		2.21	0.45	2.21	0.45	0.21	0.45

* The element would consist of some layers only that shown in the layers column

Specifically, we treat the thermostat range, internal design conditions, occupancy, infiltration rate, and hours of operation as fixed control variables (Table 4.3).

4.1.2 The thermal analysis

For the remainder of this dissertation, the proposed configurations are named depending on where the structural cores/walls are placed (opaque walls): Central for cool zone; Edge for temperate zone; Half Sides for the arid zone; Sides for the tropical zone.

4.1.3 The modeling

Autodesk's Ecotect energy simulation package was used for the thermal analysis. Ecotect 2011 is a comprehensive concept-to-detail sustainable building design. It is a popular program used by architects, its modeling procedure is simple, it is easy to rapidly manipulate the properties of models, and it consumes a reasonable amount of analysis time for large models. The Ecotect procedure starts with creating a three dimensional shell that represents the building form. This can be done in one of two ways: (1) draw plans representing the boundary of the rooms, continuing room by room to form a 3D model; or (2) import the model as gbXML file from a different 3D modeling program such as Revit. For this analysis, we prepared the building's geometry in Revit 2010, and then imported the 3D model as surfaces and rooms to Ecotect 2011. After the import, thermal properties are assigned to the building's envelope and the analysis proceeds. The basic material of an element (concrete wall, slab, glazing wall, etc.) is

assigned then the resistance (R-value) of the insulation is applied, according to specifications of IECC code as presented in Table 1.

Table 4.2 Description of the climate zones characteristics for the representative cities

City Characteristics		Boston [Cool]	Sacramento [Temperate]	Las Vegas [Arid]	Honolulu [Tropical]
		Average temperatures	high	23.3 °C	24 - 32 °C
	low	-1.5 °C	7.7- 16 °C	21-26 °C	19-24 °C
Dry bulb temperature	maximum	37.2°C [on Jul 9]	42.0°C [on Jun 14]	44.4°C [on Jul 4]	33.3°C [on Sep 2]
	minimum	-20.0°C [on Jan 23]	-2.0°C [on Feb 2]	-3.3°C [on Feb 16]	13.3°C [on Feb 12]
Annual degree-days [18°C baseline]	cooling	490	670	1904	2524
	heating	3120	1436	1234	0.0
Average daytime		11 hr, 45 min	12 hr, 24 min	11 hr, 15 min	12 hr
Average nighttime		12 hr, 15 min	11 hr, 36 min	12 hr, 45 min	12 hr
Average annual rainfall		1,080 mm plus 1,060 mm of snowfall	545 mm	110 mm	460 mm
Maximum wind speed		21.6 m/s [on Sep 6]	17.0 m/s [on Mar 4]	20.6 m/s [on Apr 12]	13.4 m/s [on Nov 15]

Table 4.3 Thermal analysis conditions

Parameters		Values	Description
Active system		Full Air conditioning	Active system for providing heating and/or cooling
Thermostat range		18 – 26 °C	comfortable range
Occupancy	People	12 m ² /p	office - typical square area for one person
	Activity	70 W/p	sedentary
Internal design conditions	clothing	1 clo/p	light business suit
	Humidity	60%	comfortable Humidity
	Air speed	0.5 m/s	pleasant breeze
	lighting level	300 lux	luminous flux per unit area
Infiltration rate	Air change rate	0.5 /hr	office - typical value
Internal heat gain		10 W/ m ²	lighting and equipment
Hours of operation		Schedule	8 am-18 pm (week)

The next step is to assign a weather file which corresponds to the climatic zones selected for this study and to provide occupancy and scheduled usage data. And finally, the program can calculate monthly and annual heating and cooling loads according to given climate conditions, (Figure 4.4).

4.1.4 Modeling assumptions

For the purpose of the present analysis, several assumptions are made: a) all the buildings have equivalent square footage, height, material usage, and thermal properties; b) all the buildings are oriented 90° with the north; c) to simplify the

analysis, the circular shape of Central configuration has been replaced by dodecagon (12-sided) shape with equivalent floor area as shown in Figure 4.3.

Ecotect calculate the heating and cooling loads based on the admittance procedure, which assume that the fluctuations between the external and internal loads can be presented by the sum of the steady-state component. This method is insensitive to the rapid change in neither temperature nor long-term heat storage. However, this method has no restrictions on the number of thermal zones or building geometry [26].

The analysis based on the local (outside and inside) mean and the fluctuations in the temperature around this mean, when outside temperature or solar load change the internal air temperature fluctuate in a similar way. “The steady-state component is calculated using a three-node model incorporating an environmental temperature node to which all zone surfaces are connected by a combined radiant and convective conductance” [33].

4.1.5 The analysis

The thermal analysis involves examining each of the four models (Central, Edge, Half Sides, and Sides) in each of the four climatic zones (cool, temperate, arid, and tropical). This constitutes sixteen different simulation runs, each of which requires approximately twenty-four hours to complete. For each climate zone, weather data (TMY files) for each city is loaded and the four models are tested under equal thermal conditions [6]. That is, the only differences among the four runs in the same climate zone are the aspect ratio and the placements of the structural core/walls. Ecotect calculates the effect of solar insolation on the heating/cooling loads of each building.

Different climate zones have different effects; for example in the tropical zone, the heating demand is negligible (effectively zero) throughout the year (see Table 4.2), and cooling loads dominate. It would follow, therefore, that in order to reduce cooling loads in the tropical zone, direct heat gain as a result of solar insolation must be minimized. In this case Yeang suggests shading the building in east and west sides. Figure 4.5 shows the sun-path diagram and how the building is shaded by its side walls (location at 12:15 pm, 20th August, Honolulu, Hawaii-USA).

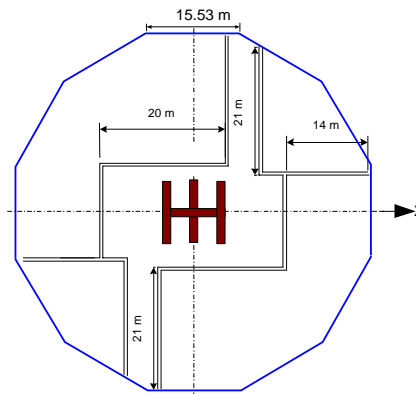


Figure 4.3 Plan view of dodecagon shape- equivalent to the Central configuration

4.1.6 Thermal analysis results

The thermal analysis results are presented in two sections. The first section demonstrates the results graphically, in four Figures (Figures 4.6 - 4.9). Each Figure represents the monthly cooling and heating loads for each of the four configurations per climatic zone. The second section is a tabulated view of annual energy use for heating and cooling loads, energy use intensity, and the difference between Yeang's recommended configuration and the configuration that resulted in the lowest energy consumption.

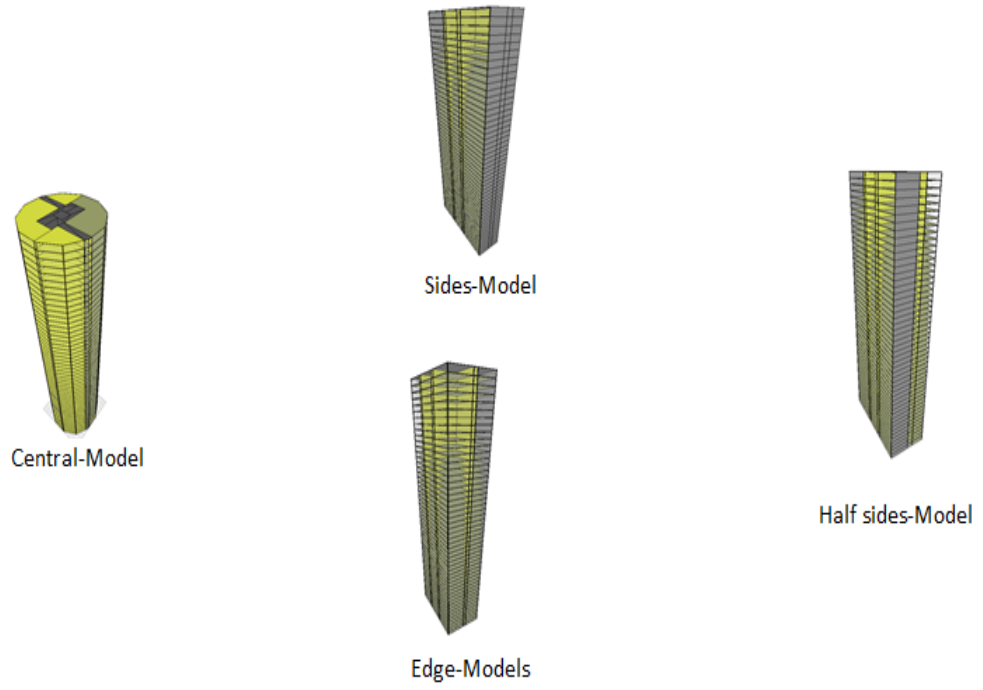


Figure 4.4 Ecotect 3D models

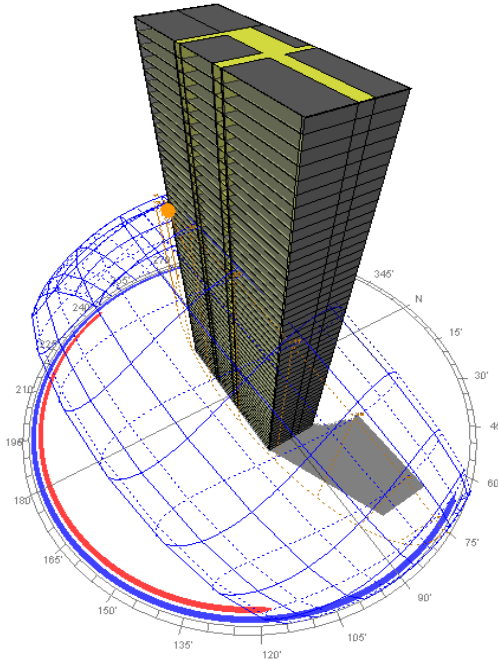


Figure 4.5 Sun-path diagram – building's walls shadow

Figure 4.6 shows the result of the thermal analysis of the four models in an arid climate (Las Vegas, NV). Generally, for all configurations the heating load is highest during the winter months (December and January). The heating demand decreases gradually thereafter until April, when the building switches to cooling mode. The maximum cooling demand occurs during the months of July and August. For this climate, the annual demand for cooling is significantly higher (approximately seven times) than heating, which is reasonable for a desert climate. Notably, the Central configuration building has the highest cooling load compared to the other models. The side configuration demands the least energy, while the Edge model ranks second and the Half Sides ranks third.

Figure 4.7 presents the thermal analysis results for a cool climate zone (Boston, MA). In general, the loads are dominated by heating demand for most of the year, which is typical for this climate. For cooling load, the comparative differences among all four models are small and confined mostly to the month of August. The demand of annual total energy is the lowest in the Sides model; the Central model has the highest energy profile; while the other two models (Edge, Half Sides) are somewhere between.

Figure 4.8 illustrates the thermal analysis in a temperate climate (Sacramento, CA). Monthly energy load simulates the seasonal changes in temperature, precipitation, and solar insolation. Moreover, in a temperate climate, the need for energy is greatest during seven months of the year. Four months (June through September) are dominated by cooling loads, which are approximately twice what is required for heating during the other three months (December through February). The results demonstrate that the

annual energy consumption is the lowest in the Sides model. The second rank is the Edge model (which was recommended by Yeang for this climate), the third is the Half Sides and the last is the Central model.

Figure 4.9 presents the thermal analysis for a tropical climate (Honolulu, HI). In this climate, the total energy demand is for cooling. In addition, the energy demand is highest in the summer and is greatly reduced during the winter season. Throughout the year, cooling is required. The model with the lowest energy profile is the Sides configuration, which was recommended by Yeang. This model maintains comfort with the lowest energy consumption, while Edge, Half Sides, and Central models come in second, third, and fourth, respectively.

The annual loads are presented in Table 4.1. Each row represents the results of examining each model configuration (Central, Edge, Half Sides, and Sides) in a climatic zone. The first row illustrates the thermal results in a cool climate. The annual energy loads for this climate are dominated by heating demand. This is an indication that the heating load should be viewed as a priority in optimizing energy efficiency rather than total heating and cooling demand. In this analysis, the Sides model resulted in the lowest EUI as well as heating demand. Yeang's recommended configuration is the Central model. The use of the Sides model in a cool climate might result in a reduction in energy consumption by 32% compared to Central, 16% compared to Half Sides model, and 9.5% compared to the Edge model. These differences are significant. The lowest ranking configuration – with the highest energy penalty– is Yeang's Central model.

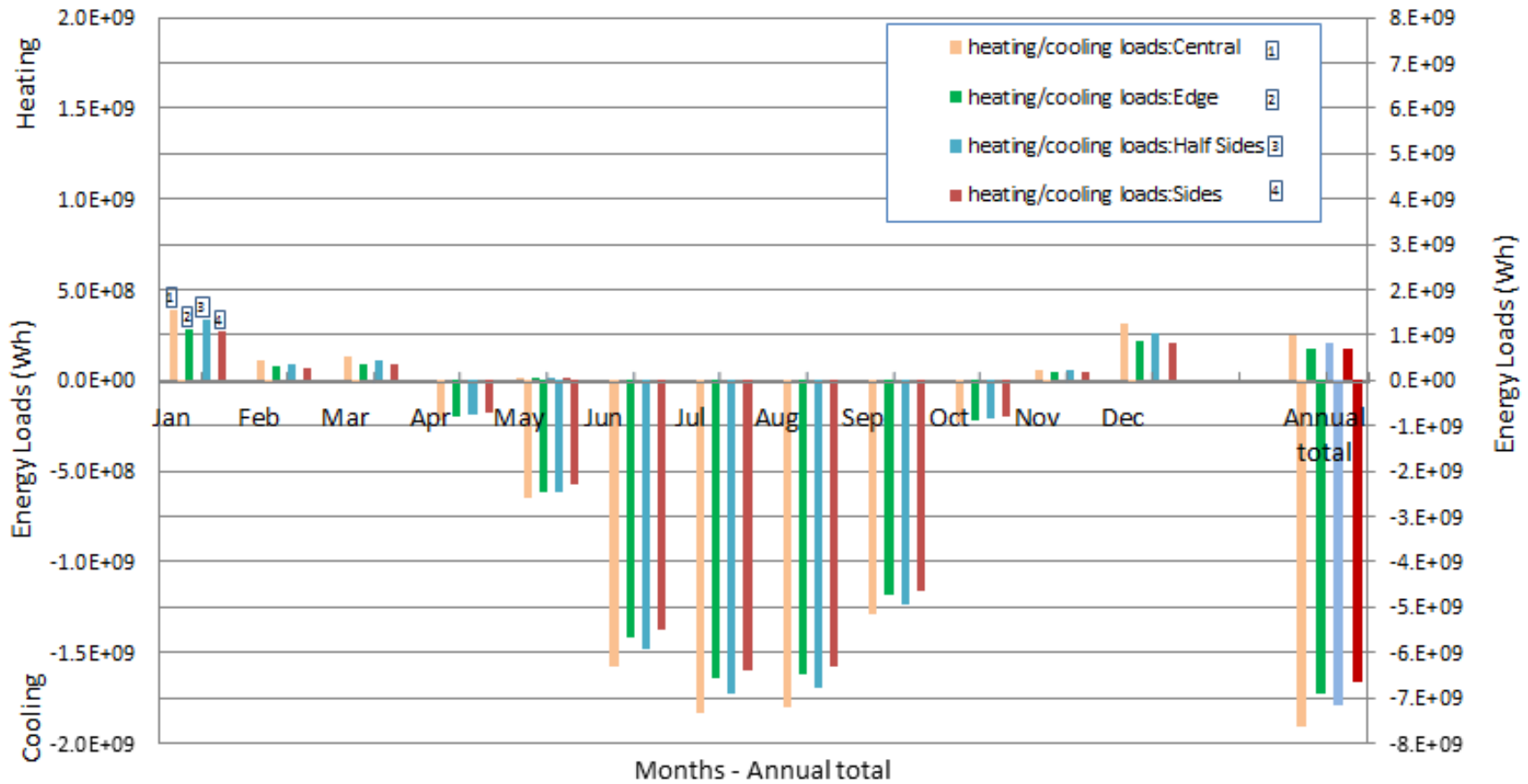


Figure 4.6 The thermal analysis result of the four models in the arid climate

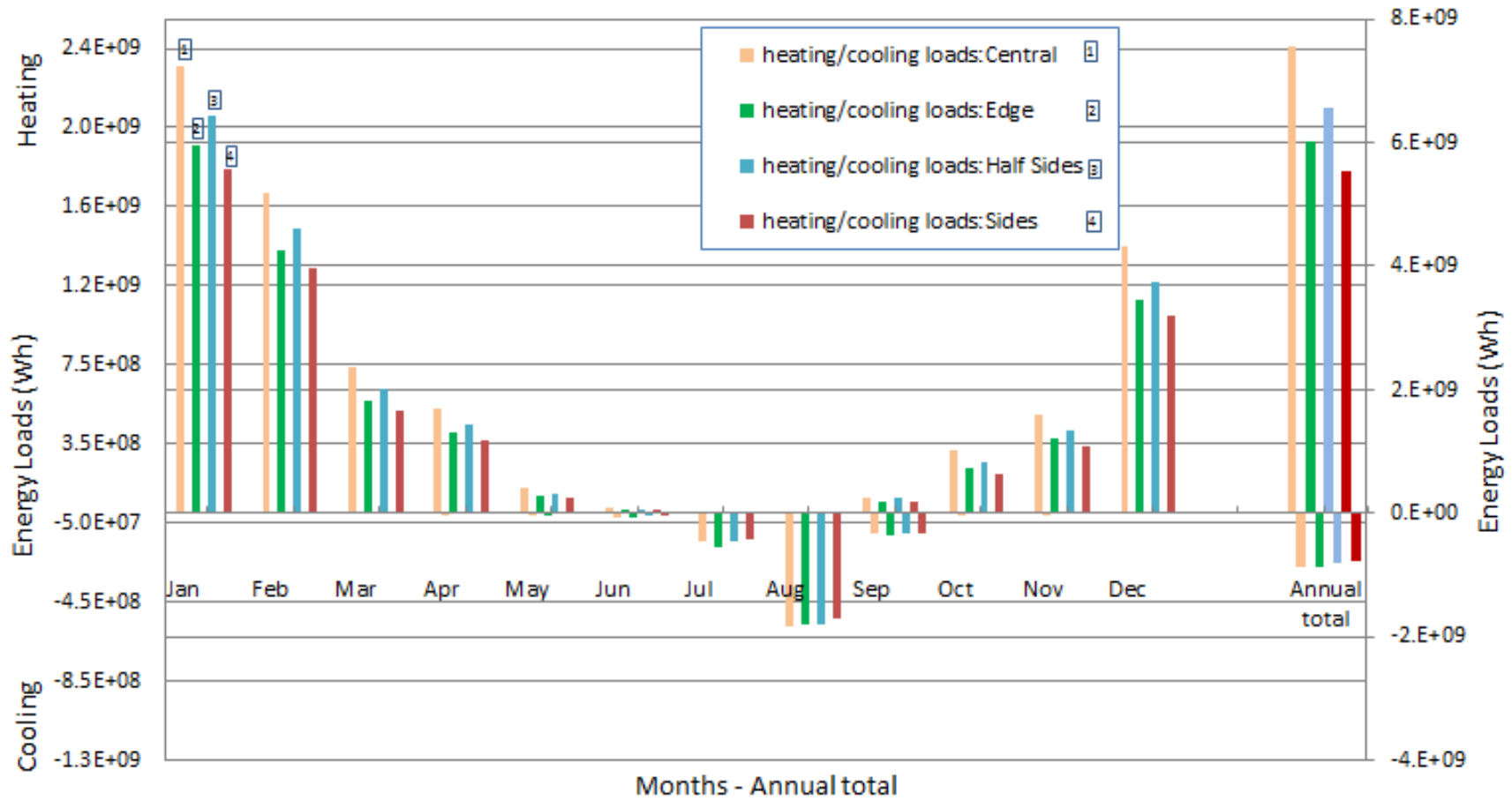


Figure 4.7 The thermal analysis result of the four models in the cool climate

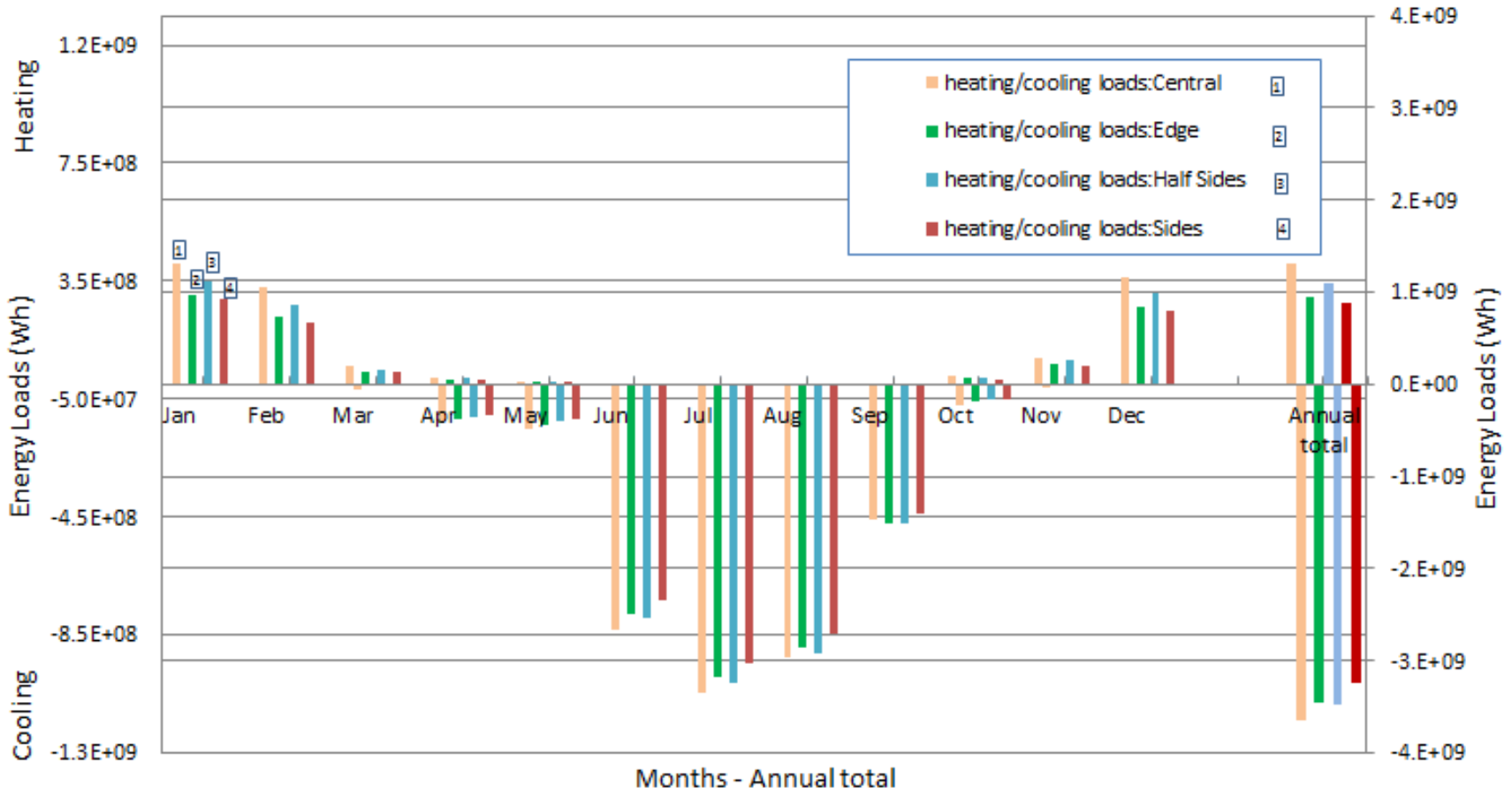


Figure 4.8 The thermal analysis result of the four models in the temperate climate

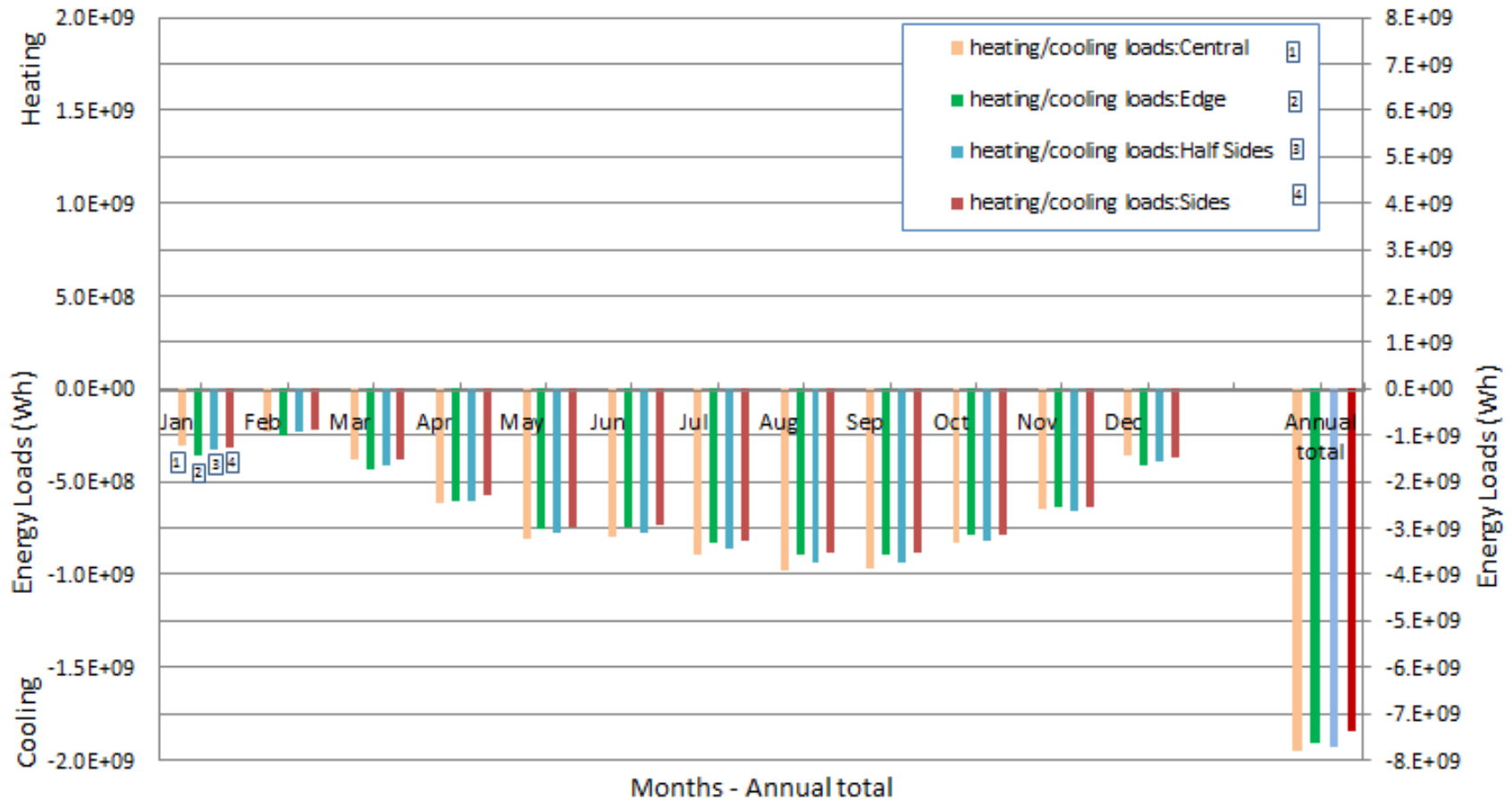


Figure 4.9 The thermal analysis result of the four models in the tropical climate

The second row illustrates the thermal results in a temperate climate. According to the data obtained from the weather file this climate is dominated by cooling loads, which represent 68% of total annual degree-days (see Table 4.2). This is consistent with the results obtained from the thermal analysis, where the cooling load averaged 76.6 % for all four building configurations. The model that consumes the least amount of cooling energy is likely the most appropriate configuration for this climate. The Sides model has the lowest cooling load by a factor of 6.0 compared with Yeang's recommended configuration (Edge), a difference that is very close to the percentage difference in annual total energy demand between the two models. The Edge model is the second ranking configuration, though the cooling load in the Half Sides model only differs by 1% compared with the Edge model (recommended configuration). The least favorable configuration is the Central model. The total energy demand of the Central model exceeds the Sides model by 20 %, the Edge model by 13%, and the Half-Side model by 8 %.

The third row represents the thermal analysis results for an arid climate. The average breakdown of cooling and heating loads are 91.6% for cooling and 8.4% for heating. Nevertheless, in all cases, the cooling load is the higher percentage of the total energy need in this climate. The cooling energy demand is the lowest in the Sides model with a difference of 7% compared to Yeang's recommendation (Half Sides), which ranked third. The difference in EUI is 3.7% between the Edge model (second option) and Half Sides model (recommended model). The least favorable configuration for this

climate is the Central model with higher energy consumption, exceeding the annual load for the Sides configuration by 17.4%.

The fourth row represents the results of the thermal analysis in a tropical climate. Based on the weather data, the annual cooling degree-days represent 100% of the total degree-days (see Table 4.2), which agrees with the results obtained from the thermal analysis. Also, the recommended model (Sides) is also the best option based on results from the thermal analysis. The differences in total energy consumption were 6% compared with the Central configuration, 5% compared with the Half Sides configuration, and 3.3% compared with the Edge configuration.

4.2 Preliminary calculation of building stiffness

Considering that the vertical core/walls are the only parts of the structural system that are found to resist the lateral loads (as in Figure 2), they were distributed in this manner in order to reduce energy consumption. We note the asymmetry in the floor plan in two configurations, the Edge and the Half Sides. Also, for the three prismatic models (Sides, Half Sides, and Edge) the walls provide the buildings with lateral resistance only in one direction; leaving the other direction too flexible against any lateral load. Beyond that, from experience we believe that these lateral resistance systems will not be sufficient for skyscrapers, and to make them adequate will require different amounts of supplementary structure, an issue we explore in subsequent chapters.

Therefore, it is obvious that additional lateral resistance systems would be needed for these buildings.

Table 4.4 Annual heating and cooling loads

Type		Central			Edge			Half Sides			Sides			Yeang's recommended configuration	% Difference [between lowest EUI and recommended]	
		Heating (Mwh)	Cooling (Mwh)	Energy Use Intensity (kwh/m ²)	Heating (Mwh)	Cooling (Mwh)	Energy Use Intensity (kwh/m ²)	Heating (Mwh)	Cooling (Mwh)	Energy Use Intensity (kwh/m ²)	Heating (Mwh)	Cooling (Mwh)	Energy Use Intensity (kwh/m ²)			
Climate	Cool	Loads	7538	875	62.3	5992	877	51.4	6553	816	54.6	5548	777	46.9	Central	32%
		Σ	8414			6869			7369			6326				
		%	89.6	10.41		87.25	12.75		88.93	11.07		87.71	12.29			
Temperate	Load	Load	1310	3646	36.7	946	3443	32.5	1103	3476	33.9	884	3248	30.6	Edge	6.0%
		Σ	4956			4389			4578			4132				
		%	26.4	73.6		21.6	78.4		24.1	75.9		21.4	78.6			
Arid	Load	Load	990	7647	63.9	696	6904	56.3	841	7167	59.3	673	6677	54.4	Half Sides	9.0%
		Σ	8637			7600			8009			7350				
		%	11.5	88.5		9.2	90.8		10.5	89.5		9.16	90.8			
Tropical	Load	Load	0.0	7824	57.9	0.0	7612	56.4	0.0	7746	57.4	0.0	7372	54.6	Sides	0%
		Σ	7824			7612			7746			7372				
		%	0.0	100		0.0	100		0.0	100		0.0	100			

% means the percentage of a load (heating or cooling) from the total load (The summation (Σ) of Heating and cooling)

In other words, the given lateral resistance systems are not realistic, and will not be adequate for these tall buildings. We investigate this in the next section.

4.2.1 Building stiffness

Considering only the vertical core/walls as the lateral load resisting system, preliminary calculations are made to investigate structural properties such lateral stiffness, torsional stiffness, and effects of wind load eccentricity. We consider here that the structural walls act as cantilevers independent of each other except for the Central model where walls compose one core.

Furthermore, the lateral stiffness is assumed to be dominated by flexural deformations, and we neglect the contribution of shear deformations on the system given the height of the models. The bending stiffness of each independent structural component i of the lateral force resisting system is proportional to the product of the elastic modulus E and the cross section moment of inertia I_i of the shear wall. We denote the stiffnesses by k_i . The total bending stiffness of the lateral force resisting system K_{core} , then, is the sum of the n individual component stiffnesses (See Table 4.5 for the coordinate system considered) and is proportional to the sum of the products EI_i :

$$K_{core} = \sum_{i=1}^n k_i \propto \sum_{i=1}^n EI_i \dots\dots\dots(4.1)$$

Where E is assumed constant for all walls; for a uniform wind load acting on a cantilever the lateral bending stiffness can be calculated as follows:

$$k = \frac{8EI}{h^4} \dots\dots\dots(4.2)$$

Where h is the height of the structural wall. The concept of torsional stiffness of thin rectangular sections, such as the shear walls in these models, is used here to calculate the torsional stiffness of the structural wall as:

$$k_t = \frac{bt^3G}{3h} \dots\dots\dots(4.3)$$

Where G is the shear modulus, b is the length of the wall, and t represents the wall thickness. A structural asymmetry in plan about the vertical axis of the building generates eccentricity of the lateral loads from the center of stiffness of the building leading to twisting in addition to translation of each floor. Here, plan eccentricity represents the horizontal distance perpendicular to each of the principal axes of the buildings determined between the position of the wind force resultant and the center of rigidity of the structural walls (see Table 5). The location of the center of rigidity from an arbitrary origin is found by using the following relationships:

$$\bar{x} = \frac{\sum_{i=1}^n k_{xi} x_i}{\sum_{i=1}^n k_{xi}} \dots\dots\dots(4.4)$$

$$\bar{y} = \frac{\sum_{i=1}^n k_{yi} y_i}{\sum_{i=1}^n k_{yi}} \dots\dots\dots(4.5)$$

Where k_{xi} and k_{yi} are the bending stiffnesses of the structural components about the x and y axes (see Table 5 for coordinate system). The existence of floor eccentricity causes uniform wind pressure to generate twist in the walls. The resulting the angle of twist is calculated as:

$$\phi = \frac{3T h}{bt^3G} \dots\dots\dots(4.6)$$

Where T is the twisting moment per unit height acting about a vertical axis of the building. This twisting moment results from the eccentricity (e), which is assumed to be the perpendicular distance between the center of pressure of the wind load P_w and the center of rigidity (c.r) of the shear walls in floor plan.

$$T = e \times P_w \dots\dots\dots(4.7)$$

4.2.4 Results

Table 5 summarizes the results of lateral stiffness calculations of the four models. The highest bending stiffness about the wall local x-axis found in the Sides model, the Central model is second and the Half Sides model third, while the Edge model is too flexible about this axis. On the other hand, the highest bending stiffness about the wall local y-axis found in the Edge model, the Central model ranked second, while the Half Sides and Sides models are too flexible about this axis. Since lateral stiffness is directly related to area moment of inertia, the same behavior as observed in cross section bending stiffness may be expected in building lateral stiffness.

The asymmetry in plan about the vertical axis of the building creates eccentricity that leads to two coupled displacement modes occurring under lateral loading (translation and rotation). This eccentricity is pronounced in two models—Edge and Half Sides models. Higher eccentricity leads to higher twisting moment and requires higher torsional stiffness. However, in the Sides and Central models the only required torsional stiffness may be to meet minimum code-prescribed requirements or to account for winds coming from an angle. Moreover, in the case of the Edge and Half Sides models the design may be substantially affected by angle of twist. Figure 4.10 shows 3D

renderings that illustrate the different deformations that building types might exhibit under wind loads, where one mode of displacement (translation) occurs in the Sides and Central models, while two modes of displacement occur simultaneously in the Half Sides and Edge models. It is clear that the form of the building and the distribution of the structural cores/walls would certainly substantially affect the building stiffness.

4.3 Summary of energy analysis and Preliminary calculation of building stiffness

Examining four different building configurations, proposed in *The Green Skyscraper* [1] for lowering the energy consumption of skyscraper in four different climate regions. By simulating each building configuration using Autodesk's Ecotect, we were able to draw two major conclusions regarding building energy consumption:

(1) The results prove Yeang's proposal that building configuration (footprint shape and the placement of structural vertical core/walls) significantly influences overall energy performance.

(2) The results demonstrated that the placement of the structural vertical core/walls in the east and west sides and with an aspect ratio of 1:3, may lead to a reduction in energy consumption of 6.0% to 32%, depending on climatic zone.

An additional based on the preliminary structural stiffness calculation. We found that for two of the proposed configurations—called Edge and Half Sides models—asymmetric distribution of the structural walls results a substantially eccentricity lead to high angle of twist due to twisting. We conclude that building configuration (footprint shape and the distribution of the structural core/wall) critically impacts the structural stiffness of a building.

Table 4.5 Lateral stiffness and torsional susceptibility of different building models

Model	K_{core}		k		k_t	T	ϕ	Floor Plan
	x -axis	y -axis	x -axis	y -axis				
Central	760E	1517E	$\frac{6080E}{h^4}$	$\frac{12136E}{h^4}$	$\frac{1.78G}{h}$	0	0	
Edge	0.5E	10659E	$\frac{4E}{h^4}$	$\frac{85272E}{h^4}$	$\frac{2G}{h}$	$20.3P_w$	$\frac{10.2P_w}{G}$	
Half Sides	465E	0.279E	$\frac{3722E}{h^4}$	$\frac{2.23E}{h^4}$	$\frac{1.12G}{h}$	$9.2P_w$	$\frac{8.2P_w}{G}$	
Sides	2025E	0.456E	$\frac{16200E}{h^4}$	$\frac{3.65E}{h^4}$	$\frac{1.82G}{h}$	0	0	

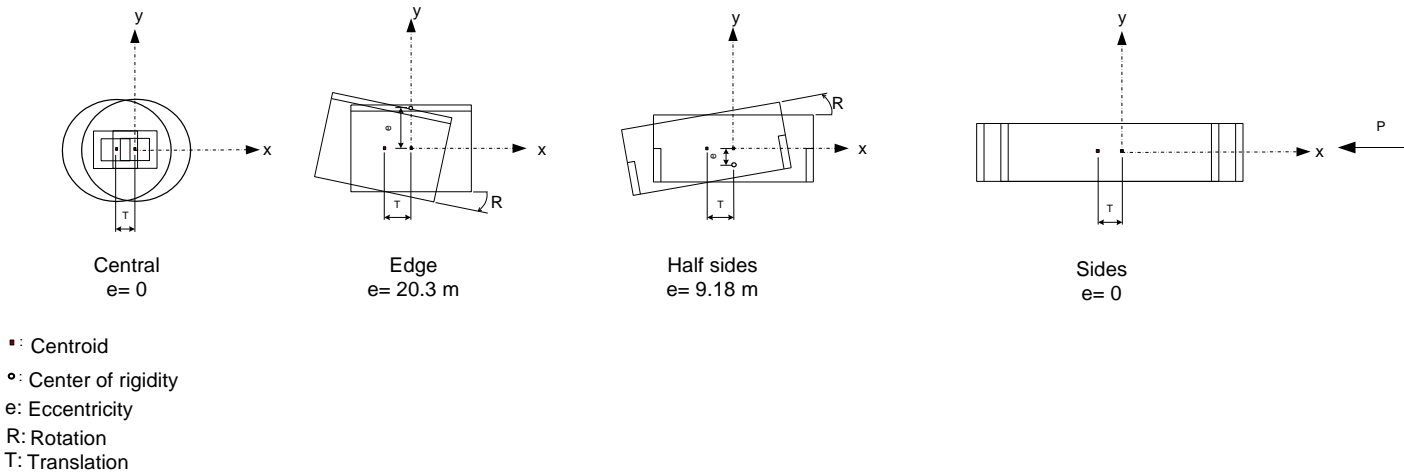
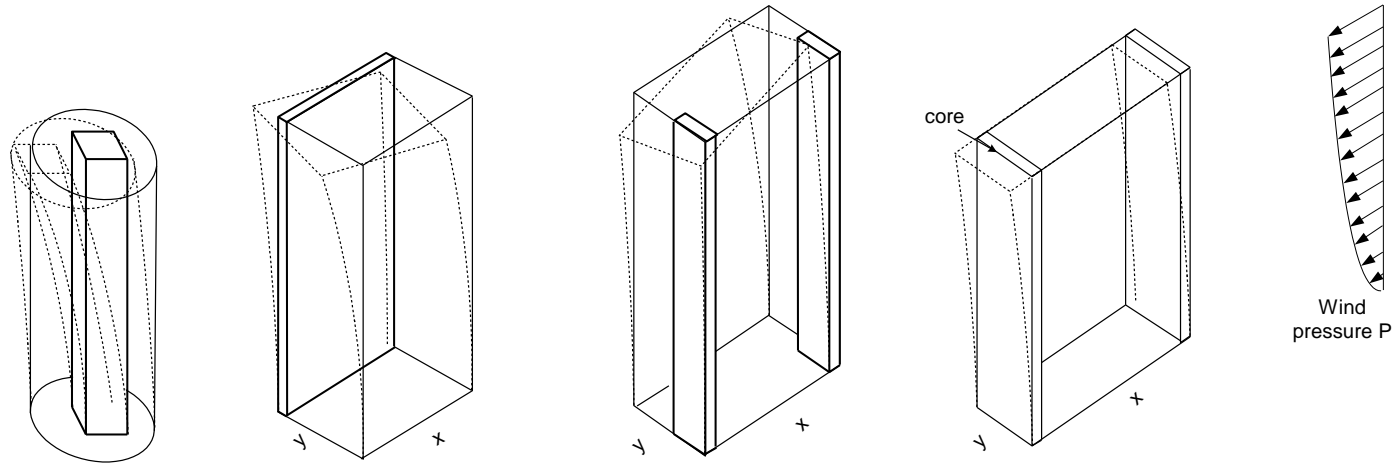


Figure 4.10 3D of how the different building types might deform under wind loads

4.4 Energy demand with equivalent percentages of opaque surfaces (EPO)

The building morphologies proposed by Yeang do not describe clearly the way in which building efficiency is quantified or the percentage of opaque and transparent materials (percentage of the windows) in the building envelope where there is no mass (core/wall). In the previous thermal analysis study, it was assumed that 10% of glazing walls is metal frame. These results in significant differences in the percentage of opaque materials in the buildings' envelope: 10% in the Central model, 37.9% in the Edge model, 28.3% in the Half Sides model, and 32.5% in the Sides model.

It suggests that any comparison of the energy consumption among the four configurations may be uneven. The percentage of opaque and transparent materials in the envelope is likely to play a major role in radiant heat gains and losses, which would affect the total energy demand/annual energy consumption. In the following section, we investigate how these different building morphologies perform with equivalent amounts of opaque material in the exterior envelopes, and limit the amount of opaque surface to 37.9% of the entire surface area for all four building configurations. This figure (37.9%) is derived from the highest percentage of opaque surface present in any of the four building configurations, a characteristic that is found in the Edge model.

4.4.1 Modeling

To ascribe 37.9% opaque surface area for all other models (the Central, the Half Sides, and the Sides), we added curtain walls such that all buildings have an equivalent percentage of opaque surface area (EPO). The curtain wall material is typically assumed

to be made from metal, and has R-values which meet IECC 2009 code. It should be noted here that the proportion of the curtain walls depends on the proportion of the opaque material that is already given in the initial proposal. Figure 4.11 shows schematics of the buildings' plan views which were assigned additional opaque material. The additional material was placed on west-east sides for the Central and Half Sides in order to reduce solar heat penetration during the hottest part of the day (afternoon). In the Sides model, the additional opaque material is placed in the north face to reduce energy loss.

The outputs of this analysis are presented in Table 4.6, which illustrates that when the buildings have EPO, it leads to some change in EUI. In the cool climate region (first row Table 4.6) the EUI for the Central model is significantly decreased from 62.32 kWh/m² (initial) to 45.27 kWh/m² (EPO), which is a 37.66% reduction (see Figure 4.12). On the other hand, the drop in the EUI for the Half Sides and the Sides models is insignificant with 4.32% and 2.42%, respectively; while in Edge model, the EUI has no change because the percentages of opaque surfaces are still the same.

Similarly, with the effect of EPO in temperate climate, the change in EUI was significant in the Central model with a difference 22.2% from the initial, while all other models (the edge, the Half Sides, and the Sides) are negligible with maximum difference is 2.17%. In arid climate, EPO also significantly reduced EUI by 23.24% in the Central model, while the other models have negligible variations. Also, in this climate the lowest EUI is in the Central model, but with a small difference of 2.97% compared with the second option of the Sides model. Lastly, the difference in EUI between the initial and

EPO in the tropical climate is slightly significant at 7% in the Central model. Otherwise, we have negligible variations.

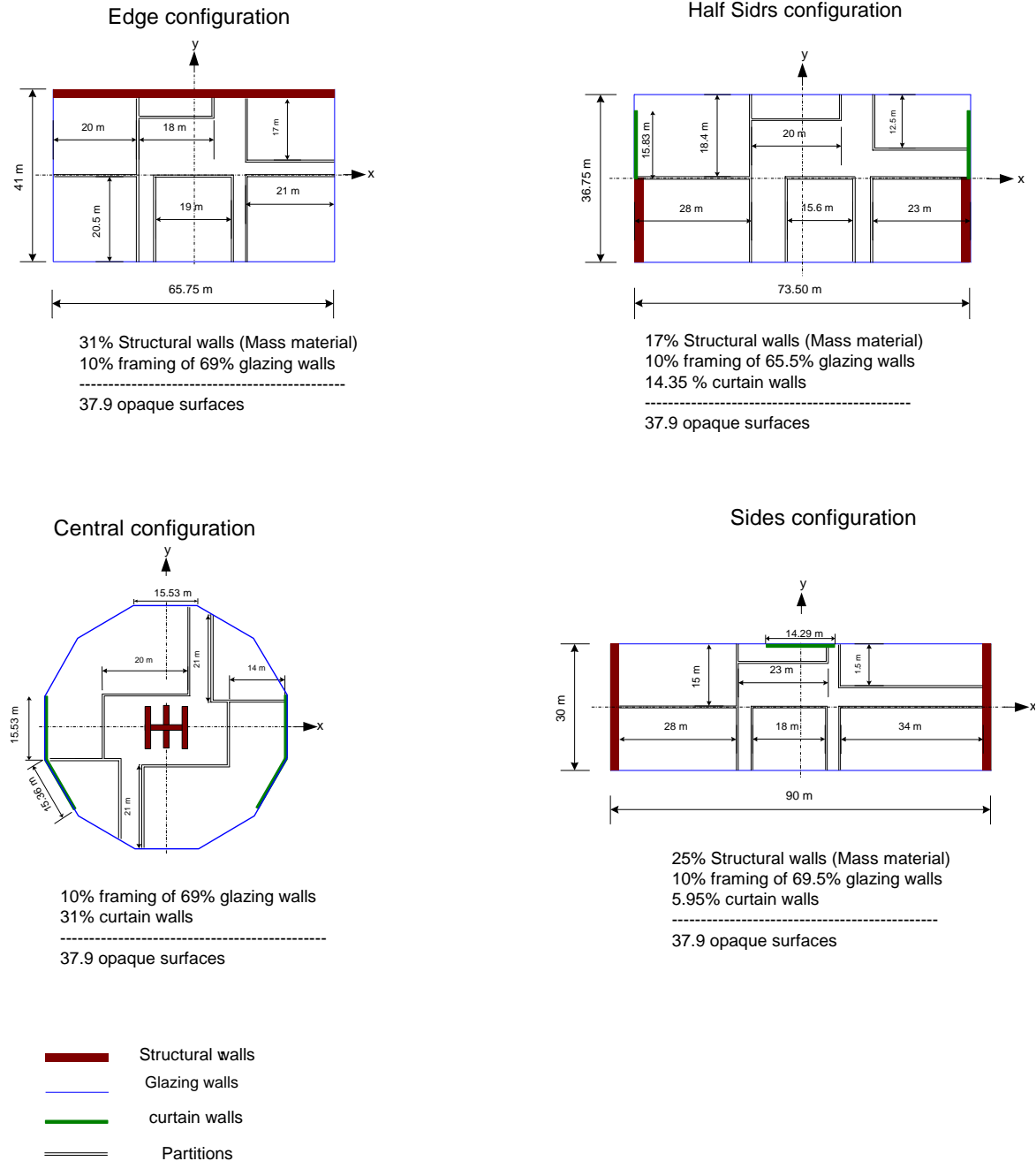


Figure 4.11 Plan views and an elevation of the buildings (EPO)

Table 4.6 Thermal analysis results of EPO

Climate	Envelope	Central	Edge	Half sides	Sides
		EUI (kwh/m2)			
Cool	Initial	62.32	50.89	54.58	46.87
	EPO	45.27	50.89	52.32	45.75
Temperate	Initial	36.71	32.51	33.91	30.6
	EPO	30.05	32.51	33.5	29.95
Arid	Initial	63.98	56.29	59.32	54.44
	EPO	51.75	56.29	56.53	53.3
Tropical	Initial	57.95	56.38	57.37	54.6
	EPO	54.17	56.38	56.83	54.32

Initial = the basic proposal by Yeang; EPO= equivalent percentages of opaque surfaces.

4.4.2 Summary of EPO analysis

By ascribing equivalent percentages of opaque surfaces, EPO, for the four given building configurations we were able to draw two major conclusions regarding building energy consumption:

1) For the Central configuration (which basically is a building that has a floor-plan aspect ratio 1:1), the energy consumption can be significantly reduced by 37.66%, 23.24% and 22.2% in Cool, Temperate, and Arid climate zones, respectively.

2) With the opaque surfaces (East and the West sides) of the Central configuration, it converts it from the worst scenario to the one of the best.

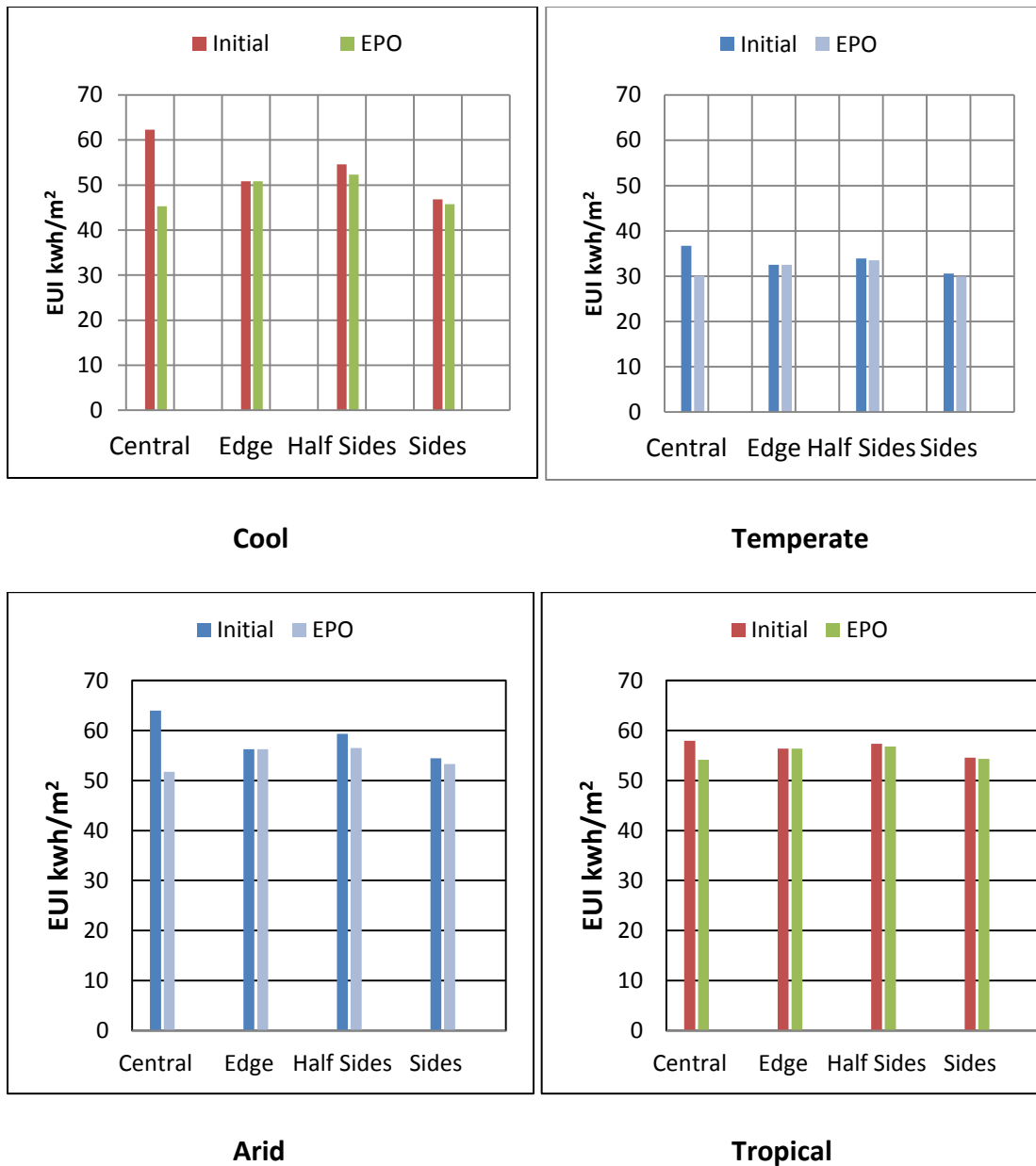


Figure 4.12 The variance in EUI between the initial and EPO for the four configurations in each climate zone

With using EPO a compromising in gaining and losing energy through the building envelope would happen. In other words, a higher percent of a glazing wall may allow more sunlight to penetrate through, but at same time because the glazing wall has a lower R-value, the losing energy would be higher as well.

4.5 Thermal mass modeling

Thermal mass is usually used in conjunction with passive design techniques. Indeed, thermal mass can be useful depending on climate and is most appropriate where there is a big difference between day and night outdoor temperatures. Thermal mass refers to the ability of building's materials to store heat (thermal storage capacity), for extended periods. The general idea behind thermal mass is this: a material with good thermal mass will absorb heat from an available source like the sun during the daytime or from the heating system in the buildings, store it, and when the sun sets and air temperature drops or the other source turns off, the heat stored in the material seeks out the cooler object. Concrete is considered a good material for thermal mass.

As the structural walls in our study are reinforced concrete, we would like to know what the effect of the thermal mass on the energy demand is. We divide this topic in two approaches: the first, based on Yeang morphologies but assuming equal proportion of structural walls in all models, the outcome will show how energy demand differs in each building type corresponding to the climate zones. The second approach would be based on increasing the wall's thickness (increasing thermal mass material) to find out how sensitive energy demand is to thermal mass.

4.5.1 Equivalent distributed of the opaque surfaces (EDO)

The first approach is to add evenly distributed walls in the building's envelope where the opaque surfaces in total become 46% in each model; this represents 40% of mass material and 10% of metal framing of the 60% glazing curtain walls, see Figure 4.14. Also, these additional mass materials have thermal properties that are the same

as in the core/wall. There is already another source of thermal mass that in all the buildings, which is the 10 cm concrete floor slabs.

The thermal analysis results shown in Table 4.7 demonstrate that by raising the percentage of the opaque surfaces to 46% leads to a significant drop in the energy demand in the Central model by 39.54% in cool climate, 24.57% in a temperate climate, 25.65% in an arid climate, and 10.27% in tropical.

In the case of the Half Sides, the reduction in energy demand is slightly significant drop of 9.8% in cool climate. Otherwise, it dropped less than 4% in other climates. Similarly, in the case of Edge and Sides models, the reduction in energy demand is not more than 4% for any of the four climates.

As a result, unlike what has been recommended regarding placement of core/walls in certain locations, we found that more opaque surfaces in a building envelope do not conflict with the overall energy performance, but can improve it. Moreover, it is important for the high structural performance to avoid the asymmetry distribution of the structural elements as much as possible. This can be more achievable given the possibility of having this wall in the building perimeter.

4.5.2 Doubling the wall's thickness

In this second approach, we investigate the potential of thermal mass to save energy. In other words, we want to know the sensitivity of energy demand to thermal mass in the structural wall. We double the thermal mass wall thickness to determine how the energy demand changes. Two building configurations (see Figure 4.14) are examined with initial wall thickness of 0.45m and 0.90m.

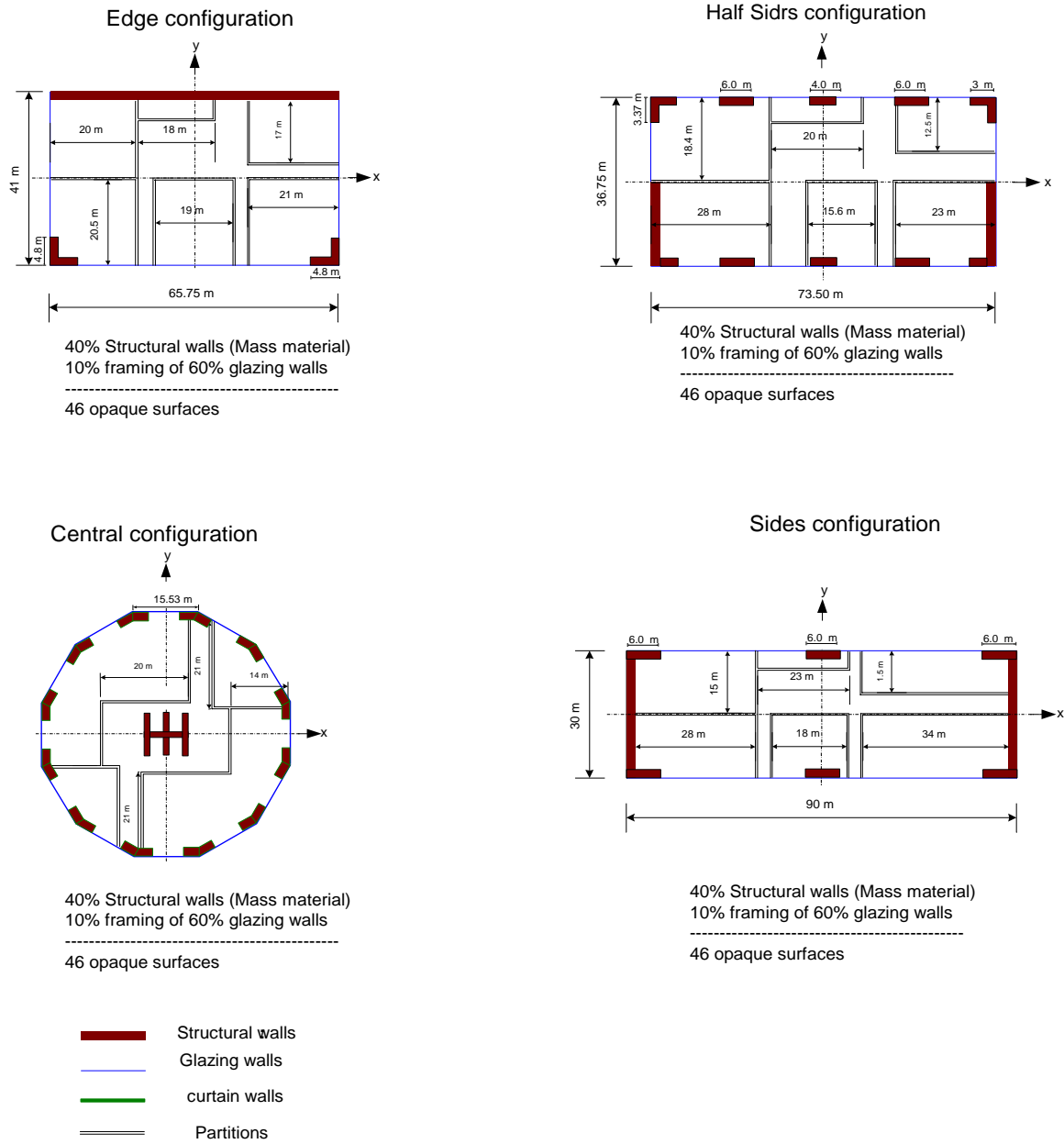


Figure 4.13 Plan views and an elevation of the buildings (EDO)

We use two different building shapes because in the Sides model the thermal mass material is located just in the east west sides, while the Central model represents the case when the thermal mass is evenly distributed in the envelope. The results are

presented in Tables 4.8 and 4.9 for the heating and cooling loads in addition to energy use intensity in all corresponding climate zones.

Table 4.7 Thermal analysis results of EDO

Climate	Envelope	Central	Edge	Half sides	Sides
		EUI (kwh/m2)			
Cool	Initial	62.32	50.89	54.58	46.87
	EDO	44.66	49.29	49.67	45.75
Temperate	Initial	36.71	32.51	33.91	30.6
	EDO	29.47	31.29	31.12	28.85
Arid	Initial	63.98	56.29	59.32	54.44
	EDO	50.92	54.39	54.48	52.13
Tropical	Initial	57.95	56.38	57.37	54.6
	EDO	52.55	55.47	54.98	52.88

The differences in the loads as well as EUI are negligible. This indicates that energy demand is not sensitive to the thermal mass for buildings that have the same inputs. However, doubling the structural wall thickness will significantly increase the amount of material use. This is directly reflected in material cost as well as in the embodied energy. On the other hand, from the structural perspective to double the wall thickness means increasing its stiffness, and accordingly the building stiffness as well.

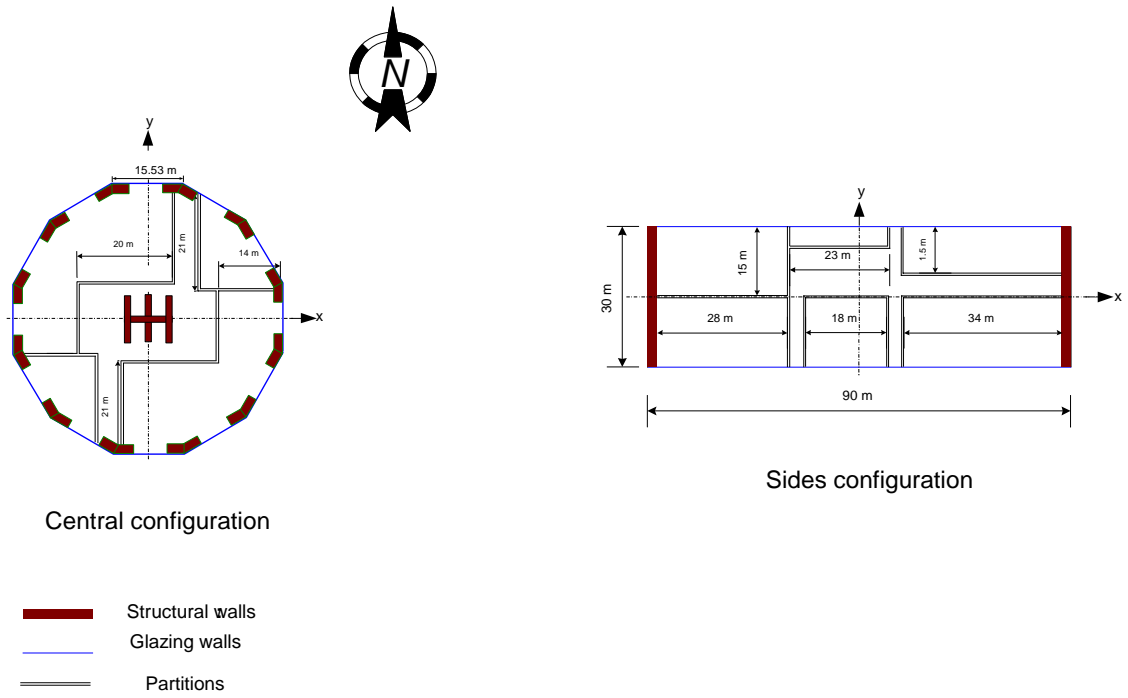


Figure 4.14 Plan views Central and Sides (thermal mass analysis)

Table 4.8. Thermal mass results of Sides configuration (initial configuration)

Climate	Wall thickness = 0.45 m			Wall thickness = 0.9 m			EUI difference %
	Heating	Cooling	EUI	Heating	Cooling	EUI	
	(kwh/m2)			(kwh/m2)			
Cool	41.10	5.76	46.87	41.03	5.74	46.78	0.19
Temperate	6.55	24.06	30.61	6.52	23.97	30.49	0.39
Arid	4.98	49.46	54.44	4	49.39	54.36	0.15
Tropical	0	54.61	54.61	0	54.28	54.28	0.61

4.5.3 Summary of EDO analysis

We obtained three major conclusions regarding building energy consumption when we made the building envelope have an equivalent percent of opaque structure:

1) The results obtained from the first approach (EDO) emphasize that adding opaque surfaces in the Central configuration envelope significantly improves energy performance. We found negligible improvements in the other configurations (Edge, Half Sides, and Sides).

2) Energy demand is insensitive to the thermal mass. Increasing thermal mass material by 100% changes the energy demand by around 0.5%.

3) The results suggest that there are more flexible options for placing the structural elements so as to avoid the asymmetrical distribution, without compromising energy performance.

Table 4.9 Thermal mass effect Sides configuration of 46% opaque

Climate	Wall thickness = 0.45 m			Wall thickness = 0.9 m			EUI difference %
	Heating	Cooling	EUI	Heating	Cooling	EUI	
	(kwh/m2)			(kwh/m2)			
Cool	38.12	6.54	44.66	38.03	6.52	44.55	0.24
Temperate	5.6	23.87	29.47	5.58	23.73	29.31	0.55
Arid	4.33	46.59	50.92	4.32	46.47	50.78	0.28
Tropical	0	52.55	52.55	0	51.88	51.88	1.3

CHAPTER 5

STRUCTURAL ANALYSIS

5.1 Introduction

Structural analysis using SAP200 is presented to determine the structural system morphology proposed solely on the basis of energy efficiency is adequate to safely support structural actions such as wind loading in accordance with ASCE 7-10 (ASCE 2007). Preliminary structural analyses have been carried out (see Appendix A) to determine for what height these given base structural systems (BSS) can meet the serviceability requirement (according to the ASCE 7-10 for loading and lateral and displacement limit). The results were as following: for the Central configuration, the BSS is adequate for a height of up to 96 m with the wind load perpendicular on Y direction, or up to 76 m with the wind load on orthogonal direction. In the case of the Sides configuration, the BSS is adequate up to 100 m with the wind load perpendicular on X. In the case of the Half Sides configuration, the BSS is adequate up to 76 m with the wind load perpendicular on X. In the case of the Edge configuration, the BSS is not adequate, because of the substantially high torsional displacement. Accordingly, given a height of 200 m, the four building types investigated need supplementary lateral load resistance (SLLR) to comply with performance expected from code defined wind loading.

The shear walls in buildings respond as cantilevers, with a relatively small base under wind loading, as the height increases, wind pressure increases, resulting in more sway, which is evident by the relationship between the deflection and the height (length) of a cantilever element. Thus, it is known that, for most of the time, the design

of a high-rise building is controlled by the lateral displacement. We thus consider the lateral displacement as a primary factor of this study. We propose to use an outrigger-braced system, which usually consists of a stiff core, connected to edge columns, where under lateral loading, the outriggers stiffen the core against overturning, generating tension in the windward columns and compression in the leeward columns [29, 30]. Furthermore, the outrigger-braced system is an efficient system that increases building stiffness and has therefore been widely used in tall building structures [34]

5.2 Description of building models variables:

As previously, we name the proposed structural configurations as a function of the initial location of structural cores or walls are initially placed. These configurations are: Central for the structural core in the building center; Edge for a structural wall along the north face; Half Sides for structural walls covering half of the east and west sides; and Sides for structural walls covering the entire east and west sides of the buildings (see figure 4.2). Other building descriptors, such as square footage, number of stories, and building height, were reasonably assumed for four high-rise office buildings. All are 50-story, 200 m tall buildings with a 4.0 m inter-story height.

There are three main structural systems in each building: 1) the base structural system core/walls (BSS) for lateral loads; 2) Non-moment steel frame for gravity loads; and 3) steel braced frame for SLLR. The BSS consists of the lateral-load proposed by Yeang on the basis of sustainability considerations. Structural walls are constructed using normal-weight reinforced concrete with an assumed compressive strength 28 MPa (note that this assumed compressive strength is not representative of all high-rise

construction, but the material selected is to illustrate the concepts in this paper). Based on the assumed concrete strength and based on the preliminary calculations of flexural strength for the shear walls [35], see Appendix A, the wall thickness increases from 0.60 m at the top, to 0.7 m at the thirty-seventh floor, 0.8 m at the twenty-fifth floor, and 0.9 m below the twelfth floor. A common assumption of including cracking in reinforced concrete walls by decreasing the gross moment of inertia (I_g) to $I_{cr} = 0.5 I_g$ was used. The SLLR system consists of a braced frame connecting the core to edge columns using an outrigger system at three levels: one quarter, one half, and the three quarters of the total building height [29]. The gravity system and SLLR are constructed using steel W-shapes and built-up sections satisfying ASTM A992 Grade 50 steel (IS Grade 420).

The fundamental periods of the proposed buildings were initially estimated using the common approximation of $T = 0.1N$ [29], where N is the total number of stories. For the subject buildings, then, $T = 0.1 \times 50 = 5.0$ sec ($f = 0.2$ Hz). Since the approximate fundamental frequency (f) is considerably less than 1 Hz, and according to the commentary section 26.2 of ASCE 7-10, these buildings are considered flexible structures.

5.2.1 Building model loading

Gravity loads consist of dead and live loads, where the assumed dead load is 2.52 kN/m² including the floor decking, allowance for floor beam weights, and allowance for superimposed dead loads; the live load used was 3.12 kN/m² including live load and a partition allowance. Lateral load resulting from wind pressures was calculated according to the directional procedure in ASCE 7-10[7]. For application of this procedure, the

assumed wind load characteristics are: basic wind speed of 58 m/s (130 mi/h) (Boston region); exposure category B (urban terrain); building classification category II; gust effect factor $G = 0.92$; wind directionality factor $K_d = 0.85$.

Typically, lateral displacements of concern in serviceability from the effects of wind are on the order of $1/600$ to $1/400$ of the building height [7]. For the subject buildings, then, with a 200 m height, the serviceability threshold for lateral displacement under wind is 0.5 m. Two wind load cases were considered: Case1, corresponding to full design wind pressure acting on the projected area perpendicular to each principal axis of the structure, considered separately along each principal building axis; and Case2, three quarters of the design wind pressure acting on the projected area perpendicular to each principal axis of the structure, considered separately for each principal axis. The purpose of load Case2 is to induce building torsion even in the case where the structural system is doubly symmetric.

5.2.2 Base structural system

For the purpose of reducing the operational energy consumption, Yeang recommended for each building configuration a position for the core and structural walls. These configurations result in a basic structural system (BSS) that are defined only with focusing on building energy consumption and are studied from the structural perspective in this paper. Buildings with asymmetric distribution of stiffness, however, are known to be susceptible to damaging torsional modes of vibration when subjected to lateral load. We note this asymmetry in the floor plan in two configurations as defined by Yeang, the Edge and the Half Sides configurations. Also, in three

configurations (Sides, Half Sides, and Edge configurations), the walls provide lateral load resistance in only one direction of the buildings, while in the orthogonal direction the buildings are too flexible to carry lateral loads. Based on these considerations, the given BSS are not adequate to meet serviceability requirements and might be deficient to satisfy strength requirements.

In order to evaluate the lateral displacements in the BSS under realistic wind load conditions, 3D analysis using SAP2000 was performed. The BSS displacement behavior for the four proposed configurations was used as a guide for a more appropriate structural design. As we mentioned, the gravity system consists of non-moment steel frames (beams and columns), while the BSS is formed by shear walls to resist the lateral load. The boundary conditions at the base are assumed as fixed supports for shear walls, pin supports for the steel gravity columns, and pinned beams ends. The BSS is the only system considered to resist the lateral loading.

Results of the analyses of the buildings under Case 1 wind loading show that the lateral displacements at the building top exceed the serviceability limit of 0.5 m (see table 1). There were no torsional displacements found for the Central and Sides models, unlike in the Half Sides and Edge models [the reason as we mentioned because of the irregularity in the rigidity in these two models (see figure 5.1)]. The displacement is high in y direction (U_y) in the Sides model when the building is subjected to y-direction wind loading (P_{wy}) although the highest wall stiffnesses in oriented parallel to this direction. This is due to the larger exposed area for this direction of wind loading that leads to high

wind pressure. These results indicate that the size and number of shear walls in the Sides model are not adequate, even though they fully cover both east and west sides

Similarly, the Half Sides model exhibits a large y -displacement (U_y) when subjected to y -direction loading, indicating that the BSS shear walls do not provide adequate stiffness to meet the serviceability requirements. Because there is really no lateral-load system in the x -direction for the Sides and Half side models, then the buildings are too flexible.

In the Edge model, on the other hand, the BSS shear wall provides stiffness only in the x direction and due to its location on only one side causes a severe stiffness irregularity. The stiffness eccentricity, defined as the perpendicular distance between the floor centroid and the center of the rigidity of the structure leads to combined translation and twisting of each floor; the lack of building stiffness in the y direction and the large stiffness eccentricity leads to the large displacement(see Figure 5.1), which greatly exceeds the serviceability limit.

In summary, the analysis with wind load Case1 resulted in displacements that are beyond the serviceability limit in all models. For this reason the models were not analyzed under Case2 loading since the buildings are already in violation of code-prescribed limits for Case1. The results show that the wall distributions for Sides, Half Sides, and Edge models provide stiffness only in one direction while the structural system is too flexible in the orthogonal direction. Asymmetry in the Edge model generates substantial eccentricity, causing a large torsional displacement mode. The core in the Central model does not have adequate stiffness in either direction to meet

the serviceability limit. Therefore, the four building types need SLLR to resist ASCE 7-10 wind loading for a building height of 200 m.

Table 5.1 lateral displacements result of BSS models

	Displacement due to wind pressure P_{wx}	Displacement due to wind pressure P_{wy}	Serviceability threshold (m) (ASCE 7-10)
	U_x (m)	U_y (m)	
Sides	1.55	1.1	0.5
Half Sides	2.1	2.16	
Edge	1.8*	4.0	
Central	1.33	2.1	

* Deformation due to torsional displacement, See Figure 2 below

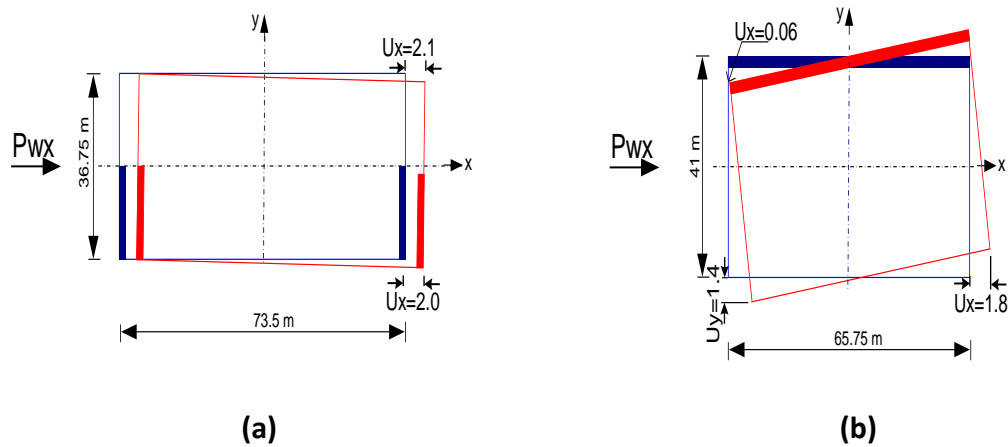


Figure 5.1 Torsional displacements: (a) Half sides; (b) Edge model

5.2.3 Supplementary lateral load resistance

The approach will be to increase the effective structural depth by connecting the core to the edge columns. The selection of the SLLR system was based in part on ensuring that the basic structural concept could be applied for all of the building types

to keep the type of system consistent, so focus could instead be placed on determining the additional material needed for the SLLR needed beyond that used in the base structure. An outrigger system was chosen then as SLLR to control drift of each building and reduce the bending demand in the core. Outrigger systems are economical and efficient lateral load systems, because the system utilizes the axial strength and stiffness of the perimeter columns to resist overturning by increasing the lever arm at different heights along the structure.

Bungale illustrates that outrigger structures are commonly used in buildings up to 70 stories [29]; Stafford-Smith and Coull illustrate that structures braced using outriggers have been successfully used in buildings from 40 to 70 stories, and they believe the system is efficient for much greater heights [30]. In this study, we use the outrigger system as SLLR to reduce the lateral displacement, Steel trusses are used as outriggers in this paper; these are located at three floor locations, which could also serve as mechanical floors 12–13, 25–26 and 37–38. Outriggers are connected to interior and exterior columns along the outrigger arm. Additionally, the exterior columns at each of these floor levers are connected using a truss perpendicular to the outrigger plane so as to engage a greater number of exterior columns in the outrigger action and better distribute axial forces, see figure 5.2. Connecting to interior columns reduces the outrigger span, and creates a stiffer 1-story outrigger (4 m height).

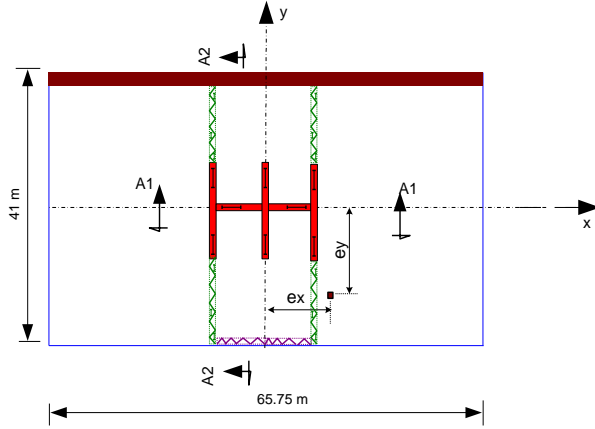
As before all of the modified buildings are analyzed for two wind load cases (Case1 and Case2). Case2 takes into account the presence of eccentricities e_x and e_y measured in the x and y axes of each structure, respectively. Stiffness eccentricity was

calculated using equation 27.4-5 in ASCE 7-10. Computed eccentricities in the x and y directions corresponding to each configuration are listed in Table 5.2.

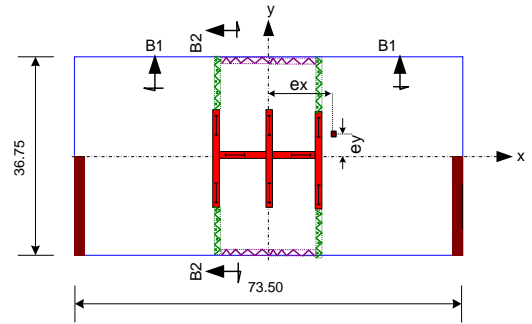
According to strength design load combinations in ASCE 7-10, if we were to size the SLLR for strength only it would not satisfy the serviceability limit, see table 2. This result indicates that the serviceability limit controlled the design, which is not unexpected in tall buildings, so the SLLR system was resized to meet the serviceability requirement of a maximum top displacement of 0.5 m, see Table 5.2 and Figure 5.3.

5.2.4 Displacements results, SLLR:

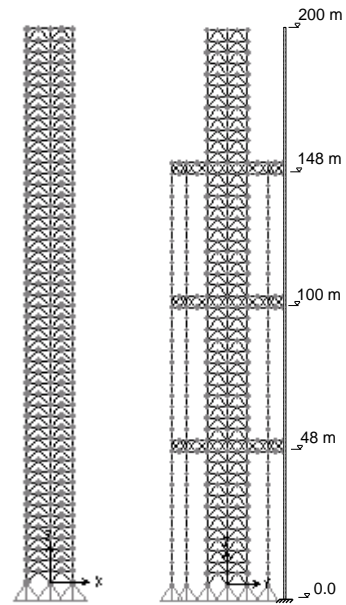
SLLR improved buildings stiffness to resist lateral displacements and allowed all buildings to meet the serviceability limit. Table 2 illustrates the lateral displacements at the roof of the buildings. In the case of Sides configuration the lateral displacement resulting from loading Case1 governed the response. The differences in maximum displacements from loading Case2 are 7% and 25% for U_x and U_y , respectively, see Figure 5.3. In the case of the Half Sides model, loading Case2 results in a higher lateral displacement than Case1, with U_y equal to 0.43 m, while U_x is governed by loading Case1 with a maximum displacement of 0.44 m. In the case of the Edge model, loading Case2 gives the highest displacements in both x and y directions, equal to 0.43 m and 0.41 m, respectively. Loading Case2 dominates in the Central model with displacements U_x equal to 0.44 m and U_y equal 0.45 m.



Plan view mechanical floors-
Edge configuration

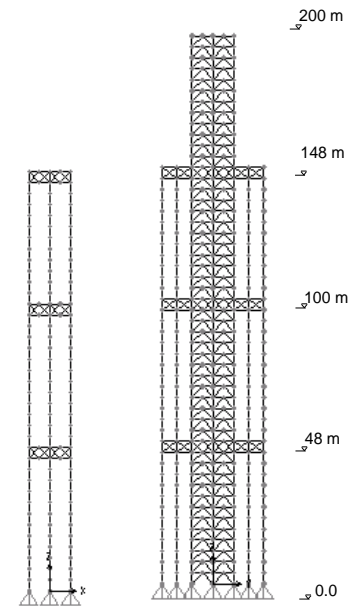


Plan view mechanical floors -Half
Sides configuration



Section A1-A1

Section A2-A2

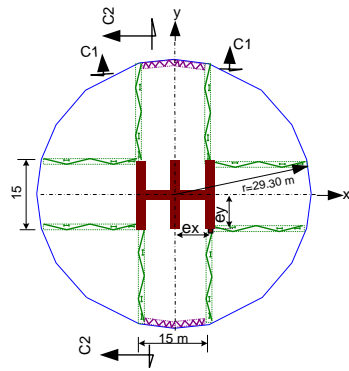


Section B1-B1

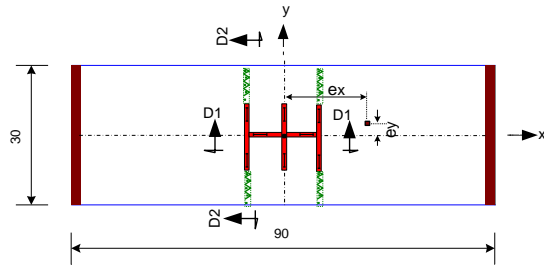
Section B2-B2

- Structural reinforced concrete shear wall
- Non-Structural : glazing walls
- Braced steel frame
- Truss
- outrigger structure

Continue



Plan view mechanical floors-
Central configuration



Plan view mechanical floors-
Sides configuration

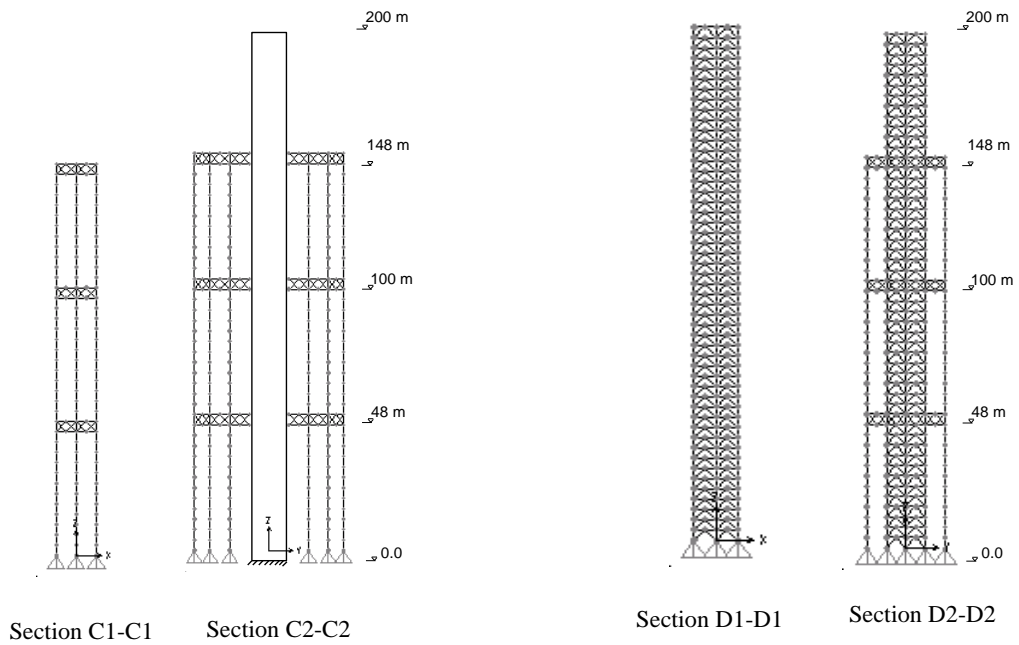


Figure 5.2 Building plan views and schematic structural system for the buildings with three outriggers with/without belt trusses (connecting columns perpendicular to the plane of outriggers)

More important than specific displacement values for each model, however, is the fact that all buildings now satisfy the serviceability criterion of a maximum roof displacement of 0.5 m established for the buildings. It is also important to note that the analyses serve to identify in a conceptual context the type of structural system required

to provide an acceptable structural solution. A detailed design of each of the structural systems proposed lies beyond the scope of this study.

5.2.5 Summary of the structural analysis

Structural analysis and design using SAP200 is performed to investigate the structural performance of the BSS, where we found that SLLR was needed. Further if we were to size the SLLR for strength only it would not satisfy the serviceability limit so the SLLR system was resized to meet the serviceability requirement of a maximum top displacement of 0.5 m. Hence, these three major conclusions regarding building structural performance:

(1) Maximum lateral displacements at the tops were close and comparable. This will allow precise comparison of the amount of material that is being added because of RLLS.

(2) In the case of the Sides configuration, because of the shear walls are placed on the sides, this played a major role in minimizing the torsion displacement. Otherwise, in the other configurations, the maximum drifts were controlled by the torsion displacement.

(3) The RLLS effectively reduced the potential torsion displacement in the Edge configurations, but resulted in larger structural elements that will reflect negatively on the cost and the embodied energy of the material, as we will see in the calculation of costs later.

A final observation: we can now calculate the amount of structural material for BSS and SLLR. Then we will (In the next chapter) calculate the total cost (operational &

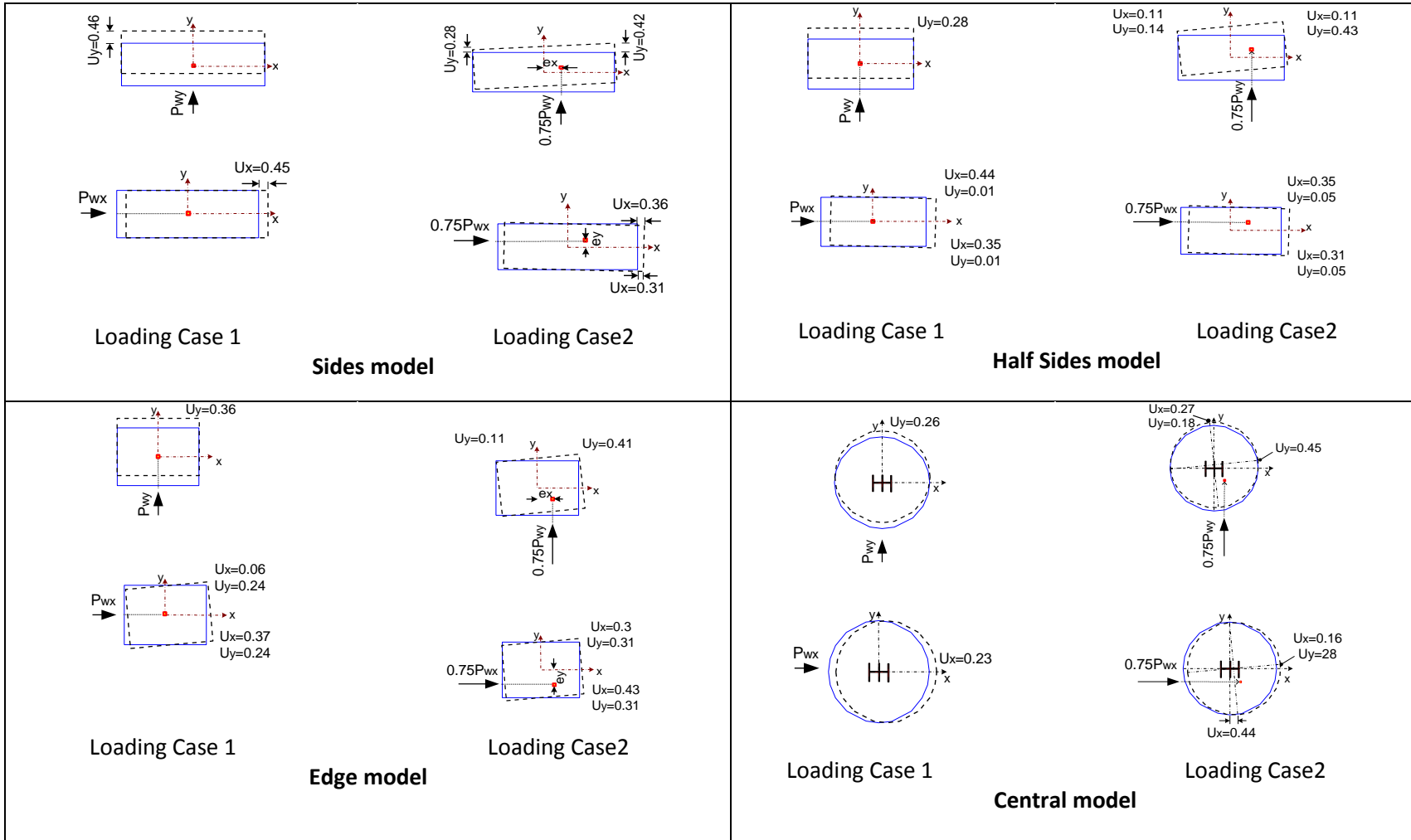
embodied energies and material) for a 50 year life span, so as to know whether the tradeoff of placing the structural cores to maximize operating energy efficiency will not cause the total cost to be too great.

Table 5.2 The lateral displacements result with SLLR

Configurations	stiffness eccentricities (m)		Maximum displacement service wind load P_{wx} and $0.75 P_{wx}$		Maximum displacement service wind load P_{wy} and $0.75 P_{wy}$		Serviceability threshold (m) (ASCE 7-10)
			With SLLR - strength checked	With SLLR - serviceability checked	With SLLR - strength checked	With SLLR - serviceability checked	
	X	Y	Ux (m)		Uy (m)		
Sides	12.7	3.9	0.87	0.45	0.88	0.46	0.5
Half Sides	10.1	5.4	0.98	0.44	1.16	0.43*	
Edge	9	12	1.24	0.43*	1.36	0.41*	
Central	8	8	1.0	0.44*	1.1	0.45*	

P_{wx} wind loading parallel to x-axis; P_{wy} wind loading parallel to y-axis.

* Deformation due to torsional displacement, See Figure 4



All displacements are in meter

Figure 5.3 Lateral displacements at the roof (service wind loads P_w and $0.75 P_w$)

CHAPTER 6

MATERIAL USED EMBODIED ENERGY AND TOTAL COSTS (OPERATIONAL, EMBODIED ENERGIES AND MATERIAL USED)

6.1 Material used embodied energy

The energy required to produce the structural elements such as concrete, steel, wood, etc., has serious environmental and financial consequences. The energy analysis, therefore, must take into consideration the added cost of embodied energy, which is the energy consumed by all of the processes associated with the production of a building. This includes the mining and manufacturing of materials and equipment as well as the transport of the materials and the administrative functions. Generally, the more highly processed a material, the higher its embodied energy is.

Materials in their basic form that have lower embodied energy intensities (such as concrete, bricks and timber) are usually consumed in large quantities. On the other hand, materials with higher embodied energy content such as steel or even aluminum are often used in much smaller amounts. As a result, the greatest amount of embodied energy in a building can be either from low embodied energy materials such as concrete, or high embodied energy materials such as steel [36].

Moreover, placing the structural cores to improve operating energy efficiency may compromise the structural performance unintentionally, thereby increasing the embodied energy of the structure. Council on Tall Buildings and Urban Habitat (CTBUH) illustrated that the embodied energy normal-weight reinforced concrete with 100Kg rebar per cubic meter is 2.12 MJ/Kg [37]. According to Lee et al. the embodied energy

virgin steel is 35.3 MJ/Kg and 9.5 MJ/Kg for recycled steel [18]: steel sections are made from 93.3% recycled steel [38], thus the estimated steel sections embodied energy would be 11.51 MJ/Kg. Once we find the quantities of the materials that are needed for the structural system (BSS and SLLR), the embodied energy is calculated as shown in Table 6.1. The quantity of each material is show in the table corresponding to each building type, and then the results are normalized based on the embodied energy for the BSS in the Sides configuration.

Table 6.1 Embodied energy of the material used (for BSS & SLLR)

configuration	Material quantity		Embodied energy GJ/t		Normalized Embodied energy		
	Steel (t) From SLLR	concrete (t) From BSS	SLLR Steel	BSS Concrete	SLLR Steel	BSS Concrete	Total
Central	10189	20719	11.51	2.12	2.57	0.96	3.53
Edge	11653	23697			2.94	1.10	4.04
Half Sides	15142	13213			3.82	0.61	4.43
Sides	8095	21542			2.04	1.0	3.04

The embodied energy is normalized with respect to material embodied energy in the Sides configuration. EEI: the embodied energy intensity.

Table 6.1 illustrates that the highest embodied energy is in the Half Sides configuration; the reason is because this model accounts for the highest amount of structural steel for SLLR, which associates with higher unit embodied energy per tonne. The embodied energy in Edge model is the highest for the BSS and second highest for SLLR the Central model demanded the lowest total embodied energy after the Sides model. It is worth noting that the Central model used to be the worst model in terms of operational energy. This may indicate that it is not necessary that buildings of lower operational energy will have lower embodied energy or vice versa.

6.1.1 Summary of the material used embodied energy

We obtained for major conclusions regarding material used embodied energy:

1) The higher embodied energy in the Half Sides configuration is because it needed the highest quantity of structural material for RLLS. This is mainly as a result of the extreme lack in BSS being adequate to resist the wind loading considered in this study.

2) Because of the potential irregularity in the rigidity in Edge configuration led to a relatively high quantity of structural material for RLLS which led to higher embodied energy in this model comparing to the others.

3) In the case of the Central model, with taking into account that the lack in BSS and also the impact of the torsion displacement (load Case2) made RLLS element to be larger, resulting a relatively high quantity of structural material for RLLS, and the high embodied energy.

4) Opposite scenario In the case of the sides, because the placement of BSS along the short sides led to reduce the impact of the torsion displacement, resulting a relatively less quantity of structural material for RLLS, and then less embodied energy.

A final observation: placing the structural cores to improve operating energy efficiency led to compromising the structural performance, thereby increasing the embodied energy of the structure. The next steps will bring the total cost of energies (operational and embodied) in addition to materials and then we can compare the tradeoff between the energy and the structural performance.

6.2 Cost analysis

The changes in global climate, population increase, concerns about the energy resource, urban infrastructure, and green buildings (which have become essential to achieve the sustainability) are all reflected on the economy. This is relevant to our study through the cost of materials for construction as well as operational and embodied energies. There are numerous costs associated with acquiring, operating, maintaining, and disposing of a building system. However, in this analysis we will focus only on the material cost for the structural lateral loads resistance systems (BSS and SLLR) and the cost for operational (cooling and heating) and embodied energies. Previously, we found that different building types with different morphologies would associate with various amounts of structural material and various energy demands; so, obviously, this would result in variation on the overall cost between these building types.

6.2.1 Cost calculation Assumptions

For the purpose of this study, several assumptions are made: 1) the energy used for cooling and heating is electricity per kilowatt-hour; this cost will be considered as constant along buildings' life span. 2) The unit cost of the embodied energy is the same as the unit cost of the operational energy. 3) All the buildings have a life span of fifty years.

6.2.2 Cost of operational energy

Based on the energy analysis and the results previously obtained (Table 4.4) we can estimate the operational energy cost for each building configuration corresponding to the energy unit price in each location. The price per-kilowatt-hour of the electricity energy is varying between the states, where it is \$0.16 Boston, MA; \$0.12 Sacramento, CA; \$0.1 Las Vegas, NV; \$0.21 Honolulu, H [39]. These differences in unit price have potential effect on the total energy cost between the regions (states), but this would not affect the comparison of our interest, because we are comparing the cost for the four buildings' configuration in each single city at a time. Table 6.1 illustrates the annual operational energy and the extreme differences in the cost associated with it.

In all the regions the upper extreme cost difference happens between the Central configuration and the Sides configuration (the Sides demands is the lowest in energy demand). On the other hand, the lower cost difference happens always between the Sides and the Edge configurations. To visualize these differences in the cost for the life span of 50 years, we estimate how many years we will have financial gain as a result from the saving if we use these configurations compared to the worst scenario (see

Figure 6.1). As can be seen in cool climate the cost of energy that is needed for Central configuration for a 50 years life span would be sufficient to Sides configuration for the same life-span period in addition to a period of 16.5 years; or in addition to a period of 11 years and 7 years if we use the Edge and the Half Sides respectively. In case of temperate climate using Sides configuration will save operational energy cost needed for 10 years extra if we use the Central configuration, while we can get enough financial gain for 6 years, and 4 years extra from the saving if we use the Edge and the Half Sides respectively. On the other hand, in the tropical climate we may say that all models are close in terms of energy costs for the given life span.

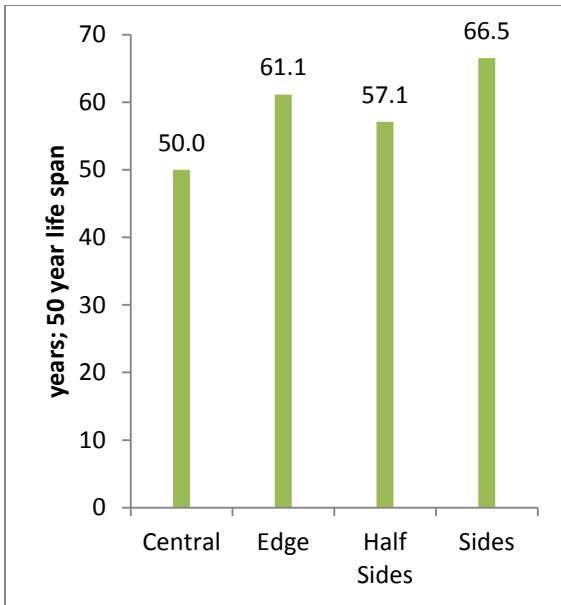
6.2.3 Cost of material used for BSS and SLLR

Input building and construction costs are determined mainly by the cost of materials, labor, and erection of the building. According to MEPS International, the cost of steel structural sections are \$908/t [40] (metric tonne) whilst the structural concrete cost is varying in different parts of the country and all over the world. However, for the Boston region, which represents the cool climate, the costs have been estimated using national RS Means data [41], where it is \$ 640 /m³ of normal weight concrete including materials, framing, placing, labor, and also including 100 kg rebar. Also, the cost of one tonne of steel structure materials is \$4300 including material, shop fabrication, shop primer, and bolted connections.

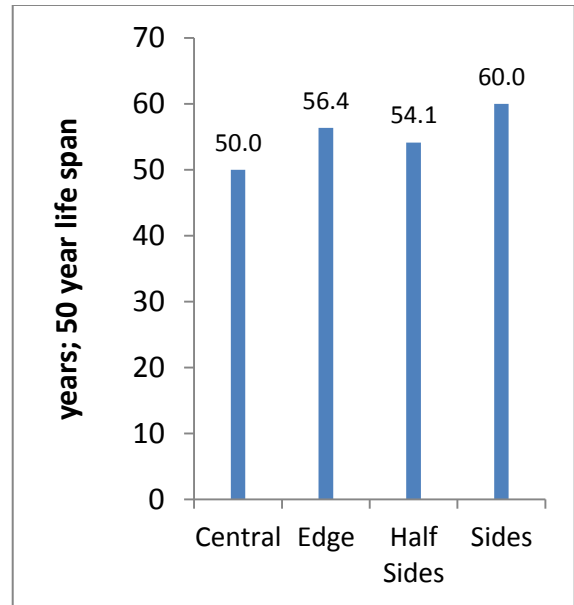
Table 6.2 The operational energy extreme differences in annual energy the cost

climate	Unit cost \$/kWh	Annual operational energy (AOE)				Extreme differences			
		Central	Edge	Half Sides	Sides	AOE % Difference		Energy cost Difference (\$)	
		kwh				Min	Max	Min	Max
Cool	0.16	8.413E+06	6.884E+06	7.368E+06	6.326E+06	9	33	89,373	334,054
Temperate	0.12	4.956E+06	4.397E+06	4.579E+06	4.132E+06	6	20	31,763	98,935
Arid	0.1	8.638E+06	7.611E+06	8.008E+06	7.350E+06	4	18	26,114	128,742
Tropical	0.21	7.824E+06	7.622E+06	7.746E+06	7.372E+06	3	6	52,528	94,887

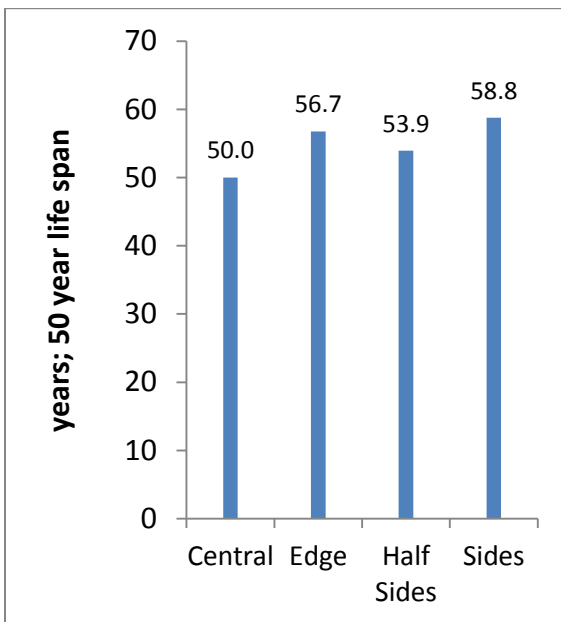
Annual operational energy includes only the heating and cooling load



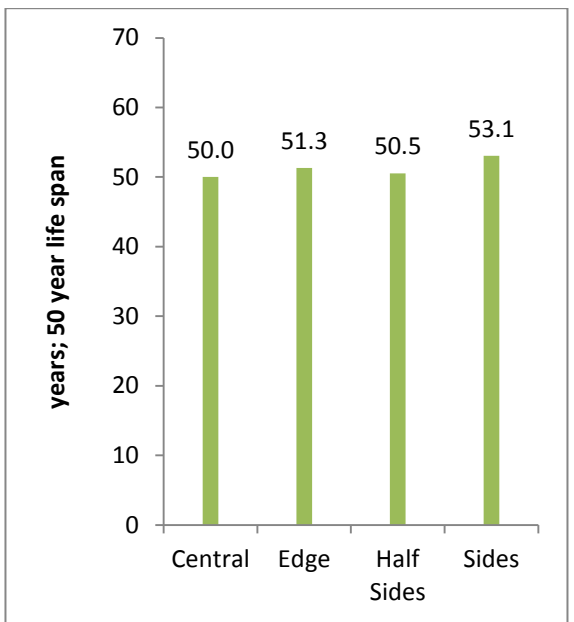
Cool



Temperate



Arid



Tropical

Figure 6.1 Financial comparison of the operational energy cost for a 50 year life span with respect to the Central configuration

Similarly, we estimated the material cost for the other locations, where in Sacramento (which represents the temperate climate), the costs are \$566 /m³ of normal concrete and \$4100 /t of steel sections; in Las Vegas (which represents the arid climate) the costs are \$547 /m³ of normal concrete and \$4240 /t of steel structure; lastly in Honolulu (which represents the temperate climate) the costs are \$702 /m³ of normal concrete and \$4170 /t of steel structure. Once we find the quantities of the materials that are used to form the structural elements for the BSS and SLLR systems (which are used to resist lateral loading), a comparison between the normalized costs for the four models can be made. Accordingly, Figure 6.2 shows material cost index for the BSS and the cost index for SLLR. The cost is normalized with respect to the BSS material cost in the Sides configuration.

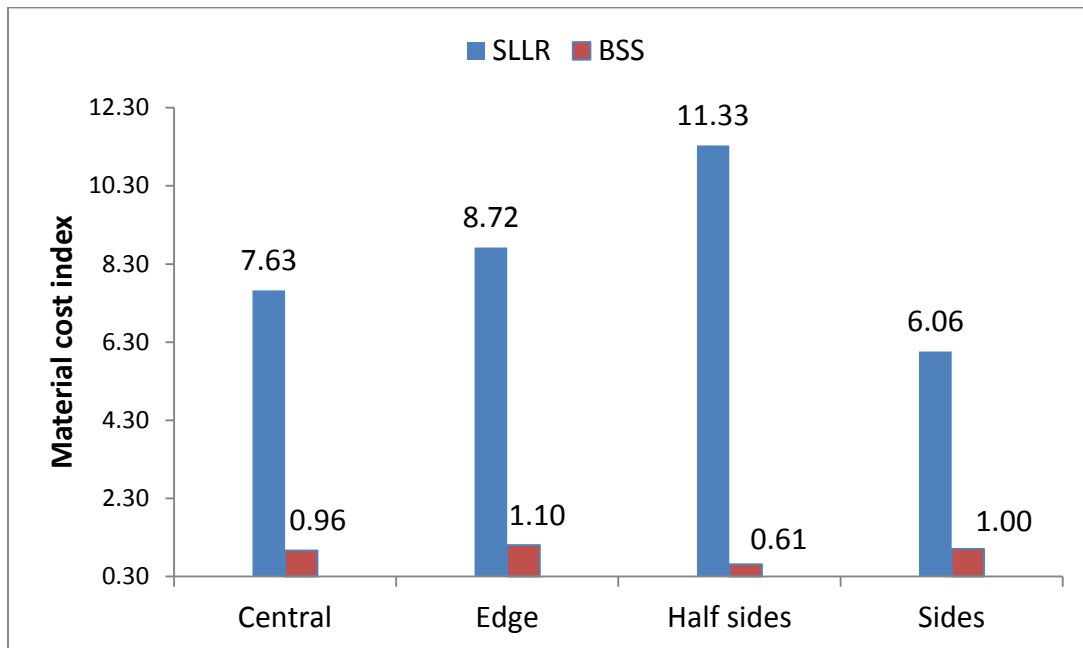


Figure 6.2 Material cost index BSS and SLLR

As can be seen, the highest added cost is in the Half Sides model; this may be reasonable because the material cost in BSS is quite low compared to the others. This is unlike the case of Edge model which demands the highest material cost in BSS. Besides, it is still costly for the SLLR. This can clearly state that the penalty of the irregularity in the rigidity in the Edge model is a high material cost, to achieve structural workability for this configuration. Both the Sides and Central models were close in terms of BSS cost, but the Side model demands the lowest cost for SLLR. Total cost index is illustrated in Table 6.3. As we have found, the worst scenario in terms of the operational energy cost was the Central configuration. However it becomes the second best to the Sides model in terms of material cost (BSS and SLLR). The Edge configuration becomes third and the worst is the Half Sides.

Table 6.3 Total material used cost index

configuration	Material quantities		Normalized cost
	Steel (t) From SLLR	concrete (m ³) From BSS	Total material (BSS+SLLR)
Central	10189	8633	1.22
Edge	11653	9874	1.39
Half Sides	15142	5505	1.69
Sides	8095	8976	1.0

The cost is normalized with respect to material cost in the Sides configuration.

6.3 Total cost: Operational, Embodied energies and Material costs

Table 5 shows the results of the summation of total operational, embodied energies and material costs for fifty years life span. In the case of the cool climate, total cost of the Half sides model is more than that in other each Individual model, while the Sides came in rank one, the Edge second, and Central third. Note here that the high operational energy cost in the Central model is reflected in the total cost; similarly, the high material cost made the Half Sides model the most costly.

In the second row, temperate climate, the difference between the four models in the total cost goes down a bit than it does in the cool climate. The Sides model has the lowest total cost of all the models, while the Central model moved from third position (in cool climate) to the second rank in this climate. The Half Sides model remains the most costly in this climate as well. Similarly we note the behavior of the total cost in the arid climate with a slightly higher cost.

In the case of the tropical climate, the Sides model remains the best, the Central model deserves second, the Edge third, and the Half Sides fourth. We note here (in this climate) that the total cost for each individual model is the largest compared with other regions; the reason is because the unit cost of the electricity energy is high in this climate, so its affect continues to appear in the total cost.

As previously, to visualize the difference in the cost for the life span of 50 years, we estimate how many years will have financial gain using these configurations comparing to the total cost in the Central configurations, see Figure 6.3. As can be seen in the cool climate, the total cost that is needed for Central configuration of 50 life-

spans would be sufficient to the Sides configuration for the same life-span period in addition to a period of 13.5 years; it would be in addition to 1.7 years if we use the Edge configuration. On the other hand, the total cost that is needed for Central configuration of 50 life-spans would be sufficient to Half Sides configuration only for 43.5 years, which means we need more finance to operate the Half Sides than the finance needed for the Central configuration.

In case of the temperate and arid climate zones, using the Sides configuration will save cost for about 10 years extra than if we use the Central configuration. Oppositely, we will need more finance if we use the Edge and the Half Sides compared to the Central configuration. The case of the tropical climate is similar but the cost saving between best configuration (Sides) and the second option (Central) gives 5.8 years extra if we use the best configuration. Otherwise, the other two configurations (Edge and the Half Sides) do not make it for a 50 years life span.

6.3.1 Summary of the cost estimating

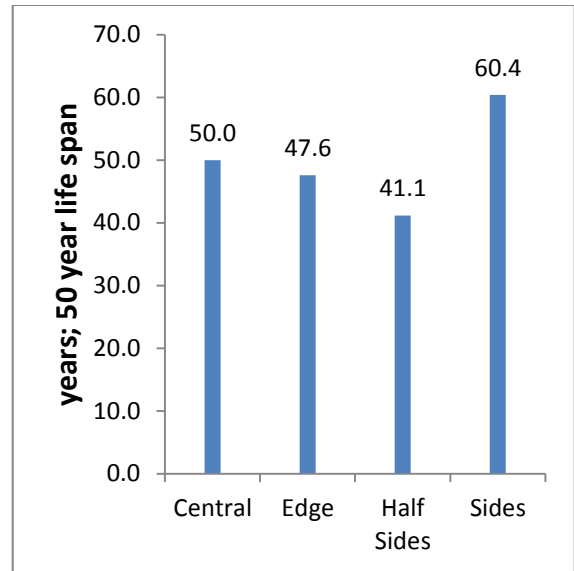
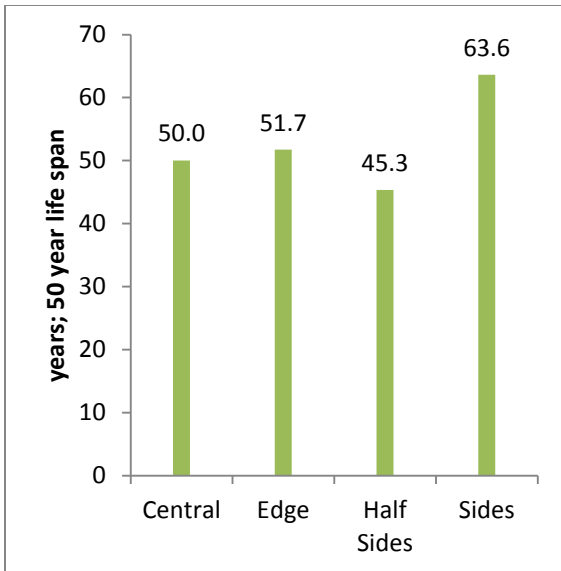
We obtained four major conclusions regarding cost estimating:

- 1) The results obtained for all individual cost estimating (operational energy , embodied energy, and material used) suggest that serious financial saving can be achieved as soon as the adoption of the Sides configuration takes place in all climate zones.

Table 6.4 Summation all costs operational, embodied energies and material for fifty years life span

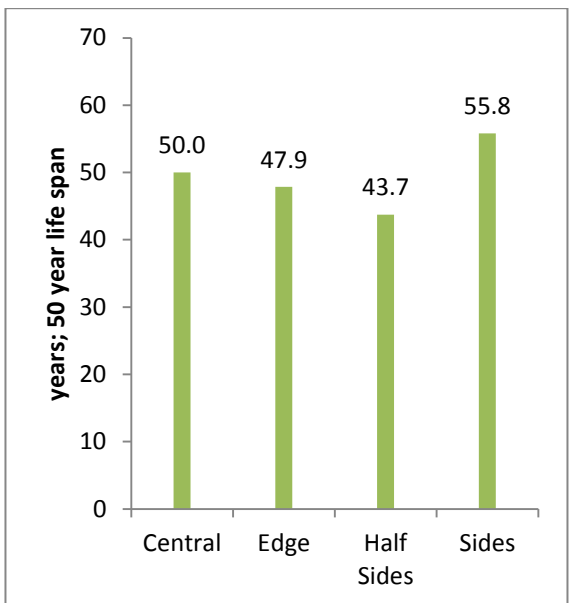
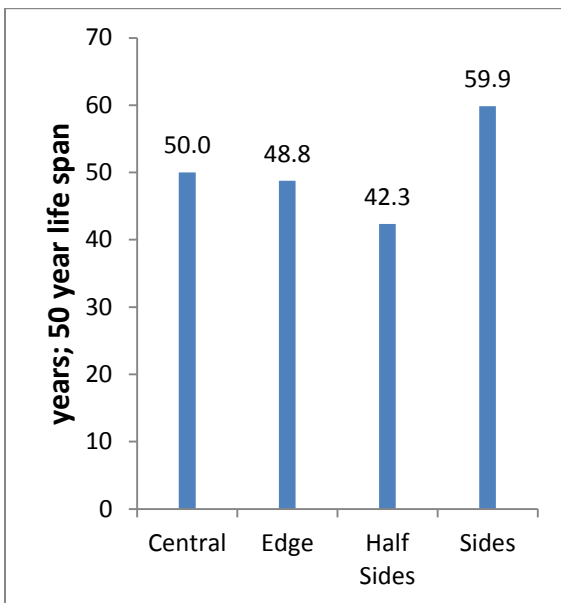
Climate	Total cost (Operational & Embodied energies cost and Material cost) \$				Cost Difference (Min. & Max)			
	Central	Edge	Half Sides	Sides	Money Difference \$		Money Difference %	
					Min	Max	Min	Max
Cool	123,809,515 	119,694,263 	136,572,398 	97,328,668 	22,365,595	39,243,730	23	40
Temperate	81,772,262 	85,890,481 	99,412,401 	67,689,155 	14,083,107	31,723,245	21	47
Arid	95,588,800 	97,986,915 	112,871,992 	79,839,888 	15,748,912	33,032,104	20	41
Tropical	140,099,572 	146,308,779 	160,139,579 	125,560,081 	14,539,492	34,579,498	12	28

■ Operational energy
 ■ Embodied energies
 ■ Material



Cool

Temperate



Arid

Tropical

Figure 6.3 Financial comparison of the total cost for a 50 years life span with respect to the Central configuration

2) The statue of the morphology in the Edge configuration gave him a good opportunity (the second rank for all climate zones) to conserve energy consumption, but the tradeoff was too great for both the structural performance and the material used and embodied energy. The main reason was because the potential irregularity in the rigidity caused substantial materials cost, which is reflected negatively on the final cost.

3) Unlike the scenario with the Central configuration, the state of the morphology gave him the worst case in terms of the energy consumption, but when we add up all costs for the 50 year life span, this model become the lowest cost after the Sides model for the temperate, arid, and tropical climate zones, while barely in the cool climate.

An observation: in the case of the Central configuration we can obtain a significant reduction on the total cost through the given ability to improve its energy performance (see section 4.4 and Appendix B).

Placing the structural cores and the manipulation with the building morphology to improve operating energy efficiency sometimes is wise approach (as in the case of the Sides configuration), but in other times the tradeoff for the structural performance too expansive (like in the case of the Sides configuration).

CHAPTER 7

SENSITIVITY OF ENERGY DEMAND TO BUILDING FOOTPRINT ASPECT RATIO AND BUILDING ORIENTATION

7.1 Introduction

Global warming and climate change are major challenges facing the nation and the world. More than two thirds of the electricity energy and one third of the total energy in the US are used to heat, cool, and operate buildings [42], representing roughly 18% of all U.S. CO₂ emissions in that year. A reduction in building energy consumption will help to mitigate the energy security and climate change impacts of buildings. The reduction in energy use may translate to a financial savings that can be achieved through the development of new technologies (for the building's envelope, mechanical, and lighting systems) that save energy and reduce CO₂ emissions. The benefit to the building owner is lower monthly utility expenses, and smaller less expensive HVAC equipment. Building energy codes are intended to promote energy efficiency by specifying minimum material, mechanical and construction standards [43].

An alternative approach is the use of passive systems that employ renewable energy sources. Passive systems avoid the need for heating or cooling through better design, construction, and operation. They utilize solar or wind energy to heat, cool, or light buildings.

Therefore, in this chapter we analyze the sensitivity of energy demand to two parameters of passive design related to building layout and site. The key parameters we investigate are building footprint aspect ratio and the building orientation that have

been considered important factors in passive design [1]. Four high-rise office buildings (glazed curtain wall) with four different aspect ratios (1:1, 1:2, 1:3, and 1:4) are thermally analyzed in four climate zones: cool, temperate, arid, and tropical. Energy demand is calculated for each model with respect to two opposing orientations (Figure 7.1). The four high-rise buildings are modeled to meet International Energy Conservation Code (IECC) 2009 requirements, which reference several American Society of Heating, Refrigeration, and Air Conditioning Engineers (ASHRAE) standards, including Std. 90.1 for commercial building construction [6].

In the following sections we describe the analytical method and the primary variables that will be measured against energy use in the four modeled buildings. We then summarize the results for each of the thirty-six scenarios and present the conclusion.

7.2 Building Materials and Method

Four models of high-rise office buildings are considered in this study to evaluate the sensitivity of energy demands to variations in: (1) footprint aspect ratio (1:1, 1:2, 1:3, and 1:4), and (2) building orientation. Since our goal is to isolate the influence of building site layout planning on energy demand, all other buildings descriptors such as the square footage, number of stories, building height, and occupancy for the four buildings are held constant across all four buildings. Specifically, we treat the thermostat range, internal design conditions, occupancy, infiltration rate, and hours of operation as fixed control variables (Table 4.3). The four buildings are 200 meters in height, 50 stories

that are 4.0 m floor-to-floor height, with a total conditioned floor area of 135,000 square meters.

The primary material for the envelope is a glazed curtain wall, which comprises of double pane standard glass with 10% metal framing. The floors are composed of layers of 10mm ceramic tiles, 5mm screed, 100 mm normal concrete, insulation (as needed to meet the R-value specified for a climate according IECC 2009), 50 mm air gap, and 10 mm plaster underneath (see Table 4.1).

To simplify the thermal analysis, we have neglected the effect of surrounding buildings, in essence assuming that the buildings are erected on flat open ground and are aligned with the cardinal directions.

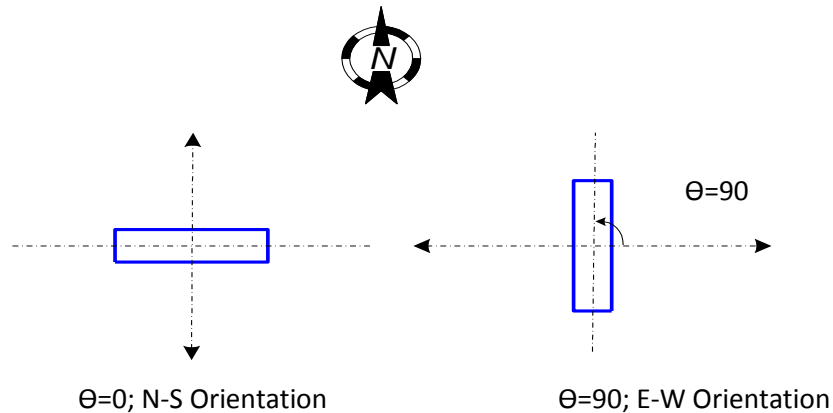


Figure 7.1 Building orientation considered in this study

The four buildings are simulated in each of the four major climate zones and as previous we have selected specific cities to represent each climate zone: Boston, Massachusetts for the cool zone, Sacramento, California for the temperate zone, Las

Vegas, Nevada for the arid zone, and Honolulu, Hawaii for the tropical zone. Building envelope materials are selected for all four models to meet the requirements of thermal properties of IECC 2009, corresponding to each climate zone.

7.3 Analytical Approach:

Autodesk's Ecotect energy simulation package was used for the thermal analysis. As previous the building geometry was prepared in Revit 2010, and then imported as surfaces and rooms to Ecotect 2011. In Ecotect, thermal properties are assigned to the envelope. The basic material of an element (floor, roof, glazing wall, etc.) is assigned first, the thermal properties of element and the insulation is then applied according to specifications of IECC 2009. The next step is to assign a weather file that corresponds to the climatic zones selected for this study and to provide occupancy and scheduled usage data. Finally, the program calculates monthly and annual heating and cooling loads according to the prescribed conditions.

7.3.1 Thermal analysis

The thermal analysis involves examining each of the four models (1:1, 1:2, 1:3, and 1:4) in each of the four climatic zones (cool, temperate, arid, and tropical). For each climate zone, weather data (TMY files) for each city is loaded and the four models are tested under equivalent interior thermal and schedule conditions. That is, the only differences among the four runs in the same climate zone are the building width to length ratio (aspect ratio) for one orientation at a time.

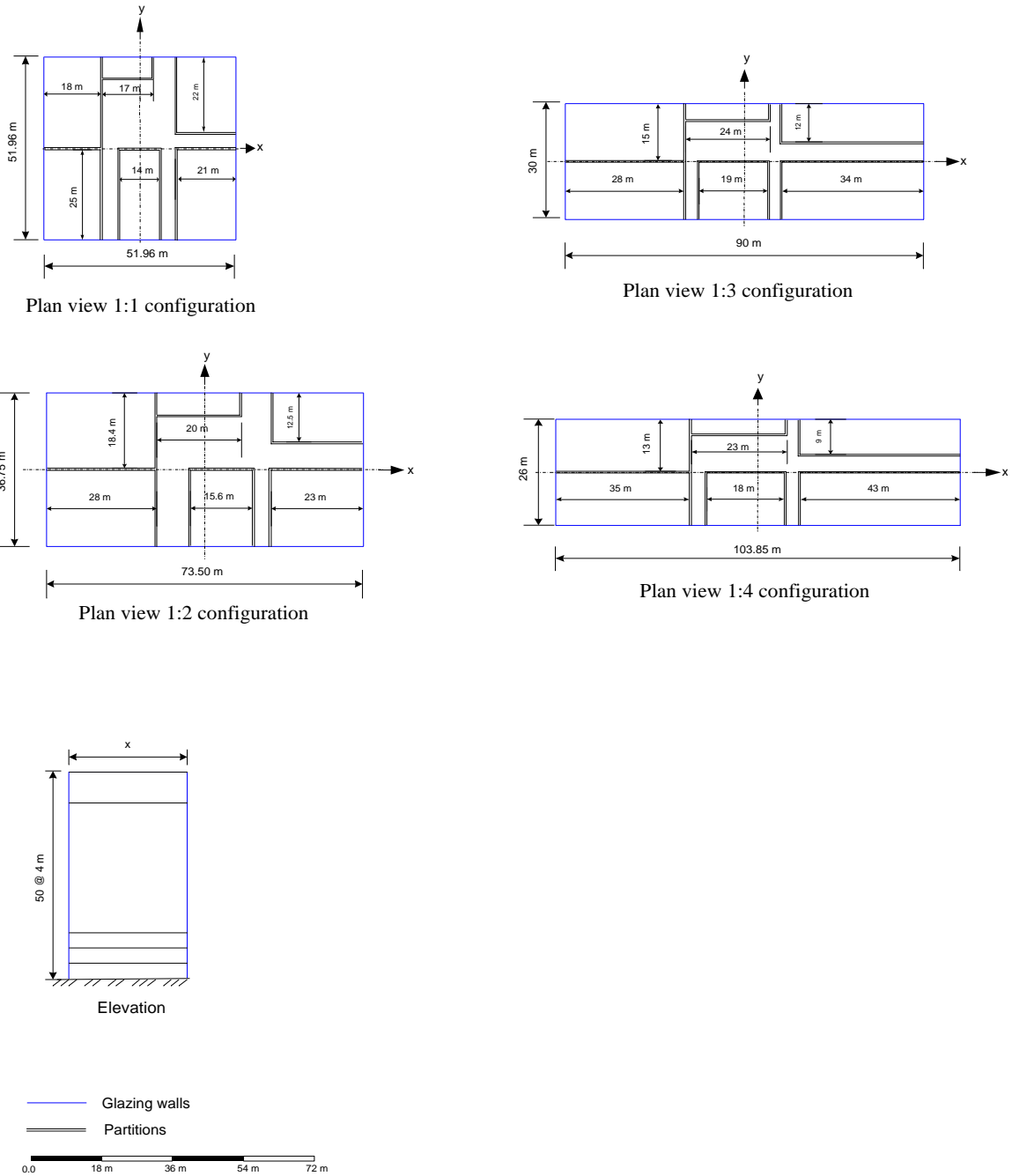


Figure 7.2 Building plan view and envelope thermal properties

Ecotect calculates the overall heat gain/loss; and then with choose the way the comfort zone is calculated for each day of the year. We use the Flat Comfort Bands method, which sets upper and lower limits for comfort temperatures. If the internal zone

temperature is either above or below the temperature limits for the prescribed comfort zone, then thermal environmental conditions are unacceptable to a majority of the occupants within that space. Factors that determine thermal environmental conditions are temperature, thermal radiation, humidity, air speed, and personal factors such as activity and clothing. Environmental factors are influenced by: 1) Direct solar gain, or radiant flow through transparent surfaces; 2) Internal (sensible) heat gain from lights, people, and equipment; 3) Conductive heat flow through opaque (envelope) elements; 4) Radiant flow through opaque (envelope) elements; 5) Ventilation and infiltration heat flow through cracks and openings; 6) Inter-zonal heat flow between adjacent zones, which for this analysis is negligible. Conductive and radiant flows through opaque elements are treated together and described as “Fabric” in Ecotect. Personal factors such as activity (metabolic rate) and clothing (insulation of clothing) are treated as constant for all building occupants.

In this study there are two main stages of the thermal analysis. The first stage is to find the sensitivity of the energy demand (heating and cooling loads) to the change of the surface area ratio (SAR), which relates to floor-plan aspect ratio:

$$SAR = \frac{(floor\ perimeter \times floor\ height)}{floor\ plan\ area} \dots \dots \dots (7.1)$$

This analysis consists of thirty-two different simulation runs (of four models in two orientations in four climate zones = 4×2×4), where annual cooling and heating loads are calculated for each model. The results corresponding to the N-S orientation are provided in Table 7.1; and the difference in the total energy demand between the N-S and E-W orientations is not significant, as shown in Figure 7.3. Using the model of 1:4

aspect ratio as an example, the monthly and yearly energy demand ratios (EDR) for each of the four climate zones are shown in Table 7.2.

$$EDR = \frac{\text{energy demand of East – West orientation}}{\text{energy demand of North – South orientation}} \dots \dots (7.2)$$

Also the passive solar heat gain ratio (PSHGR) of the model of 1:4 aspect ratio is displayed in Figure 7.4. Moreover, the total heat gain and heat gain ratio (HGR) of the month of July are broken down into individual sources of direct (solar) gain, internal gain, fabric, and ventilation. Table 7.3 presents the percentage of each of these heat sources and how they vary by orientation. The total energy demand for each orientation are not significantly different, even though the E-W oriented models have a much higher potential for passive solar heat gain.

The next stage of the thermal analysis investigates why the differences in the energy demand are negligible. One possible reason maybe is because of the thermal properties of the IECC 2009 envelope. In the initial analysis, the glazing walls were modeled with U-factors and SHGC set according to the regional climate. These walls were subsequently modeled using single-pane glazing, which has inferior thermal properties ($U=6.0 \text{ W/m}^2\text{K}$ & $SHGC=0.94$). The simulation was run again to evaluate the total energy demand for each of the two orientations. The results of the new simulation runs show that buildings oriented E-W require 12% more energy than those oriented N-S, and that the passive solar heat gain in July is significantly increased.

7.3.2 Demand sensitivity–glazing walls built to code

For each building in the climate zones of Cool, Temperate, and Arid, the change in energy demand is slightly significant, where by increasing the surface area (up to 20%), energy demand is increased by 5.1-7.9% (table 7.1) depending on the climate zone. In the tropical climate, however, the energy demand is insensitive to the variations in SAR, where the average increment percent is 0.4% and the total increase is 0.84%.

Of course, an increase in the surface area (SAR) is likely to lead to an increase in the materials used, may impact construction costs and embodied energy. Furthermore, increases in the surface area may result in an increase in the area exposed to wind pressure, which might lead to the need of a larger size of structural element, which also impact construction costs and embodied energy.

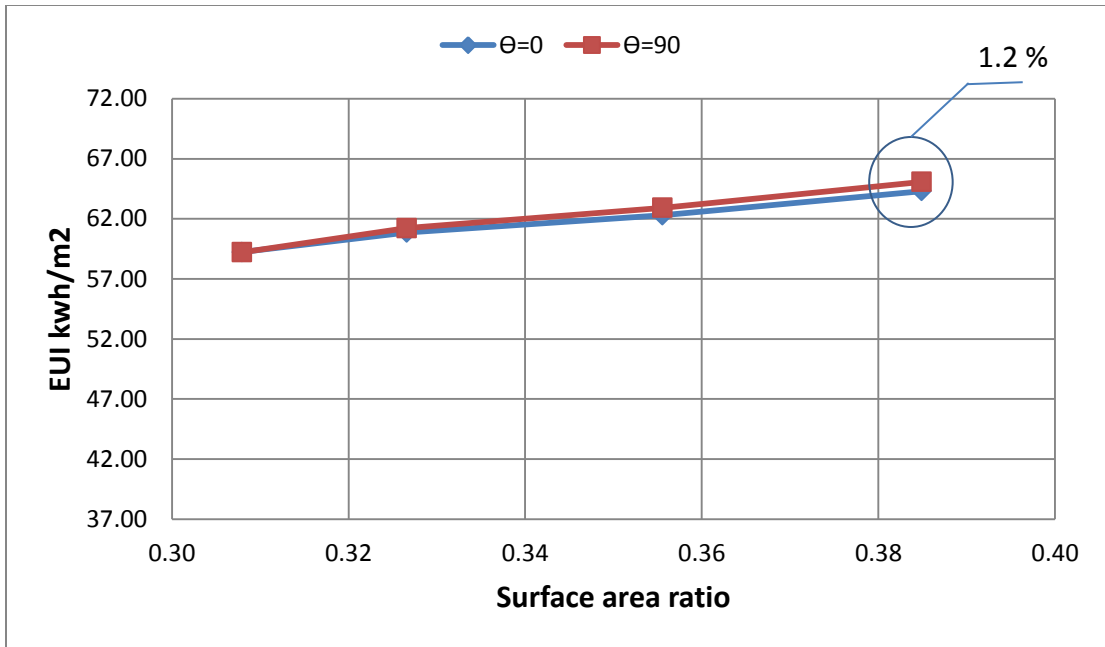
The differences in the total energy demand for two building orientations (N-S & E-W) in each climate zone are nearly negligible (see Figure 7.3). The horizontal axis represents the SAR corresponding to the four building's aspect ratios (1:1, 1:2, 1:3, and 1:4), while the vertical axis represent EUI.

These small differences in EUI raise questions about the results presented in Figure 7.4, where the monthly breakdown shows solar heat gains and losses resulting from building oriented E-W are much greater than if the building were oriented N-S. The sources of total energy demand for the month of July are presented in Table 7.3, and it is clear that the influence of solar loads is small compared to internal, fabric, or ventilation loads.

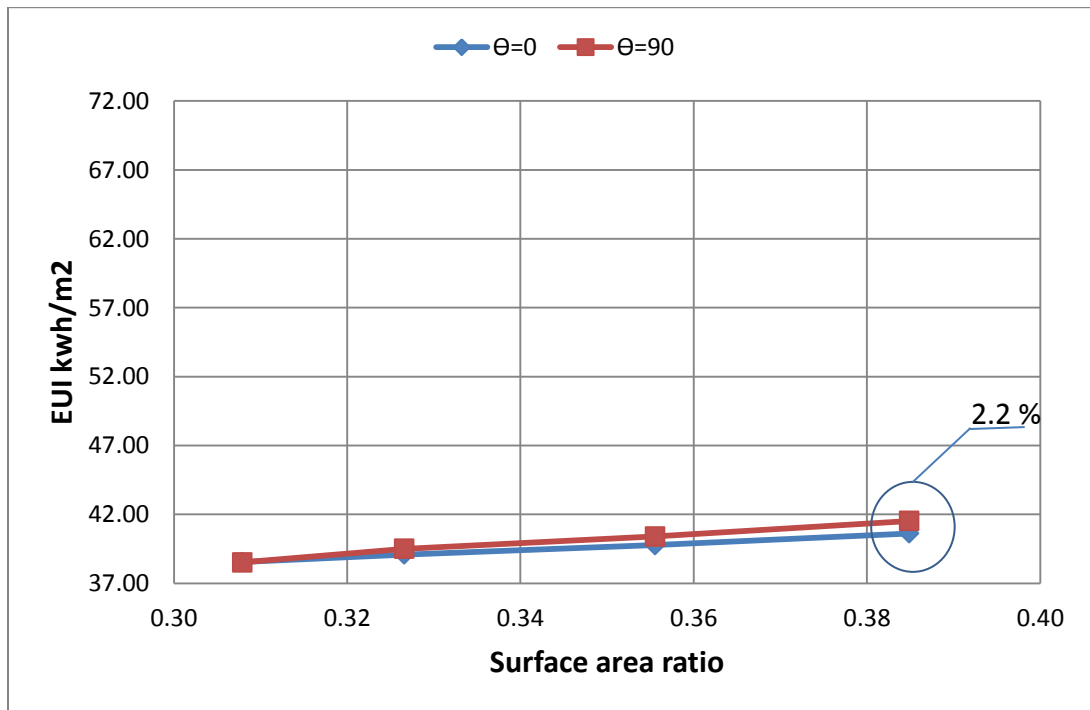
Table 7.1 Energy demand verses SAR (N-S orientation)

Width to length ratio - increase in SAR												
Type	1:1			1:2			1:3			1:4		
	Heating	Cooling	EUI	Heating	Cooling	EUI	Heating	Cooling	EUI	Heating	Cooling	EUI
Climate	kwh/m ²			kwh/m ²			kwh/m ²			kwh/m ²		
Cool	49.8	9.4	59.2	51.9	9	60.9	53.6	8.7	62.3	55.9	8.4	64.3
Temperate	7.9	30.7	38.55	8.4	30.7	39.1	8.9	30.8	39.8	9.7	31	40.6
Arid	5.8	57	62.8	6.1	57.9	64.0	6.5	59	65.5	7	60.4	67.4
Tropical	0.0	62.5	62.5	0.0	62.75	62.6	0.0	63.4	63.4	0.0	64.1	64.1

EUI: Energy Use Intensity

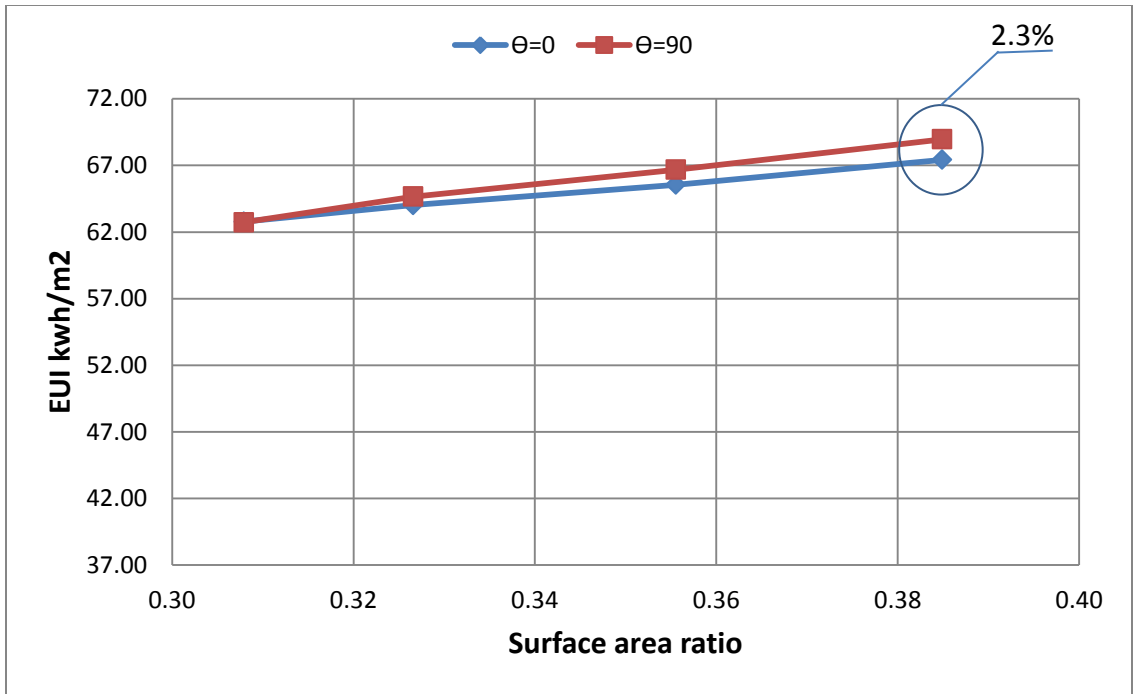


Cool

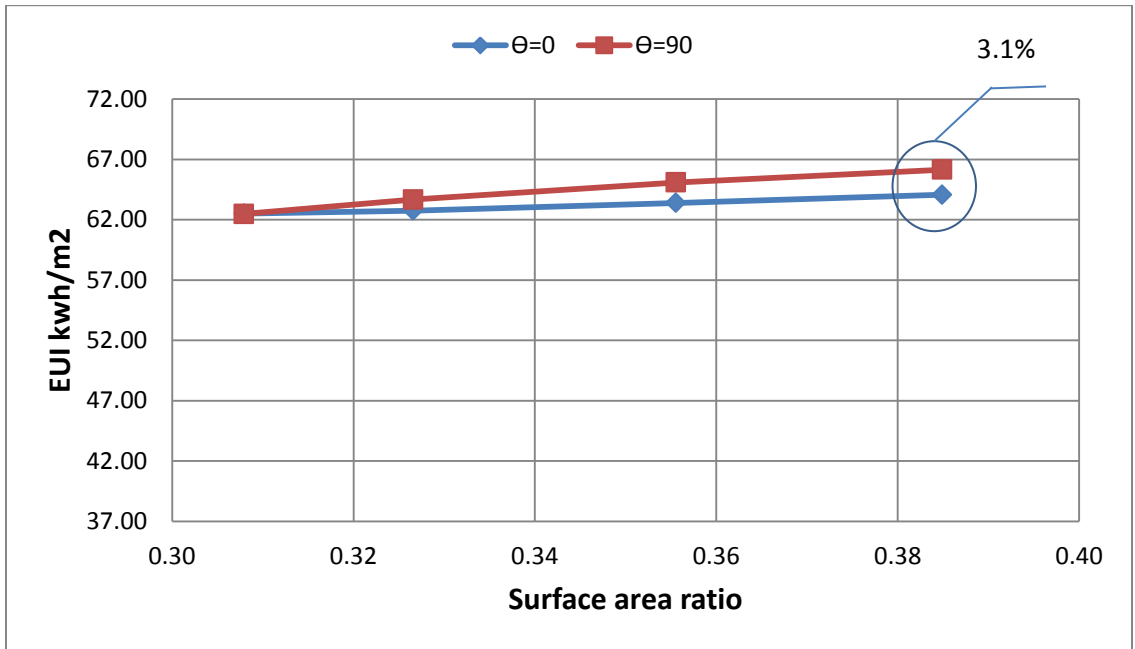


Temperate

(Continue)



Arid



Tropical

Figure 7.3 Sensitivity of EUI to the change in surface area ratio

The amount of heat gain from passive sources represents 5-20% of the total heat gain. This is consistent for both orientations, and the effect is trivial compared to the total heat gain.

7.3.3 Demand sensitivity with non-code-compliant glazing on walls.

The second stage of thermal analysis is an investigation of the sensitivity of built-to-code glazing systems on passive solar heat gain, compared to single-pane glazing, which has poorer thermal properties. The outcome demonstrates that code requirements for glazing systems results in reductions in direct heat gain to become represent 5% rather than 24% of total heat gain(N-S),while become represent 8% rather than 34% of total heat gain(E-W), (Table 3 & Table 5 for arid climate). Code-built glazing also reduces total energy demand by 12%, which also explains why there is such a small effect from varying building orientation on monthly and yearly energy demand.

Table 7.2 Energy demand ratio, EDR, (model of 1:4 aspect ratio)

Months	Energy demand ratio (EDR)			
	Cool	Template	Arid	Tropical
Jan	1.01	1.01	1.03	0.96
Feb	1.01	1.02	0.97	0.99
Mar	1.01	0.99	0.99	1.05
Apr	0.99	1.02	1.04	1.07
May	0.97	1.04	1.05	1.06
Jun	0.99	1.04	1.03	1.05
Jul	1.011	1.034	1.026	1.055
Aug	1.02	1.02	1.02	1.05
Sep	1.00	0.99	1.01	1.03
Oct	1.01	0.98	0.99	1.01
Nov	1.02	1.00	0.99	0.99
Dec	1.02	1.02	1.03	0.97
yearly	1.01	1.02	1.02	1.03

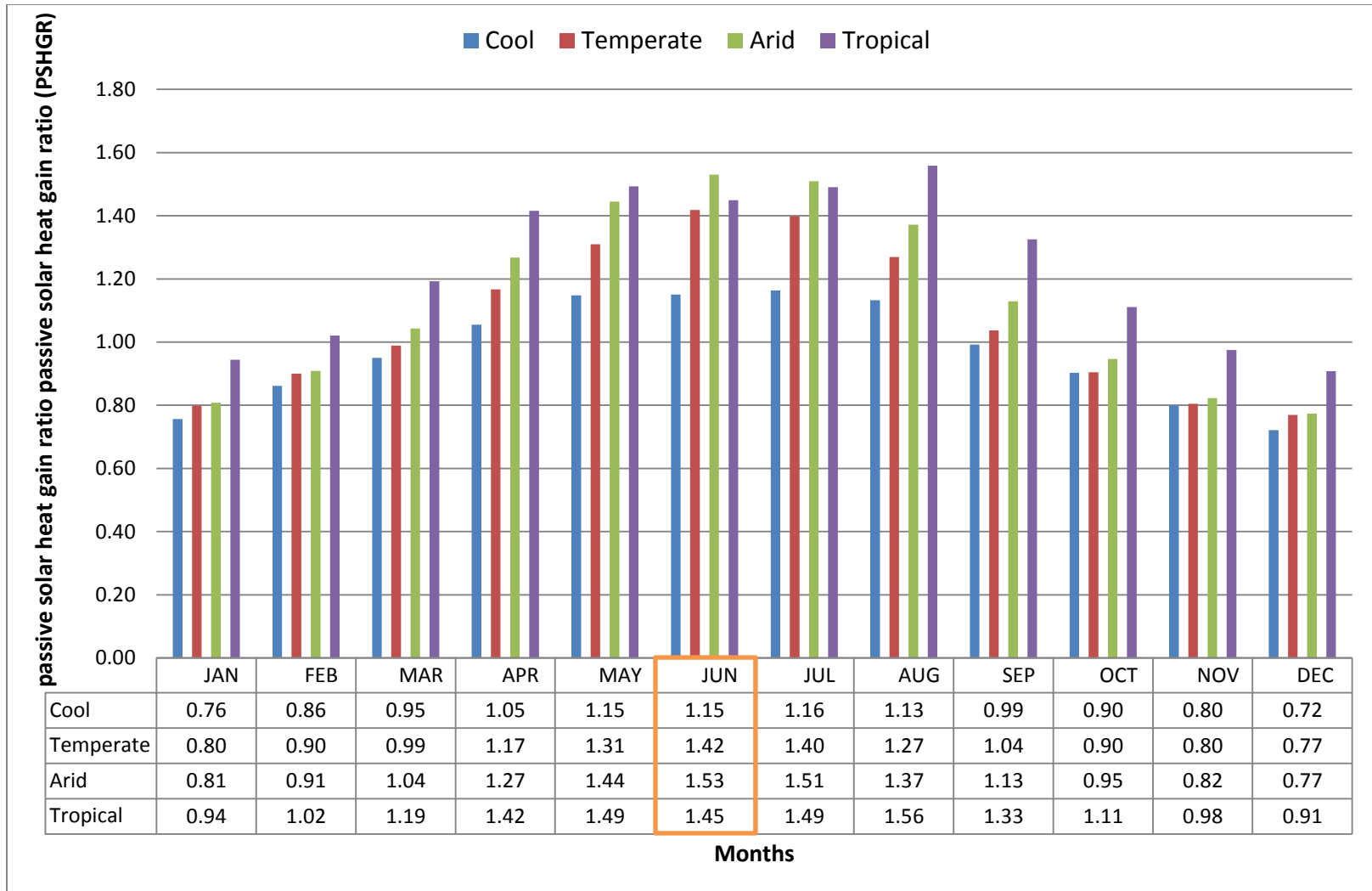


Figure 7.4 Monthly passive solar heat gain ratio (model of 1:4 aspect ratio)

Table 7.3 Sources of heat gain (Wh) in July- built to code envelope (model of 1:4 aspect ratio)

Climate	Cool					Temperate				
Orientation	θ=0		θ=90		July HGR	θ=0		θ=90		July HGR
Direct	1.1E+08	17%	1.3E+08	20%	1.16	1.1E+08	8%	1.5E+08	11%	1.40
Internal	5.1E+08	78%	5.1E+08	75%	1.00	5.1E+08	40%	5.1E+08	38%	1.00
Fabric	2.1E+07	3%	2.3E+07	3%	1.11	2.8E+08	22%	2.9E+08	22%	1.02
Ventilation	1.3E+07	2%	1.3E+07	2%	1.00	3.8E+08	30%	3.8E+08	29%	1.00
Total	6.573E+08		6.783E+08		1.032	1.277E+09		1.325E+09		1.038
Climate	Arid					Tropical				
Orientation	θ=0		θ=90		July HGR	θ=0		θ=90		July HGR
Direct	1.1E+08	5%	1.6E+08	8%	1.51	9.9E+07	10%	1.5E+08	14%	1.49
Internal	5.1E+08	25%	5.1E+08	24%	1.00	5.1E+08	50%	5.1E+08	47%	1.00
Fabric	6.1E+08	30%	6.2E+08	29%	1.01	2.2E+08	21%	2.3E+08	21%	1.05
Ventilation	8.3E+08	40%	8.3E+08	39%	1.00	2.0E+08	19%	2.0E+08	18%	1.00
Total	2.068E+09		2.129E+09		1.03	1.029E+09		1.087E+09		1.057

Table 7.4 Breakdown heat gain (Wh) in July in Arid climate – regular glass envelope
(model of 1:4 aspect ratio)

	Heat gain (Wh)				July HGR
	$\theta=0$		$\theta=90$		
Direct	7.4E+08	24%	1.2E+09	34%	1.62
Internal	5.1E+08	16%	5.1E+08	14%	1.00
Fabric	1.0E+09	33%	1.0E+09	29%	1.01
Ventilation	8.3E+08	27%	8.3E+08	23%	1.00
Total	3.099E+09		3.564E+09		1.15

7.3.4 Summary of results

By simulating each building configuration using Autodesk’s Ecotect, we can draw two major conclusions regarding building energy demand:

(1) For the buildings in Cool, Arid, and Temperate climate zones, the energy demand may be considered marginally sensitive to changes in surface area ratio (SAR). Increasing the envelope surface area by 20% leads to energy demand increases of 5.1-7.9% depending on the climate zone. The energy demand for buildings in the Tropical climate zone is insensitive to variations in SAR.

(2) The energy performance of high-rise office buildings is not sensitive to the passive solar gain as long as the exterior envelopes are built to IECC 2009 requirements for thermal performance.

CHAPTER 8

CONCLUSIONS AND RECOMMENDATIONS AND FUTURE WORK

8.1 Conclusions

The energy performance of a high-rise office building is highly impacted by its morphology. This study proves that building configuration (footprint shape and the placement of structural vertical core/walls) significantly influences overall energy performance. Furthermore, placement of the structural vertical core/walls in the east and west sides and building footprints with an aspect ratio of 1:3 (Sides configuration) lead to significant reduction in the energy demand in the four major climatic zones.

Significant improvements in energy performance can be gained by adding opaque surfaces in the Central configuration envelope (thermal analyses EPO and EDO). Moreover, envelopes with more opaque surfaces increase the opportunity for placing the structural elements so as to avoid the asymmetrical distribution, which would lead to improving the structural performance without compromising energy performance.

It is often noted that the thermal mass contributes to reductions in building energy consumption, and concrete materials have good thermal mass properties. However, in this study, we do not obtain the expected result of improving the energy performance (where increasing thermal mass material by 100%, the energy demand changed by around 0.5%) by increasing the amount of thermal mass in the building envelope.

In the case of the sides configuration placing the structural cores to improve the operating energy efficiency works well without compromising the structural

performance; it is desirable to be in that place, because the placement of the shear wall along the short sides leads to reduce the impact of the torsion displacement, resulting in relatively less quantity of structural material, and then less embodied energy and cost.

The state of the morphology in the Edge configuration gave it a good opportunity (the second rank for all climate zones) to conserve energy consumption, but the tradeoff was too great for both the structural performance and the material used embodied energy. The main reason was because the potential irregularity in the rigidity, which caused a substantial growth in materials cost that reflected negatively on the final cost.

Finally, high quality thermal properties of code-built envelope systems offer more flexibility to designers with regard to the building site planning (geometry, layout, and orientation) without creating negative impacts on total energy demand. On the other hand, this limits the possibility of maximizing the advantages of passive heat gain. And, because built to code buildings are not significantly sensitive to direct solar gain, it leaves little room for other passive design strategies for energy conservation such as shading devices, landscaping, and thermal mass.

8.2 Recommendations

As we have found, in the case of the Central configuration, adding opaque surfaces to the East-West sides significantly improves energy performance. Our recommendation is to consider these opaque surfaces as shear walls to optimize structural performance.

As mentioned, thermal mass is generally thought to be a good way to reduce overall energy demand, though our study indicates otherwise. Our recommendation is to investigate new opportunities to take advantage of the presence of the thermal mass. We can start by investigating the effective thickness, investigating the effect of the insulation on the thermal mass, and investigating the relationship between the thermal mass exposed surface and the insolation, etc.

Making good use of natural light reduces the need of artificial lighting and helps provide a feeling of well-being to office workers. Buildings are lit by a combination of daylight entering through windows and skylights and electric-light sources. Maximizing the use of natural light is a very important element in the sustainable design. One of the objectives of the envelope with glazed curtain walls is to use the natural lighting. Also, in some cases the shape of the building is designed so natural daylight reduces the need for artificial lighting. Therefore, our recommendation is to include the effect of natural lighting on the energy demand for the given buildings' morphologies.

8.3 Future work

Based on the conclusions, positioning the opaque surfaces on the East-West sides significantly improves energy performance for two building configurations (the Sides and the Central), and also the placement of these opaque surfaces made for the structural purposes is highly desirable (to reduce torsional displacement under lateral loading).

Thus, the first future work would focus on optimizing each of these configurations (the Sides, the Central) for each of the four climate zones. This optimizing should

consider energy and structural performances, trade-off between the cost of the high performance envelope versus the increased the energy performance.

Second future work would find out how the structural performance of these two configurations would change, if the building height is increased and how this affects the total cost (energy and material) for a given building life span.

Third future work would include a finance comparison between use insulation material and use of thermal mass, which inherently have a good characteristic of thermal insulation; taking into account the embodied energy for both the insulation and thermal mass materials.

Lastly, investigate how the energy demand would change if the system type is Mixed-Mode System (rather than a full Air-conditioning system), which is a combination of air-conditioning and natural ventilation. This investigation may require changes in the building morphologies for natural ventilation; the latter may possibly affect the building structural performance.

APPENDIX A

PRELIMINARY ANALYSIS

A.1 Preliminary structural walls analysis

A preliminary investigation is made to find out for each model what height the current lateral resistance systems can likely withstand under the wind loads. The approach here is to calculate the maximum bending and torsion stresses and the maximum disablement on the walls, and then compare them with the limits. The limits here are maximum bending stress is $0.3F'_c$, where F'_c is the compressive strength for normal weight concrete (28 Mpa), displacement $\frac{\Delta}{h} \cong \frac{1}{500}$ [29], where Δ is the lateral drift, and h is the wall height, and maximum torsion stress is $0.33\sqrt{f'_c}$. Based on ASCE 7-10, wind loads have been calculated for each model (Sides, Edge, Half Sides, and Central).

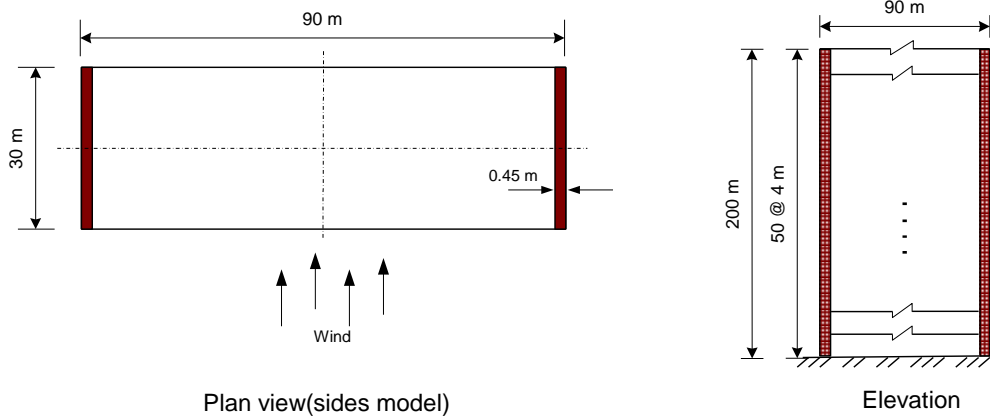
A.1.1 Wind Loading: Calculation Example

Sides model use here as calculation example that illustrates the procedure for calculating the wind load. Plan view and the building elevation are shown below. Based on the expression in ASCE 7-10 Eq. (27.3-1) the velocity pressure is given by.

$$q_z = 0.613 k_z k_{zt} k_d V^2 \text{ (n/m}^2\text{)} \dots \dots \dots (A.1)$$

Where q_z is the velocity pressure, V is the basic wind speed at 10m height, k_d is the directionality factor, k_{zt} is the topographic factor, and k_z is the exposure coefficient. Based on Tables 1.5-1, 26.6-1, and Figures 26.5-1A, 26.8-1 in ASCE 7-10 the parameters are assigned values of: $k_{zt}=1$; $k_d=1$; and for risk category II the basic wind speed $V=58$

m/s (130 mi/h), Boston region. The exposure coefficient (according to Table 27.3-1 in ASCE 7-10) given by.



Sides model plan view and elevation

$$k_z = 2.01 \left(\frac{z}{z_g} \right)^{2/\alpha} \quad 15 \text{ ft.} \leq z \leq z_g \dots\dots\dots (A.2,a)$$

$$k_z = 2.01 \left(\frac{15}{z_g} \right)^{2/\alpha} \quad z \leq 15 \text{ ft.} \dots\dots\dots (A.3,b)$$

Where α is the power law coefficient, z_g is the nominal height of boundary layer; from the Table C26.7-12 in ASCE 7-10 the parameters are assigned values of: $\alpha=7.0$; $z_g=366$.

Given all these values for the velocity pressure parameters, the wind pressure is.

$$q_z = 2062 k_z \dots\dots\dots (A.4)$$

At this point the velocity pressure is determined; now calculate the design wind load, which is based on the expression (ASCE 7-10 Eq. (27.4-1)).

$$P = q_z G C_p - q_h (G C_{pi}) \dots\dots\dots (A.5)$$

Where P is the design wind pressure, G is the gust effect factor, C_p is the external pressure coefficient, q_h is the velocity pressure evaluated at height $z = h$, and $G C_{pi}$ is the topographic factor. Based on Tables 26.11-1, and Figure 27.4-1, in ASCE 7-10 the parameters are assigned values of: $G C_{pi} = \pm 0.18$; $C_p = 0.8$ in windward wall, -0.5 in leeward wall, and -0.7 in sides walls. The gust effect factor assumed to be $G=0.92$. Given these values for the design wind pressure parameters:

$$P = 1897k_z C_p \pm 628 \dots\dots\dots (A. 6)$$

The figure below shows the pressure loading that are obtained from Eq.(A.6) with using the calculated values of k_z by Eq.(4.8). So the lateral- force resistance system must resist this loading, which wind blows on the front or rear of the building.

A.1.2 Stresses and Displacement: Calculation Example

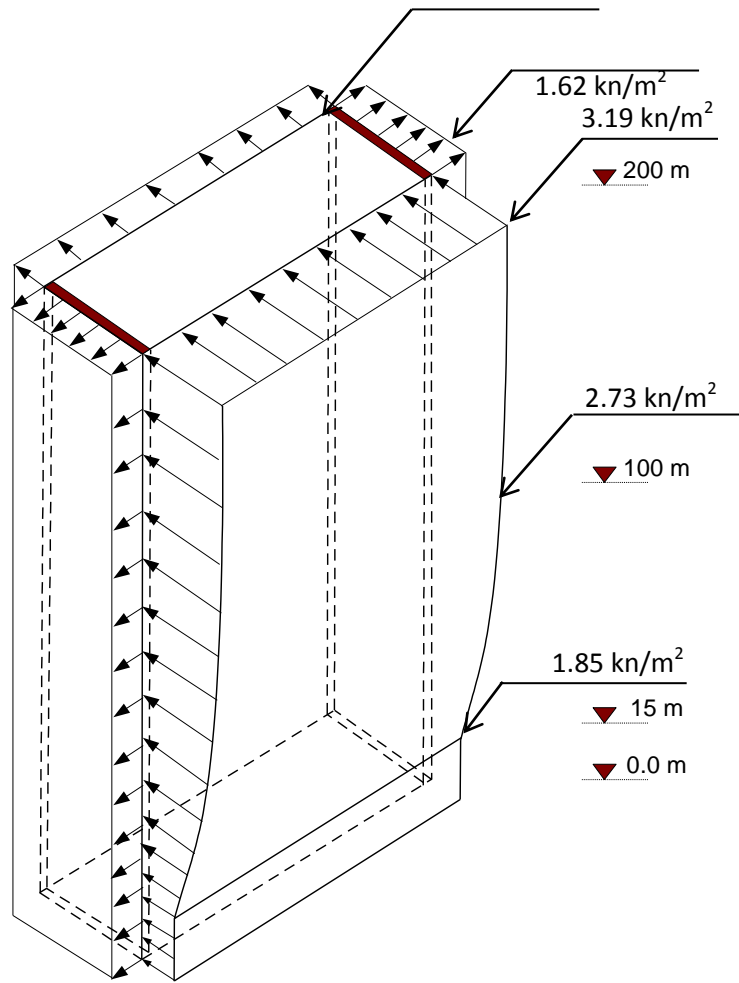
We assumed the wind load has a trapezoidal distribution. Based on beam theory approach the maximum bending stress can be calculated by flowing equation:

$$\sigma = \frac{M C}{I} \dots\dots\dots (A. 7)$$

Where σ is the bending stress, M is the maximum bending moment at the base, I is the moment of inertia of the wall cross section, and C is the perpendicular distance from compressive face to the neutral axis. The torsional stress is calculated as:

$$\tau = \frac{3T}{bt^2} \dots\dots\dots (A. 8)$$

0.97 kn/m²



Wind pressure on the building surfaces

Where T is the twisting moment per unit height acting about a vertical axis of the building. This twisting moment results from the eccentricity (e), which is assumed to be the perpendicular distance between the center of pressure of the wind load P_w and the center of rigidity (c.r) of the shear walls in floor plan.

$$T = e \times P_w \dots \dots \dots (A.9)$$

Calculating the lateral displacement at the free end, by using the following equation:

$$\Delta = \frac{w_a h^4}{8E_c I} + \frac{(w_b - w_a) 11h^4}{120 E_c I} \dots \dots \dots (A. 10)$$

Where Δ is the displacement at the free end, E_c is the normal weight concrete modulus of elasticity, h is the wall height, w_a is the wind load at point a, w_b is the wind load at point b.

Following the same steps for each model the stresses and displacements in the strongest direction of the building were calculated. The results were as following: for the Central configuration, the BSS is adequate for a height of up to 96 m with the wind load perpendicular on Y direction, or up to 76 m with the wind load on orthogonal direction. In the case of the Sides configuration, the BSS is adequate up to 100 m with the wind load perpendicular on X. In the case of the Half Sides configuration, the BSS is adequate up to 76 m with the wind load perpendicular on X. In the case of the Edge configuration, the BSS is not adequate, because of the substantially torsional stress.

A.1.2 The eccentricity e for flexible structures

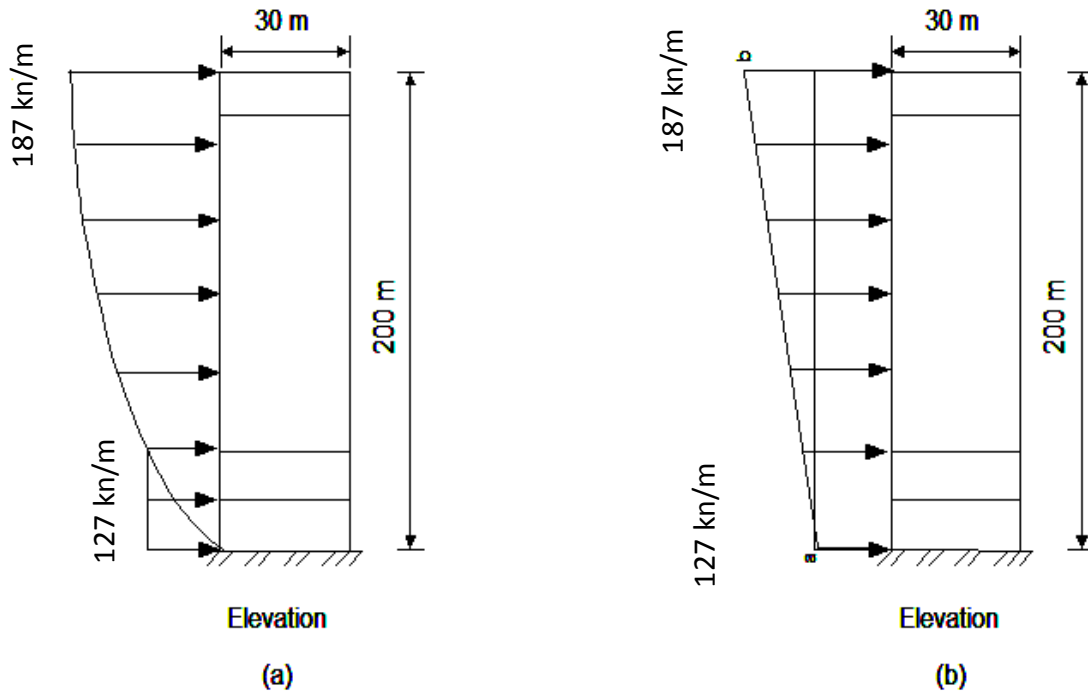
Loading in Case2 is taking into account the presence of the eccentricity e (e_x , e_y) for the x, y principal axis of the structure, respectively. This eccentricity is calculated based on the equation 27.4-5, ASCE 7-10 as following:

$$e = \frac{e_Q + 1.7I_z \sqrt{(g_Q Q e_Q)^2 + (g_R R e_R)^2}}{1 + .7I_z \sqrt{(g_Q Q)^2 + (g_R R)^2}} \dots \dots (A. 9)$$

where $e_Q = \pm 0.15 B$ as it is determined for rigid structures where B in (m); e_R in (m) is the distance between the elastic shear center and center of mass of each floor; g_Q is taken as 3.4.

$$g_R = \sqrt{2 \ln(3600 f)} + \frac{0.577}{\sqrt{2 \ln(3600 f)}} \dots \dots (A.10)$$

$$I_{\bar{z}} = c \left(\frac{10}{\bar{z}} \right)^{1/6} \dots \dots \dots (A.11)$$



Wind load: (a) Actual load distribution; (b) Trapezoidal distribution

Where $I_{\bar{z}}$ where is the intensity of turbulence at height \bar{z} where \bar{z} is the equivalent height of the structure defined as $0.6h$, but not less than z_{min} for all building

heights h . z_{min} and c are constants depend on the exposure (see table below); Q is the background response is given by

$$Q = \sqrt{\frac{1}{1 + 0.63 \left[\frac{B + h}{L_z} \right]^{0.63}}} \dots \dots \dots (A. 12)$$

where h is the height of other structure in (m); L_z is the integral length scale of turbulence at the equivalent height given by:

$$L_z = l \left(\frac{\bar{z}}{10} \right)^{\bar{\epsilon}} \dots \dots \dots (A. 13)$$

where l and $\bar{\epsilon}$ are constants listed in table below.

$$R = \sqrt{\frac{R_n R_h R_B (0.53 + 0.47 R_L)}{\beta}} \dots \dots \dots (A. 14)$$

$$R_n = \frac{7.4 N_1}{(1 + 10.3 N_1)^{5/3}} \dots \dots \dots (A. 15)$$

$$N_1 = \frac{f L_z}{\bar{V}_z} \dots \dots \dots (A. 16)$$

$$\bar{V}_z = \bar{b} \left(\frac{\bar{z}}{10} \right)^{\bar{\alpha}} V \dots \dots \dots (A. 17)$$

Terrain exposure B constants (ASCE 7-10)

	l (m)	$\bar{\epsilon}$	c	$\bar{\alpha}$	z_{min} (m)	\bar{b}
Exposure B	97.54	1/3	0.3	1/4	9.14	0.45

where \bar{V}_z mean hourly wind speed at height \bar{z} in (m/s); V is the basic wind speed in in (m/s); β is the damping ratio; \bar{b} and $\bar{\alpha}$ are constants as listed.

$$R_l = \frac{1}{\eta_l} - \frac{1}{2\eta_l^2} (1 - e^{-2\eta_l}) \quad \text{for } \eta_l > 0 \dots\dots\dots (A.18)$$

$$R_l = 1 \quad \text{for } \eta_l = 0 \dots\dots\dots (A.19)$$

$$\eta_l = 15.4f \frac{L}{\bar{V}_z} \dots\dots\dots (A.20)$$

$$R_h = \frac{1}{\eta_h} - \frac{1}{2\eta_h^2} (1 - e^{-2\eta_h}) \dots\dots\dots (A.21)$$

$$\eta_h = 4.6f \frac{h}{\bar{V}_z} \dots\dots\dots (A.22)$$

$$R_B = \frac{1}{\eta_B} - \frac{1}{2\eta_B^2} (1 - e^{-2\eta_B}) \dots\dots\dots (A.23)$$

$$\eta_B = 4.6f \frac{B}{\bar{V}_z} \dots\dots\dots (A.24)$$

where L in (m). Based on these equations, the critical cases of the eccentricities as listed for the x, y principal axis corresponding to each configuration, e (8, 8) for the Central model; (9, -13) for the Edge model; (10.14, 4.83) for the Half Sides model; and e(12.72, 3.9) for the Sides model.

A.1.3 Shear wall thickness determination

Assuming the wall thickness change about each 12-story. Based on the flexural strength, we may estimate the preliminary thickness of the shear wall along its height.

$$M_u \leq \phi M_n \dots\dots\dots (A.25)$$

where M_u is the external moment due to external loading; M_n is the nominal moment (design resisting moment at section); Φ is the strength reduction factor. M_n can be calculated as following [44]:

$$M_n = 0.5A_s f_y l_w \left(1 + \frac{N_u}{A_s f_y} \right) \left(1 - \frac{c}{l_w} \right) \dots \dots \dots (A. 26)$$

Where A_s is the total area of vertical reinforcement at section (in^2); f_y specified yield strength of vertical reinforcement (psi); L_w is the horizontal length of the shear wall (in); N_u is the axial load (lb). C is the distance from the extreme compression fiber to the neutral axis (in); $\beta_1=0.85$ for concrete strength f'_c up to 4000 psi.

$$\frac{c}{l_w} = \frac{w + \alpha}{2w + 0.85\beta_1} \dots \dots \dots (A. 27)$$

$$w = \frac{A_s}{l_w h} \times \frac{f_y}{f'_c} \dots \dots \dots (A. 28)$$

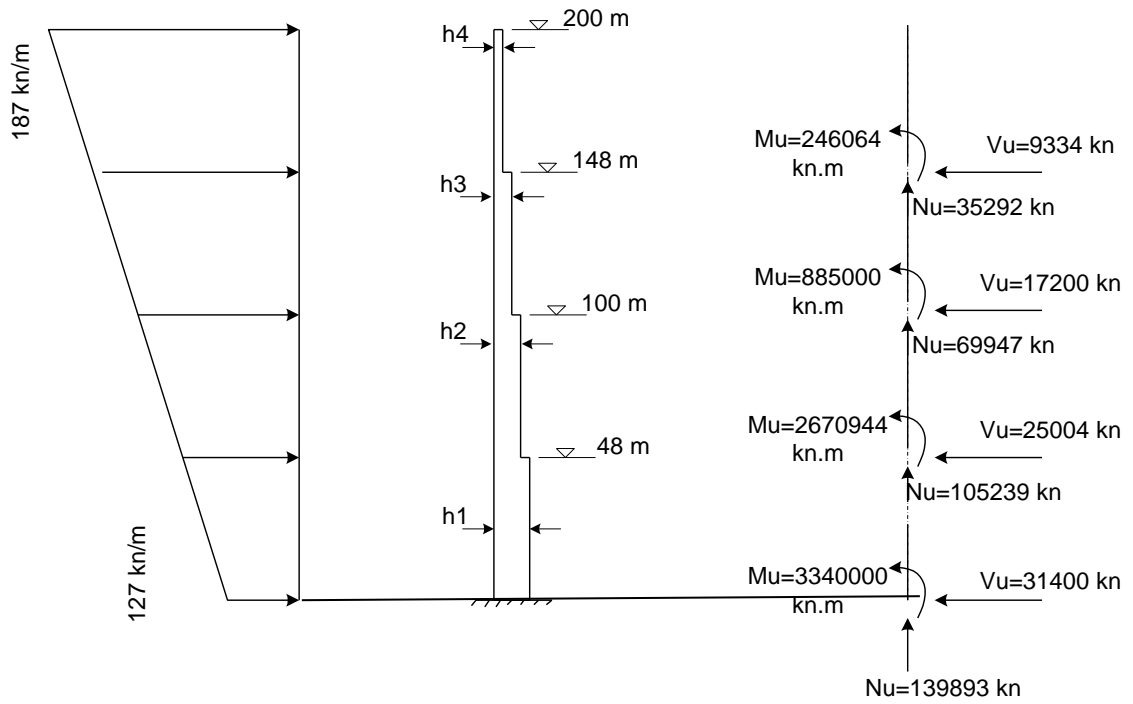
$$\alpha = \frac{N_u}{l_w h f'_c} \dots \dots \dots (A. 29)$$

A.1.3.1 Calculation example

Given the result analysis for the Sides model (For M_u and N_u); $L_w=98.4$ ft. ; $f'_c=4$ ksi; $f_y=60$ ksi; $\beta_1=0.85$; $\Phi = 0.9$; Note the gravity loads are included wall self-weight 390 kip/ft, dead load 52.63 psf, and live load 65.16 psf. Note the dead and the live loads are in each floor on tributary area of 1210 ft^2 .

To start assume wall thickness at the base is h1 = 2.952 Ft. (0.90 m)	
$\alpha = \frac{31451 \times 1000}{98.4 \times 2.952 \times 4000 \times 12 \times 12} = 0.19$	N _u =31451 kip
$w = 0.032 \times \frac{60}{4} = 0.483$	
$\frac{c}{l_w} = \frac{0.483 + 0.19}{2 \times 0.483 + 0.85 \times 0.85} = 0.312$	
$\begin{aligned} \phi M_n &= 0.9 \times 0.5 \times 1349 \times 60000 \times 98.4 \\ &\times 12 \left(1 + \frac{31451 \times 1000}{1349 \times 60000} \right) (1 \\ &- 0.312) \left(\frac{1}{1000 \times 12} \right) = 2999000 \text{ kip.ft} \end{aligned}$	As=1349 in ² (1100 #10) S=2.21 in
$\frac{\phi M_n}{M_u} = 1.22 \geq 1 \quad o.k$ Hence, use h1= 2.952 Ft. (0.90 m)	M _u = 2463309 kip.Ft
Now assume wall thickness h2 = 2.624 Ft. (0.80 m)	
$\alpha = \frac{23660 \times 1000}{98.4 \times 2.624 \times 4000 \times 12 \times 12} = 0.16$	N _u =23660 kip
$w = 0.024 \times \frac{60}{4} = 0.361$	
$\frac{c}{l_w} = \frac{0.361 + 0.16}{2 \times 0.361 + 0.85 \times 0.85} = 0.36$	
$\begin{aligned} \phi M_n &= 0.9 \times 0.5 \times 894.16 \times 60000 \times 98.4 \\ &\times 12 \left(1 + \frac{23660 \times 1000}{894.16 \times 60000} \right) (1 \\ &- 0.36) \left(\frac{1}{1000 \times 12} \right) = 2190916 \text{ kip.ft} \end{aligned}$	As=894.16 in ² (900 #9) S=2.7 in
$\frac{\phi M_n}{M_u} = 1.11 \geq 1 \quad o.k$ Hence, use h2= 2.624 Ft. (0.80 m)	M _u = 1969868 kip.Ft

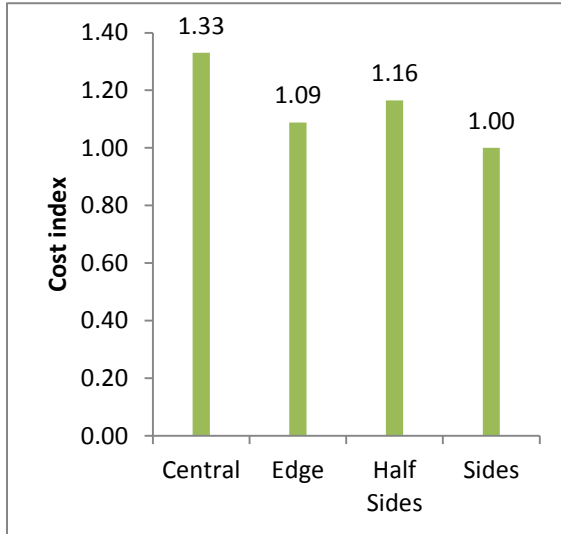
Now assume wall thickness h3 = 2.296 Ft. (0.70 m)	
$\alpha = \frac{15725 \times 1000}{98.4 \times 2.296 \times 4000 \times 12 \times 12} = 0.12$	Nu=15725kip
$w = 0.00424 \times \frac{60}{4} = 0.063$	
$\frac{c}{l_w} = \frac{0.063 + 0.12}{2 \times 0.063 + 0.85 \times 0.85} = 0.21$	
$\begin{aligned} \phi M_n &= 0.9 \times 0.5 \times 138 \times 60000 \times 98.4 \\ &\times 12 \left(1 + \frac{15725 \times 1000}{138 \times 60000} \right) (1 \\ &- 0.21) \left(\frac{1}{1000 \times 12} \right) = 832190 \text{ kip.ft} \end{aligned}$	As=138 in2 (450 #5) S=5.35 in
$\frac{\phi M_n}{M_u} = 1.27 \geq 1 \quad o.k$ Hence, use h3= 2.296 Ft. (0.70 m)	Mu= 652703 kip.Ft
finally assume wall thickness h4 = 1.968 Ft. (0.60 m)	
$\alpha = \frac{7934 \times 1000}{98.4 \times 1.968 \times 4000 \times 12 \times 12} = 0.071$	Nu=7934kip
$w = 0.00275 \times \frac{60}{4} = 0.041$	
$\frac{c}{l_w} = \frac{0.041 + 0.071}{2 \times 0.041 + 0.85 \times 0.85} = 0.14$	
$\begin{aligned} \phi M_n &= 0.9 \times 0.5 \times 76.66 \times 60000 \times 98.4 \\ &\times 12 \left(1 + \frac{7934 \times 1000}{76.66 \times 60000} \right) (1 \\ &- 0.14) \left(\frac{1}{1000 \times 12} \right) = 477529 \text{ kip.ft} \end{aligned}$	As=76.66 in2 (250 #5) S=9.6 in
$\frac{\phi M_n}{M_u} = 2.63 \gg 1 \quad o.k$ Hence, use h3= 2.296 Ft. (0.60 m)	Mu= 181477 kip.Ft



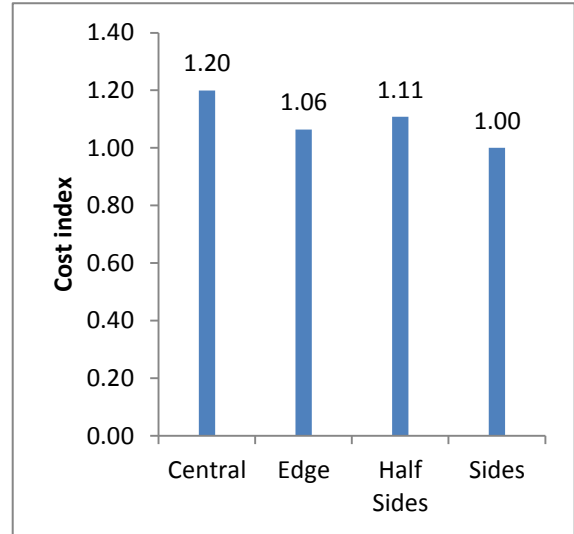
External forces (Sides Model)

APPENDIX B

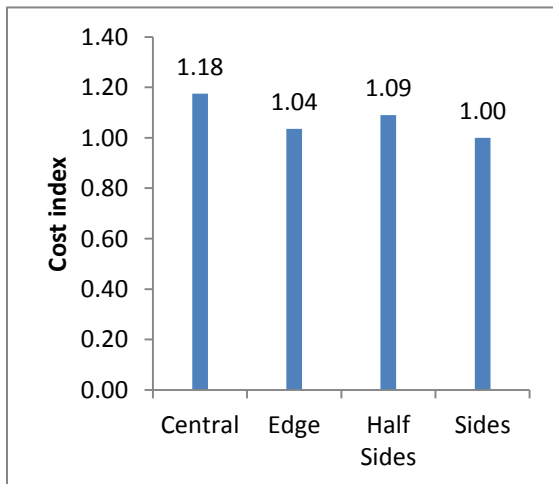
COST INDEX



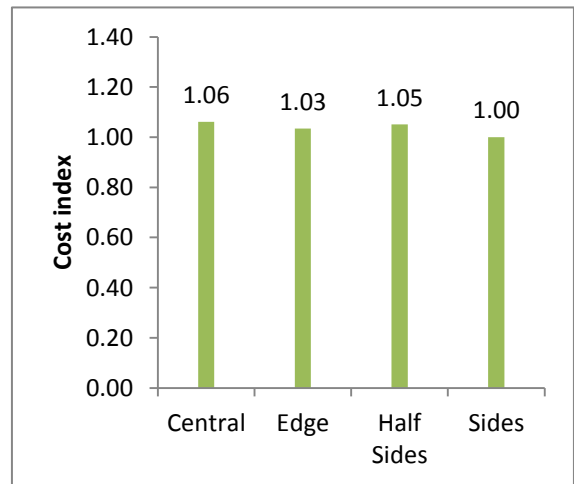
Cool



Temperate

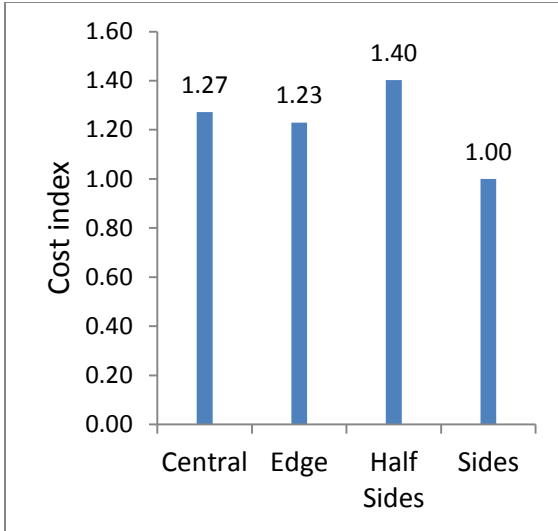


Arid

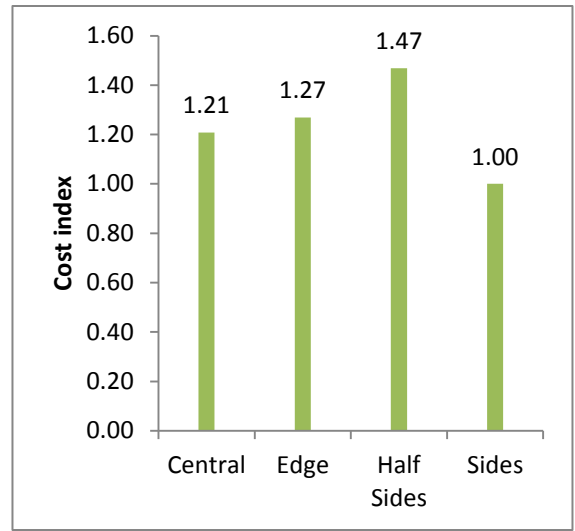


Tropical

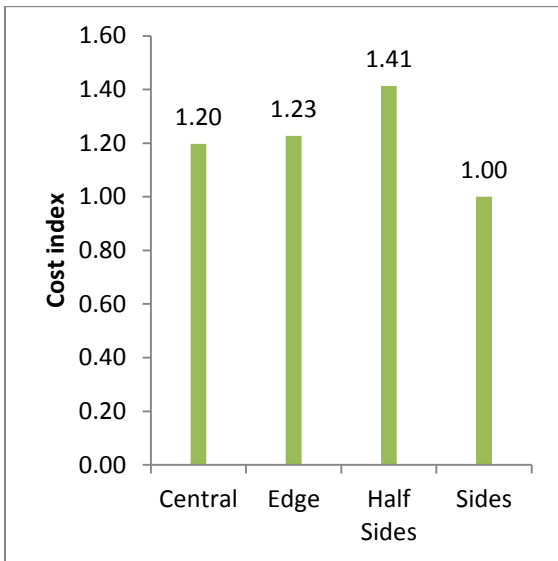
Operational cost index based on the cost normalization with respect to the cost in the Sides model



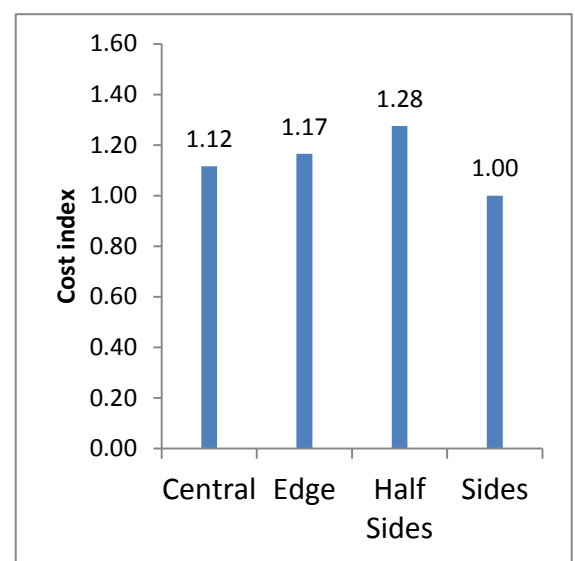
Cool



Temperate

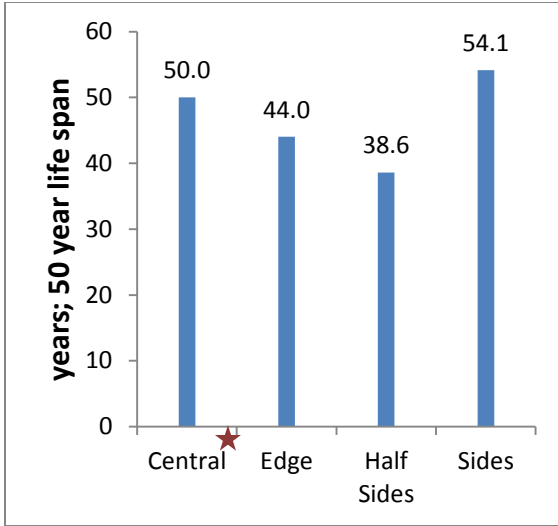


Arid

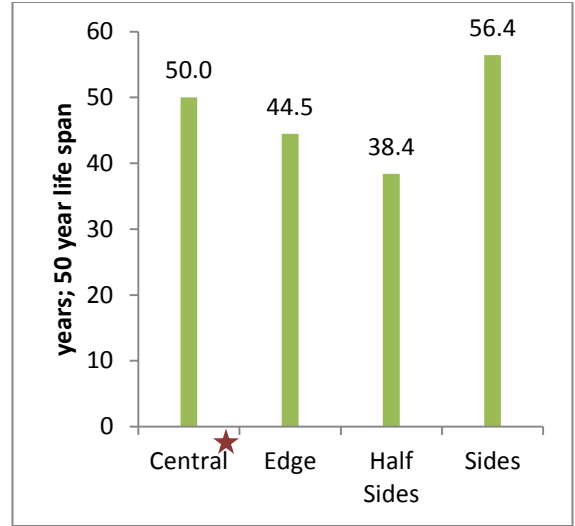


Tropical

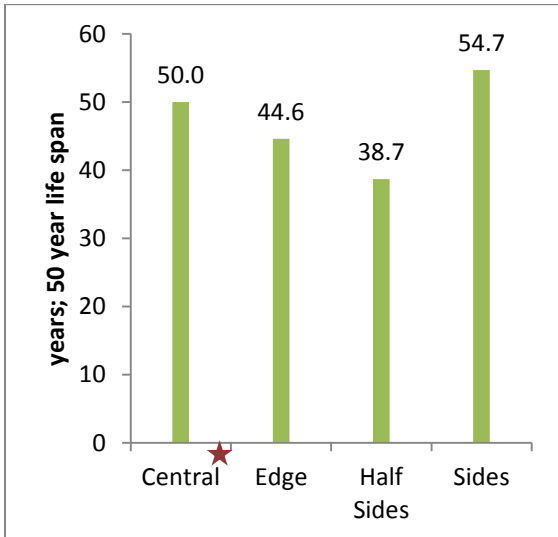
Total cost index (Operational and Embodied energies and Material used) based on the cost normalization with respect to the cost in the Sides model



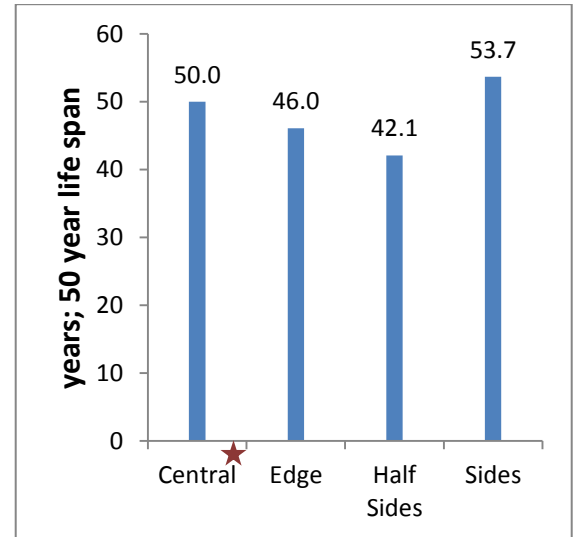
Cool



Temperate



Arid



Tropical

★ Indicates the operational energy is considered according to thermal analysis with EPO (section 4.4)

Financial comparison of the total cost for a 50 years life span with respect to the Central configuration

BIBLIOGRAPHY

- [1] Yeang K., *The Green Skyscraper*. Prestel, Munich, 1999.
- [2] Jenks, M. and Burgess, R. *Compact cities: Sustainable urban forms for developing Countries*. Spon Press, New York, 2004.
- [3] Straube, J. Green building and sustainability. *Building science digest*, 5: 24, 2006.
- [4] United States Green Building Council. Green building research. <<http://www.usgbc.org>>, 03 June 2009.
- [5] Reed, W. *The Integrative design guide to green building*. Hoboken, New Jersey, 2009.
- [6] The U.S. Department of Energy Building Energy Codes Program. *International Energy Conservation Code 2009*. International code council, INC., 2010.
- [7] ASCE. *ASCE Standard 7-10 Standard*. American Society of Civil Engineers, Virginia, 2010.
- [8] Walker, M.A. Energy series: What about House Design and Room Location. *Virginia cooperative extension*, 2009.
- [9] Cheung, C., Fuller, R., and Luther, M. Energy-efficient envelope design for high-rise apartments. *Energy and Buildings* 37: 37–48, 2004.
- [10] Jones, W., Balcomb, J., Kosiewicz, C., et al. *Passive solar design Handbook*. Volume 3: Passive solar design analysis. Prepared for U.S. department of energy, Washington, D.C., 1982.
- [11] Mazria, E. *Passive solar energy book*. Rodalie press, Pennsylvania, 1979.
- [12] Chow, W.K. Wind induced indoor airflow in a high rise building adjacent to a vertical wall. *Applied Energy* 77:225-234, 2004.
- [13] Li, L., Mak, C.M. The assessment of the performance of a wind catcher system using computational fluid dynamics. *Building and Environment* 42:1135-1141, 2007.
- [14] Mak, C.M., Niu, J.L., Lee, C.T., et al. A numerical simulation of wing walls using computational fluid dynamics. *Energy and Buildings* 39:995-1002, 2007.
- [15] Anderson, J.E., Silman R. The role of the structural engineer in green building. *The Structural Engineer* 87:28-31, 2009.
- [16] Webster, M.D. Relevance of structural engineers to sustainable design of buildings. *Structural Engineering International*. 14:181-185, 2004.

- [17] Kestner, D., Goupil, J., and Lorenz, E. *Sustainability Guidelines for the Structural Engineer*. American Society of Civil Engineers, Reston, Virginia, 2010.
- [18] Lee, B., Trcka, M., Hensen, J. Embodied energy of building materials and green building rating systems — a case study for industrial halls. *International Conference on Sustainable Energy Technologies*, Shanghai, China, 2010.
- [19] Technical Manual Design for lifestyle and the future. Australia's guide to environmentally sustainable homes. < <http://www.yourhome.gov.au>>, 2010.
- [20] Technical Manual. Embodied Energy. < <http://www.yourhome.gov.au/technical/fs52.html> >, 2010.
- [21] Ashley, E., Lemay, L. Concrete's contribution to sustainable development. *The Journal of Green Building* 1552-6100, 2008.
- [22] Buzzle. Thermal equilibrium. < <http://www.buzzle.com/articles/thermal-equilibrium.html>>, 2010.
- [23] Sylvie Boulanger. Special Issue: Sustainability and Steel. *Advantage steel*, 20:5-23, 2004.
- [24] Fathy, H. *Architecture for the poor*. The University of Chicago Press.1973.
- [25] Strine Environments. Thermal mass < <http://www.strinedesign.com.au/environments/thermalmass.cfm>>, 2011.
- [26] CIBSE. *Environmental design- guide A*. London, 2006.
- [27] A Guide to Heating & Cooling Load Estimation. < <http://www.scribd.com/doc/38684860/4/part-4-heat-gain-through-lighting-fixtures>>, 2010.
- [28] ASHRAE. *ASHRAE Handbook-Fundamentals*. American Society of Heating, Refrigerating and Air-Conditioning Engineers, Inc. Atlanta, 2001.
- [29] Bungale S. Taranath. *Wind and earthquake resistant buildings structural analysis and design*. Marcel Dekker, NEW YORK, 2005.
- [30] Bryan Stafford and Alex Coull. *Tall building structures: analysis and design*. A Wiley-Interscience Publication, Canada, 1991.
- [31] Kotttek, M., Grieser, J., Beck, C., et al. World map of the Koppen-Geiger climate classification updated. *Meteorologische Zeitschrift*. 15:259-263, 2006.
- [32] U.S. Department of energy, Energy plus. <<http://www.energy.gov/index.htm>>.2010.

- [33] Rees, S.J., Davies, M.G., Spitler, J.D., et al. Qualitative comparison of North American and U.K. cooling Load calculation methods. *HVAC& Research*, 1: 75-99, 2000.
- [34] Chang, KL., and Chun, CC. Outrigger system study for tall building structure with central core and square floor plate. *Structural engineer*, CTBUH, Seoul, 853-869, 2004.
- [35] A. E. Cardenas, J. M. Hanson, W. G. Corley and E. Hognestad, Design provisions for shear walls, *Journal of the American Concrete Institute*, 3: 221-230, 1973.
- [36] Technical manual design for lifestyle and the future .Embodied energy. <<http://www.yourhome.gov.au/technical/fs52.html> >, 2011.
- [37] CTBUH Journal. Tall building in numbers. *Issue III*, 50-51, 2009.
- [38] AISC. Designing for Sustainability. <<http://www.aisc.org/content.aspx?id=17560>>, 2011.
- [39] U.S. energy information administration. Consumption & Efficiency. < <http://www.eia.gov/>>, (2011)
- [40] Independent steel industry analysts. <<http://www.meps.co.uk/index.htm>>, 2011.
- [41] RC Means. Means Cost Works. <[http:// www.meanscostworks.com](http://www.meanscostworks.com)>, 2011.
- [42] WBDG. Energy Codes and Standards. < <http://www.wbdg.org/>>, 2011.
- [43] US department of energy. Building technologies program. < <http://www.energycodes.gov>>, 2012.
- [44] A. E. Cardenas, J. M. Hanson, W. G. Corley and E. Hognestad. Desing proisions for shesr walls. *Journal of the American Concrete Institute*, 3: 221-230, 1973.
- [45] John H.Lienhard V and John H.Lienhard IV. *A Heat Transfer* .Dover Publications, INC., Mineola, New York, 2011.
- [46] Daniel D.Chiras. *The natural house A Complete Guide to Healthy, Energy-Efficient, Environmental Homes*. Chelsea Green Publishing Company, 2000.
- [47] Egor P.Popov. *Engineering mechanics of solids*. Prentice Hall, New Jersey, 1990.
- [48] Russell C. Hibbeler. *Structural Analysis*. Prentice Hal New Jersey, 2002.
- [49] ASHRAE STANDARED. *Energy Standard for Buildings Except Low-Rise Residential Buildings*. ASHRAE, Atlanta, 2010.